DEVELOPMENT OF CYCLIC RAMP-TO-BASIN CARBONATE DEPOSITS, LOWER MISSISSIPPIAN, WYOMING AND MONTANA

by

Maya Elrick

Dissertation submitted to the Faculty of the
Virginia Polytechnic Institute and State University
in partial fulfillment of the requirements for the degree of
DOCTOR OF PHILOSOPHY
in
Geology

APPROVED:

J.F. Read, Chairman

R.K. Bambach

L. Glover III

C. Coruh

N.L. Gilinsky

July, 1990
Blacksburg, Virginia

LD
5655
V856
1990
E675
.2

ABSTRACT

The Lower Mississippian Lodgepole/lower Madison Formations (20-225 m thick) developed along a broad (>700 km) storm-dominated cratonic ramp. Three types of shallowing-upward cycles (5th order) are recognized across the ramp-to-basin transition. Peritidal cycles consist of very shallow subtidal facies overlain by algal-laminated tidal flat deposits, which are rarely capped by paleosol/breccia layers. Shallow subtidal cycles consist of stacked ooid grainstone shoal deposits or deeper subtidal facies overlain by ooid-skeletal grainstone caps. Deep subtidal cycles occur along the outer ramp and ramp-slope and consist of sub-storm wave base limestone-argillite, overlain by graded limestone, and are capped by storm-deposited skeletal-ooid grainstone. They pass downslope into rhythmically interbedded limestone and argillite with local deep-water mud mounds; no shallowing-upward cycles occur within the ramp-slope facies. Average cycle periods calculated along the outer ramp range from 30-110 k.y. The cycles likely formed in response to 5th order (20-100 k.y.) sea level oscillations.

The cycles are stacked to form three 3rd to 4th order depositional sequences which are defined by regional transgressive-regressive facies trends. The ramp margin wedge (RMW) developed during long-term sea level fall lowstand conditions and consists of cyclic crinoidal bank and oolitic shoal facies which pass downdip into deep subtidal cycles. The transgressive systems tract (TST),

which onlapped the ramp during long-term sea level rise, includes thick deep and shallow subtidal cycles; peritidal cycles are restricted to the inner ramp. The highstand systems tract (HST) developed during long-term sea level highstand and fall, and along the ramp is composed of early HST shallow subtidal cycles which are overlain by late HST peritidal cycles; shallow through deep subtidal cycles composed the HST along the ramp-slope.

Two-dimensional computer modeling of the cyclic sequences suggests that for the assumed water depths of facies, minimum 5th order amplitudes of 20-25 m were required to generate deep subtidal cycles along the ramp-slope. These amplitudes generated poorly developed peritidal cycles during the HST. Models run with amplitudes less than 10 m generated peritidal cycle-dominated HSTs, however, unreasonably shallow depths to storm-wave base were required to generate deep subtidal cycles and thick peritidal cycles were also generated during RMW and TST deposition, which is not observed in the actual sequences. Other factors, in addition to 5th order sea level oscillations, must have played a role in generating synchronous peritidal and deep subtidal cycles during the HST. These may include long-term climatic changes which influenced the depths to storm-wave reworking, or 5th order amplitudes may have varied during a single long-term sea level cycle. The moderate amplitude sea level oscillations may reflect the initial effects of Carboniferous glaciation that occurred in Gondwanaland.

ACKNOWLEDGEMENTS

My sincere thanks go to Fred Read for being an enthusiastic, positive and very approachable advisor who taught me to ask the important questions and how to answer those important questions. Thanks also to Bill Sando and Charlie Sandberg of the U.S.G.S. Bill generously shared his time and field notes for most of the sections I visited. Charlie offered much advice on the regional geology and biostratigraphy of the Mississippian. Many thanks to my field assistants David Jordan, Dave Pauling, May Devan, and Becky Cottingham who put up with sometimes ridiculous conditions and my odd eating habits. I would like to thank Emin Demirbag for his help with the VAX computer system and our many conversations about spectral analysis, and Vincent Miranda who helped with the computer modeling. My four years in Blacksburg would not be as memorable as they are without the academic and emotional support given by my good friends and colleagues in the carbonate lab, Dave Osleger, Isabel Montanez and Roger Barnaby. I appreciate and will miss the companionship of many in Derring Hall. My special thanks go to Bob Downs for his friendship and support.

Financial assistance was provided by NSF grants EAR 88-16664 and 87-07737 to J. F. Read, by Texaco, Mobil, Chevron, and Marathon oil companies, and by grants-in-aid from Sigma Xi, the Geological Society of America, and the Colorado Scientific Society.

TABLE OF CONTENTS

CHAPTER 1: DEVELOPMENT OF CYCLIC RAMP-TO-BASIN CARBONATE DEPOSITS, LOWER MISSISSIPPIAN, WYOMING AND MONTANA 1

INTRODUCTION 2

REGIONAL SETTING AND STRATIGRAPHIC FRAMEWORK 4

REGIONAL FACIES, SHALLOWING-UPWARD CYCLES AND DEPOSITIONAL ENVIRONMENTS 15

Ramp-Slope Facies 30

Deep Ramp Facies 34

Foreshoal Facies 43

Crinoidal Bank Facies 45

Ooid Shoal Facies 45

Peritidal Facies 47

Basal Dolomite/Siliciclastics 51

REGIONAL FACIES RELATIONSHIPS 52

Depositional Sequence 1 54

Depositional Sequence 2 59

Depositional Sequence 3 63

ORIGIN OF SHALLOWING-UPWARD CYCLES 66

COMPUTER MODELLING PARAMETERS 70

COMPUTER MODELING RESULTS 85

Ramp Margin Systems Tract 92

Transgressive Systems Tract 94

Maximum Flooding Surfaces 103
Highstand Systems Tracts 103
Sequence Boundaries 106
Discussion 107
CONCLUSIONS 110
REFERENCES - CHAPTER 1 114
CHAPTER 2: SHORT-TERM PALEOCLIMATIC FLUCTUATIONS IN RHYTHMICALLY BEDDED RAMP-SLOPE DEPOSITS, LOWER MISSISSIPPIAN OF SOUTHWESTERN MONTANA 128
ABSTRACT 129
INTRODUCTION 131
SETTING AND STRATIGRAPHY 132
METHODS 137
LITHOLOGIES 138
DEPOSITIONAL INTERPRETATION 144
SPECTRAL ANALYSIS 147
DISCUSSION 152
CONCLUSIONS 159
REFERENCES - CHAPTER 2 161
APPENDIX 167

LIST OF TABLES

TABLE 1.....16

TABLE 2.....72

TABLE 3.....155

LIST OF FIGURES

Figure 1. Map of northern Rocky Mountains.....5
Figure 2. Map of study area.....7
Figure 3. Biostratigraphic chart.....9
Figure 4. Regional cross-section.....11
Figure 5. Cycle types.....13
Figure 6. Interpreted range of water depths.....31
Figure 7. Variation in average cycle thickness.....36
Figure 8. Photographs of cycles and breccias.....38
Figure 9. Photographs of laminites and storm layers.....40
Figure 10. Depositional sequence 1.....49
Figure 11. Depositional sequence 2.....55
Figure 12. Depositional sequence 3.....60
Figure 13. Synthetic sequence 1.....86
Figure 14. Synthetic sequence 2.....88
Figure 15. Synthetic sequence 3.....90
Figure 16. Observed and synthetic columns 1.....96
Figure 17. Observed and synthetic columns 2.....98
Figure 18. Observed and synthetic columns 3.....100
Figure 19. Map of northern Rocky Mountains.....133
Figure 20. Lower depositional sequence cross-section.....135
Figure 21. Photographs of rhythmic interbeds.....139
Figure 22. Photomicrographs of limestone and argillite.....141
Figure 23. Portion of time-series.....148

Figure 24. Complete residue time-series 150
Figure 25. Power spectrum 153

LIST OF PLATES

PLATE 1.....folded in back

DEVELOPMENT OF CYCLIC RAMP-TO-BASIN CARBONATE DEPOSITS, LOWER MISSISSIPPIAN, WYOMING AND MONTANA

INTRODUCTION

The common building block of Precambrian through Holocene carbonate platform deposits are regularly repeating rock types or cycles (Wilson, 1975; James, 1984). The scale of cyclicity varies from formation-scale cycles that are 10-100's m thick (3rd to 4th order depositional sequences), outcrop-scale cycles which are several meters thick (5th order shallowing-upward cycles), to very small-scale cycles or rhythmites which are 10's cm thick. Similar types of cycles are also recognized in many shallow-marine clastic sequences (Wright, R., 1986; Eriksson and Simpson, 1990; Harris and Eriksson, 1990).

The origin of 5th order, shallowing-upward cycles has been attributed to autocyclic mechanisms that involve processes inherent within the depositional environment which govern the production or distribution of carbonate sediment (Ginsburg, 1971; James, 1984) or allocyclic mechanisms such as eustatic sea level changes (Goodwin and Anderson, 1985; Grotzinger, 1986; Goldhammer *et al.,* 1987, 1990; Bova and Read, 1987; Koerschner and Read, 1989), climatic change (deBoer and Wonders, 1984; Arthur *et al.*, 1984, Fischer *et al,* 1985; Herbert and Fischer, 1986; Weedon, 1986) or episodic subsidence (Cisne, 1986; Atwater, 1986).

Most studies on cycle carbonates have concentrated on the development of peritidal cycles (Goldhammer *et al.,* 1987; Strasser, 1988; Koerschner and Read, 1989) and have rarely examined how the

peritidal cycles relate to time-equivalent shallow and deep subtidal cycles (cycles that are composed wholly of facies deposited in subtidal environments) that occur in offshore parts of the platform. Furthermore, there have been few studies that have examined how the small-scale cycles are stacked to form larger scale depositional sequences (Grotzinger, 1986; Goldhammer and Harris, 1989; Koerschner and Read, 1989; Goldhammer *et al.*, 1990).

This paper describes the facies makeup and distribution of various types of cycles that occur across a Lower Mississippian carbonate ramp-to-basin transition and their arrangement within larger-scale depositional sequences. The detailed field data was combined with two-dimensional computer modeling techniques to assess how the cycles formed and to more quantitatively understand how specific input variables affect the development of cycles and sequence generation. The modeling results suggest that short-term (20-100 k.y.) sea level fluctuations likely controlled the development of the small-scale cycles in both shallow and deeper water settings, while long-term (0.5-3.0 m.y.) sea level oscillations influenced systems tracts makeup and depositonal sequence geometries.

REGIONAL SETTING AND STRATIGRAPHIC FRAMEWORK

Lower Mississippian carbonates of the Lodgepole/lower Madison Formations are exposed throughout the northern Rocky Mountains (Fig. 1). The formations developed on a westward-thickening cratonic ramp that was over 700 km wide, and over 1600 km long (Sando, 1976; Poole and Sandberg 1977; Gutschick and Sandberg, 1983). The ramp was bordered on the east by the Transcontinental Arch, and on the west by the Antler foredeep and its orogenic highlands (Fig. 1). During Lower Mississippian time, the ramp was intersected by the Central Montana Trough, which connected the Antler foredeep to the Williston Basin (Fig. 1). The ramp-to-basin transition is exposed on the authochthon east of the leading edge of the Mesozoic-early Cenozoic Sevier foreland fold and thrust belt (Fig. 1). Nineteen stratigraphic sections were logged in detail across this ramp-to-basin transition (Fig. 2).

The Lodgepole Formation of southwestern Montana is over 225 m thick, whereas the time-equivalent lower Madison Formation of Wyoming thins to less than 20 m in eastern Wyoming (Fig. 4). These formations overlie a regional Late Devonian-Early Mississippian unconformity, and are conformably overlain by the Mission Canyon/upper Madison Formations (Fig. 3). The Lodgepole Formation is composed of three members, in ascending order: the Cottonwood Canyon, Paine, and Woodhurst Members. The lower Madison Formation is composed of the Cottonwood Canyon/Englewood

Figure 1. Major paleogeographic and tectonic features of the northern Rocky Mountain region during Lower Mississippian time. Included is the Mesozoic-Cenozoic Sevier thrust front. Boxed area shown enlarged in Figure 2.

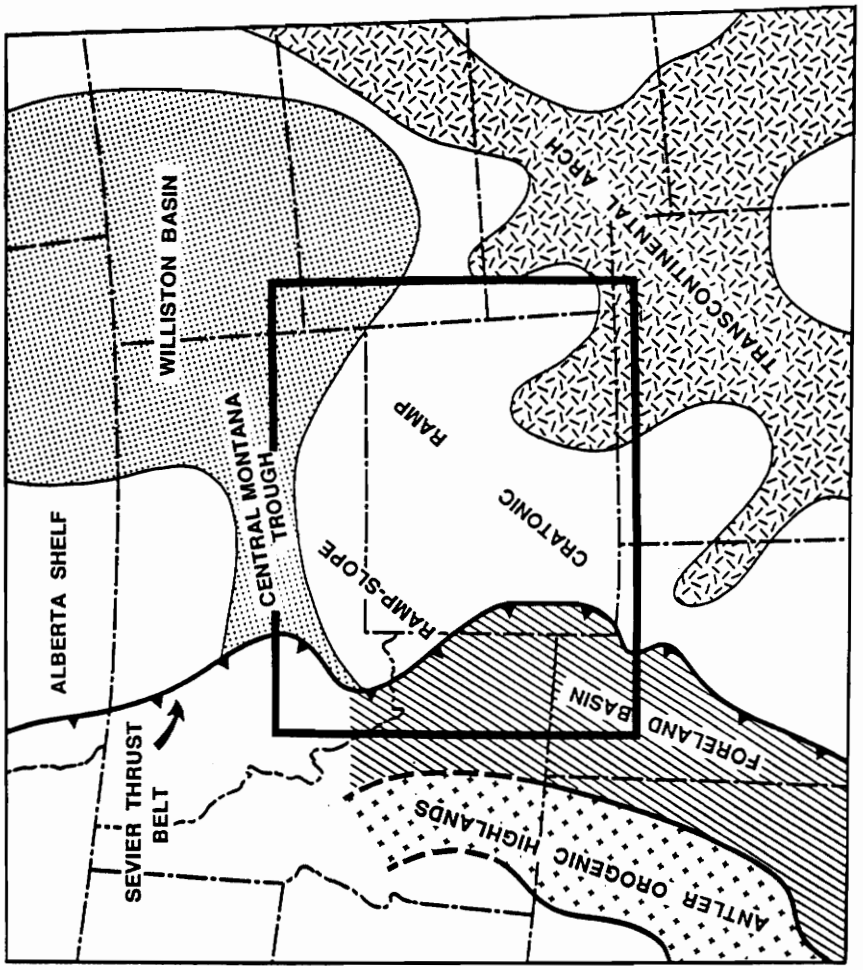
WILLISTON BASIN
TRANSCONTINENTAL ARCH
ALBERTA SHELF
CENTRAL MONTANA TROUGH
RAMP
CRATONIC
RAMP-SLOPE
BASIN
FORELAND
SEVIER THRUST BELT
ANTLER OROGENIC HIGHLANDS

Figure 2. Study area in Wyoming, southern Montana, and eastern Idaho with the location of measured sections and line of cross-section. Fine stippled pattern outlines shallow ramp regions, coarse stipple represents deep ramp to ramp-slope regions. Thrust fault is the leading edge of Mesozoic-Cenozoic Sevier fold and thrust belt. HC- Hartville Canyon, RC- Red Canyon, BC- Blue Creek, SR- South Rock, BG- Big Goose, LT- Little Tongue, LBC- Little Bighorn Canyon, CF- Clarks Fork, SH- Shoshone, W- Wiggins, WR- Washakie Reservoir, B- Benbow, BM- Baker Mountain, L- Livingston, S- Sacajawea, LO- Logan, DF- Dry Fork, AC- Ashbough Canyon, LF- Little Flat Canyon.

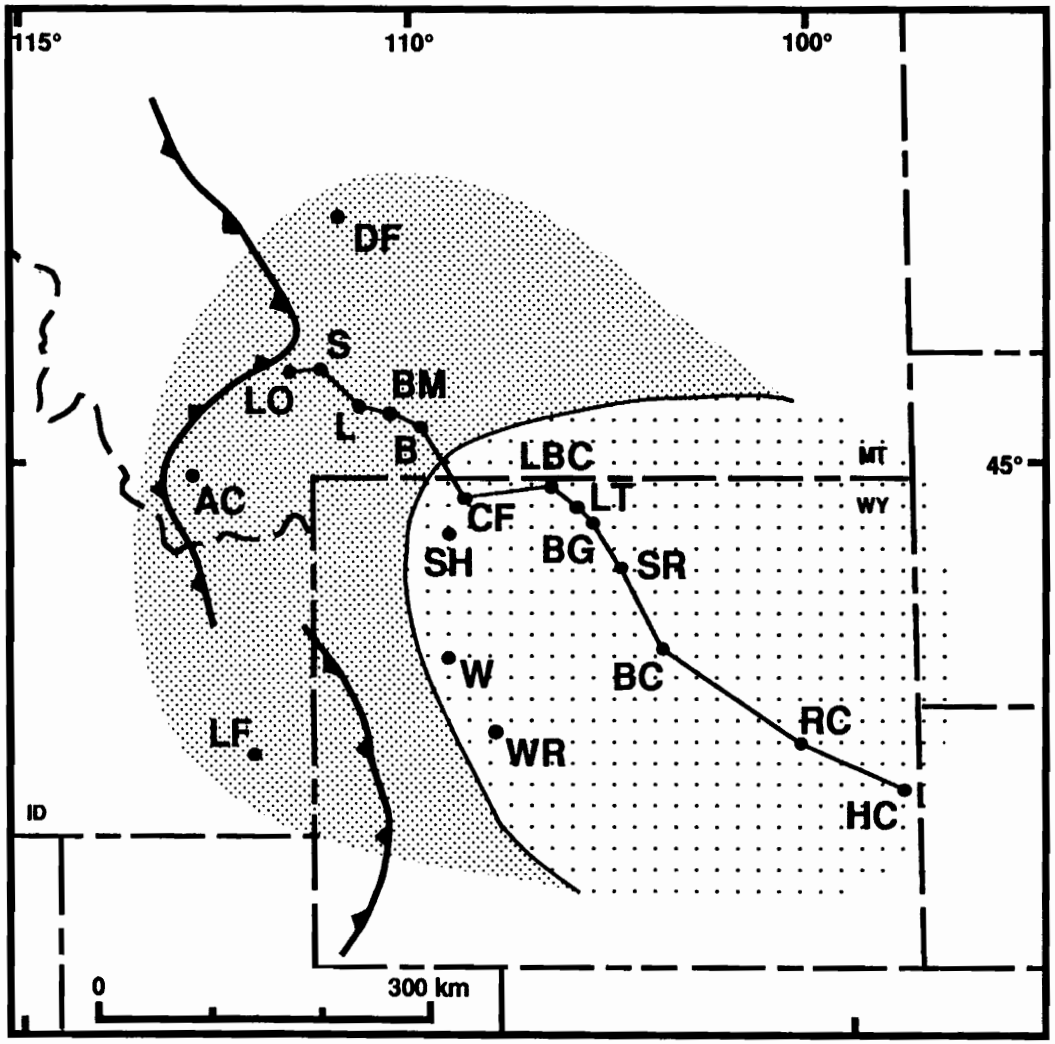
115°
110°
100°
45°
DF
S
LO
BM
L
B
LBC
MT
WY
LT
AC
CF
SH
BG
SR
W
BC
RC
WR
LF
HC
ID
0
300 km

Figure 3. Chronostratigraphic and biostratigraphic chart for the Lodgepole and lower Madison Formations. Biostratigraphy modified from Gutschick *et al.*, (1982), Sando (1985), and DNAG time scale (Palmer, 1983).

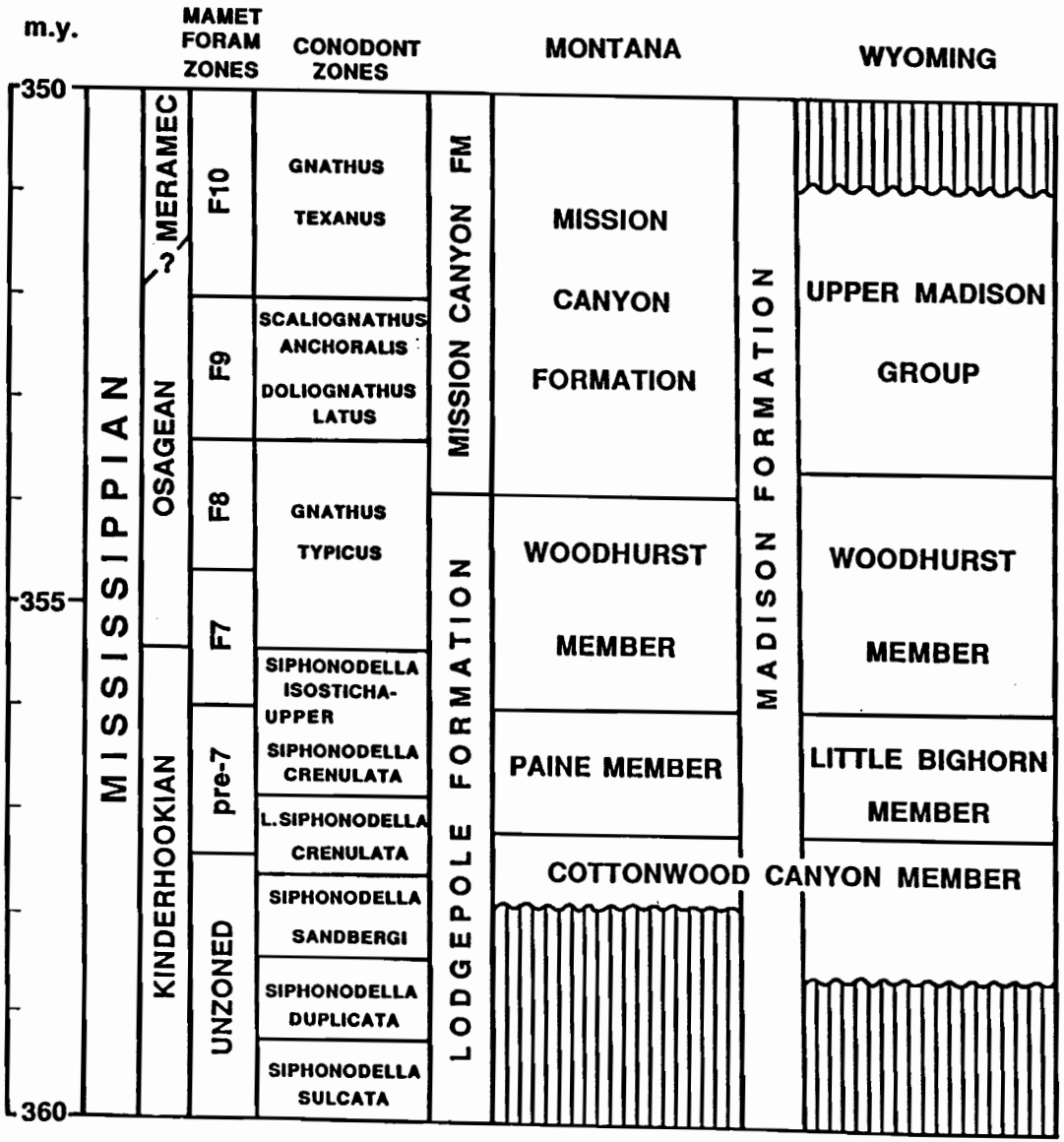
m.y.
MAMET FORAM ZONES
CONODONT ZONES
MONTANA
WYOMING
350
355
360
MISSISSIPPIAN
OSAGEAN
KINDERHOOKIAN
MERAMEC
F10
F9
F8
F7
pre-7
UNZONED
GNATHUS TEXANUS
SCALIOGNATHUS ANCHORALIS
DOLIOGNATHUS LATUS
GNATHUS TYPICUS
SIPHONODELLA ISOSTICHA-UPPER
SIPHONODELLA CRENULATA
L. SIPHONODELLA CRENULATA
SIPHONODELLA SANDBERGI
SIPHONODELLA DUPLICATA
SIPHONODELLA SULCATA
MISSION CANYON FM
LODGEPOLE FORMATION
MISSION CANYON FORMATION
WOODHURST MEMBER
PAINE MEMBER
COTTONWOOD CANYON MEMBER
MADISON FORMATION
UPPER MADISON GROUP
WOODHURST MEMBER
LITTLE BIGHORN MEMBER

Figure 4. Regional cross-section >700 km long showing depositional sequences 1-3 that are correlated using regional transgressive-regressive facies trends.

LODGEPOLE FORMATION
LOWER MADISON FORMATION
MT WY
SEQUENCE 1
SEQUENCE 2
SEQUENCE 3
RELATIVE SEA LEVEL
RISE
NW
SE
LO S
L BM B
CF
LBC LTBQ SR
BC
RC
HC
ENGLEWOOD FORMATION
WOODHURST
LITTLE BIGHORN
COTTONWOOD CANYON
PAINE
20 m
0
200 km
PERITIDAL FACIES
OOID SHOAL FACIES
CRINOIDAL BANK FACIES
FORESHOAL FACIES
DEEP RAMP FACIES
RAMP-SLOPE FACIES with MUD MOUNDS
BASAL DOLOMITE/SILICICLASTICS
SEQUENCE BOUNDARY

Figure 5. Cycle types occurring across the ramp-to-basin transition. Detailed facies descriptions and lateral distributions are given in the text and Table 1. A) Deep subtidal cycles (section LO); note symmetric cycle near base. B) Stacked shallow subtidal ooid grainstone cycles from section LBC. C) Stacked shallow subtidal oolitic intraclast cycles from section SR. D) Fining-upward shallow subtidal cycles from section SH at edge of ooid shoal complex. E) Coarsening-upward shallow subtidal cycles from section CF from basinward edge ooid shoal complex. F) Peritidal cycles containing paleosol/regolith caps from section RC.

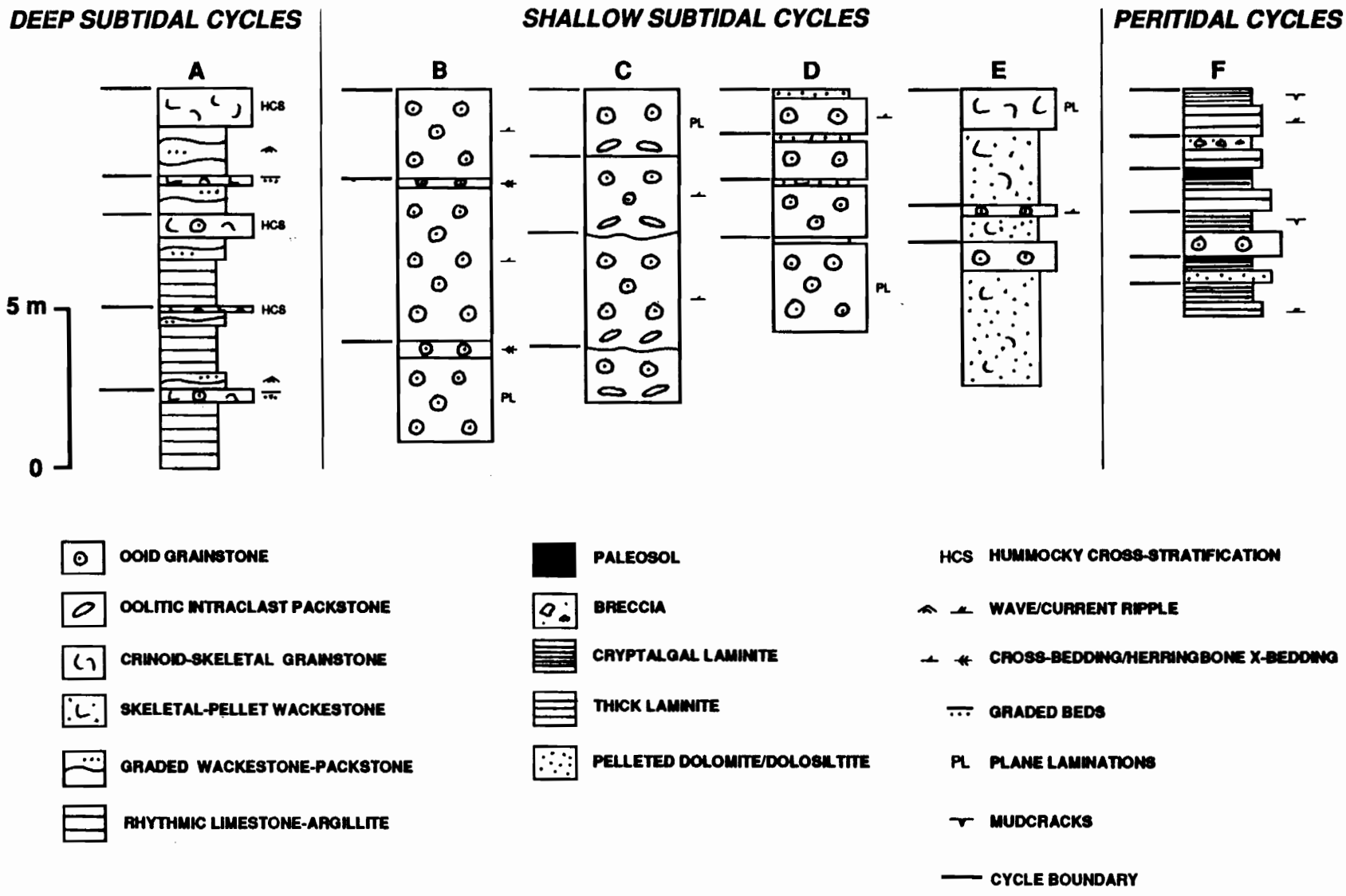
DEEP SUBTIDAL CYCLES
SHALLOW SUBTIDAL CYCLES
PERITIDAL CYCLES
A
B
C
D
E
F
HCS
PL
5 m
0
OOID GRAINSTONE
OOLITIC INTRACLAST PACKSTONE
CRINOID-SKELETAL GRAINSTONE
SKELETAL-PELLET WACKESTONE
GRADED WACKESTONE-PACKSTONE
RHYTHMIC LIMESTONE-ARGILLITE
PALEOSOL
BRECCIA
CRYPTALGAL LAMINITE
THICK LAMINITE
PELLETED DOLOMITE/DOLOSILTITE
HCS HUMMOCKY CROSS-STRATIFICATION
WAVE/CURRENT RIPPLE
CROSS-BEDDING/HERRINGBONE X-BEDDING
GRADED BEDS
PL PLANE LAMINATIONS
MUDCRACKS
CYCLE BOUNDARY

Formation, Little Bighorn, and Woodhurst Members (Fig. 3; Sando, 1982). Based on regional conodont, foraminifera, and coral biostratigraphy (Gutschick *et al.,* 1980; Sando, 1985), the Lodgepole/lower Madison Formations are middle Kinderhookian to early Osagean in age (Fig. 3).

The time resolution of conodont and foraminifera biozones is not sufficient to allow for precise biostratigraphic correlation between sections (*cf.* Gutschick *et al.,* 1980; Sando, 1985). Instead, sections were correlated using distinctive regional facies patterns which are shown on the ramp-to-basin cross-section in Figure 4. Correlation of these regional facies defines three depositional sequences (discussed below). Rock types and their arrangement within the regional facies are summarized in Table 1 and their interpreted depositional environments are outlined below.

REGIONAL FACIES, SHALLOWING-UPWARD CYCLES AND DEPOSITIONAL ENVIRONMENTS

Regional facies in the Lower Mississippian sequences (Fig. 4) include ramp-slope, deep ramp, crinoid bank, foreshoal, ooid shoal, peritidal, and basal dolomite/clastic facies. The component rock types within these regional facies are summarized in Table 1. The rock types are commonly arranged in cyclic units that include deep subtidal, shallow subtidal, and peritidal cycles (Fig. 5).

Table 1. Detailed characteristics of rock types within regional facies and cycles.

RAMP-SLOPE FACIES

Rhythmically interbedded limestone and argillite

Occurrence

Paine Member occurs as thick intervals (60-79 m) at sections LO, S, AC, and DF; also forms base (0.1-8.0 m) to deep subtidal cycles along deep ramp.

Lithology

Rhythmically interbedded limestone (5-30 cm) and argillite (1-10 cm).
Even-bedded limestone: Lime mudstone to laminated pellet packstone with <15 wt% quartz silt, muscovite/illite and organic matter.
Nodular limestone: Lime mudstone to crinoid wackestone (with pellet packstone matrix).
Argillite: Bryozoan-crinoid wackestone (argillaceous microspar matrix with <100 μm dolomite rhombs) with up to 60 wt% quartz silt, muscovite/illite, and organic matter.

Color

Limestone: medium gray
Argillite: yellow gray

Deep-water mud mounds

Occurrence

Basal part of Paine Member and upper 50 m Woodhurst Member at secton S (10-25 m tall, 75-185 m wide; Fig. 4).

Lithology

Inner core facies: bryozoan grainstone with abundant marine cement.
Outer core: lime mudstone/bryozoan wackstone.
Flank facies: crinoid wackstone through packstone.
Mounds developed on clayey, bryozoan-crinoid wackestone through grainstone, and are onlapped and capped by rhythmically interbedded limestone-argillite facies (Stone, 1972).

Color

Yellow brown to gray

Table 1. continued

Sedimentary structures	Sedimentary structures
Even-bedded limestone layers contain millimeter-thick, wavy to planar, graded laminae of pellet silt to mudstone. No structures observed in argillite layers.	Massive to poorly bedded. Depositional dips within mud mounds are between 5°-30°, sparse stromatactis structures, and syn-depositional brecciation.
Biota	Biota
Even-bedded limestone: Rare bryozoans, crinoids, and rugose corals (in life position), calcispheres and abundant sponge spicules. *Nodular limestone:* Crinoids, syringoporid-type and(in life position) rugose corals, brachiopods, sponge spicules, and calcispheres. *Argillite:* Large fenestrate bryozoan fragments, articulated crinoid stems and calyxes, brachiopods, trilobites, and abundant trace fossils (*Scalarituba, Zoophycus, Cosmoraphe(?)*).	Fenestrate and ramose bryozoan, common articulated crinoids, brachiopods, rugose and *Syringapora* corals, ostracodes, trilobites, gastropods, and cephalopods.

Table 1. continued

DEEP RAMP FACIES

Occurs as deep subtidal cycles (1-10 m thick): rhythmically interbedded limestone and argillite overlain by thin-bedded, normally graded limestone, capped by skeletal/ooid grainstone. Weakly cyclic intervals (34-47 m) of cherty skeletal wackestone/packstone at sections BM, L, and base of Paine Member (3-10 m) at sections S and LO.

Ooid-skeletal grainstone caps

Occurrence

Ooid or ooid-skeletal packstone/grainstone form caps (0.3-2.0 m) to some deep subtidal cycles. Skeletal packstone/grainstone form common caps (0.1-1.5 m) to deep subtidal cycles.

Lithology

Ooid or ooid-skeletal packstone/grainstone with argillaceous mudstone interbeds and drapes.
Crinoid-skeletal packstone/grainstone with common argillite drapes.

Graded limestone

Occurrence

Middle portion or base (0.3-6.0 m) of shallow and deep subtidal cycles.

Lithology

Graded layers (3-20 cm) of skeletal packstone/grainstone, pellet-skeletal wackestone/packstone to argillaceous wackestone; (argillaceous microspar with <0.1 μm dolomite rhombs) partially dolomitized.
Grades basinward into:
Graded layers (5-30 cm) of skeletal packstone-grainstone, pellet-skeletal grainstone, to argillaceous wackestone with trace amounts of quartz silt.

Table 1. continued

Color	Color
Medium gray	*Limestone:* Medium gray *Argillite:* yellow gray
Sedimentary structures	Sedimentary structures
Ooid caps: graded layers, plane-laminations, cm-thick argillite interbeds, hummocky-stratification, and rare symmetric megaripples. *Skeletal caps:* sharp, erosional base with argillite rip-ups, grading, hummocky-stratificaton, symmetric megaripples, plane-laminations, and fine-grained drapes.	*Landward graded facies* are laterally discontinuous over ≈1-2 m, scours, plane-laminations, wave-ripples, mud drapes; abundant bioturbation obliterates many primary structures. *Seaward graded facies* are more laterally continuous over 10's m, layers characterized by scoured base, overlain by graded and hummocky-stratified layers with rip-ups composed of the underlying argillite, overlain by plane-laminated, and wave-rippled pellet grainstone (2-15 cm), capped by laminated to burrowed argillaceous wackestone (1-10 cm) drapes. Bioturbation within individual graded layers decreases from the top of argillite layer down into underlying limestone layers. Graded layers may scour and erode underlying argillite drapes.

Table 1. continued

Biota	Biota
Ooid caps: Pelmatozoans and rugose corals. *Skeletal caps:* Pelmatozoans, brachiopods, bryozoans, benthic foraminifera, and trilobites.	Crinoids, brachiopods, bryozoans, rugose corals, sponge spicules, trilobites, calcispheres, and abundant trace fossils including *Chondrites, Cruziana(?), Zoophycus, Asterophycus(?),* and *Cosmorhape(?),* and abundant escape structures.

Cherty skeletal wackestone/packstone

Occurrence

Paine Member at sections BM and L (34-47) and base of Paine Member at sections S and LO (3-10 m).

Lithology

Skeletal wackestone/packstone with trace quartz silt and glauconite grains, and up to 40% chert layers and nodules.

Color

Medium gray to yellow gray

Sedimentary structures

Faint plane-laminations, sparse cross-bedding (Smith, 1977) and rare, thin graded layers.

Table 1. continued

Biota

Abundant sponge spicules, crinoids, brachiopods, bryozoans, and bioturbation.

CRINOID BANK FACIES

Shallow subtidal cycles (0.5-9.0 m thick): *Coarsening-upward cycles:* skeletal-pellet wackestone or graded limestone overlain by crinoidal packstone/grainstone. *Fining-upward cycles:* crinoid-skeletal packstone/grainstone overlain by pelleted dolomite or skeletal-pellet wackestone.

Crinoidal packstone/grainstone

Occurrence

Occur as thick (2-15 m), poorly bedded intervals along outer ramp and ramp-slope (sequence 2).
Skeletal packstone/grainstone also occur as channel-fills along the inner and outer ramp (channels 1.5 m deep, and up to 2 m wide); 16 occurrences of channeling observed.

FORESHOAL FACIES

Shallow subtidal cycles (0.5-9.0 m thick) *Coarsening-upward cycles:* skeletal-pellet wackestone overlain by cross-bedded ooid-skeletal grainstone or crinoid-skeletal packstone/grainstone.

Crinodal dolowackestone and skeletal-pellet wackestone

Occurrence

Little Bighorn Member (10-35 m). *Skeletal-pellet wackestone* forms base (0.5-9.0 m) to some shallow subtidal cycles.

Table 1. continued

Lithology	**Lithology**
Fine- to coarse-grained crinoid packstone/grainstone or skeletal packstone/grainstone; may contain pellet packstone or argillaceous wackestone interbeds/drapes (2-10 cm).	*Little Bighorn Member*: Nodular crinoidal dolowackestone with wispy argillite seams, locally abundant silicified nodules/geodes, and rare <5 cm thick laminite interbeds at base. *Skeletal-pellet wackestone:* skeletal wackestone with pellet packstone matrix.
Color	**Color**
Medium gray	Yellow gray to light gray
Sedimentary structures	**Sedimentary structures**
Bank deposits: Poorly stratified to massive. *Channel-fill deposits* : Imbricated rip-ups, herringbone, trough, and planar cross-bedding.	Sparse laminations to burrow-homogenized, rare cross-laminations, and graded lenses of fine skeletel debris.
Biota	**Biota**
Pelmatozoans, brachiopods, rugose corals, benthic foraminifera, mollusks, ostrocodes, trilobites, sponge spicules, bryozoan, and calcispheres.	*Little Bighorn Member*: crinoids, syringaporid-type corals, rugose corals. *Skeletal-pellet wackestone:* ostracodes calcispheres, pelmatozoans, brachiopods, benthic foraminifera, and abundant trace fossils.

Table 1. continued

OOID SHOAL FACIES

Shallow subtidal cycles (0.5-9.0 m thick):
Stacked ooid grainstone cycles: cross-bedded ooid-oolitic intraclast grainstone which grades into plane-laminated or herringbone-stratified ooid-skeletal grainstone.
Fining-upward cycles: cross-bedded ooid-skeletal grainstone overlain by thin pelleted dolomite/dolosiltite.
Coarsening-upward cycles: skeletal-pellet wackestone or graded limestone overlain by ooid-skeletal grainstone.

Ooid grainstone

Occurrence

Inner and outer ramp Woodhurst Member. Forms base (0.3-1.5 m) of some peritidal cycles and caps of (0.3-8.0 m) shallow subtidal cycles. Also occur as thick (5-26 m) noncyclic intervals of massive grainstone.

Lithology

Ooid/ooid-skeletal grainstone; radial-concentric ooids are micritized or have chalky textures, commonly mixed with rounded skeletal grains and peloids; dolomitized along inner ramp.

Color

Yellow gray to light gray

Oolitic intraclast grainstone

Occurrence

Inner and outer ramp Woodhurst Member (0.3-3.0 m).
Forms base to some shallow subtidal cycles

Lithology

Platy to elongate oolitic intraclasts (8+ cm long) are composed of cemented ooids, peloids, and rounded skeletal aggregates.

Color

Yellow gray

Table 1. continued

Sedimentary structures	Sedimentary structures
Erosional base with rip-up clasts, plane-laminations, planar and trough cross-bedding (sets 10-30 cm thick), sparse herringbone cross-stratification (peritidal cycles), thin interbeds of cryptalgal laminite, and dolomudstone drapes.	Massive to cross-bedded.
Biota	Biota
Pelmatozoans, benthic foraminifera, rugose and syringaporid-type corals, and brachiopods.	Syringporid-type and rugose corals, benthic foraminifera, crinoids, and brachiopods.

PERITIDAL FACIES

Cycles (0.3-5.0 m thick): Ooid grainstone or pelleted dolomite base overlain by thick laminite which grades into cryptalgal laminite; rarely capped by thin paleosol or breccia layers.

Pelleted dolomite/dolosiltite	**Thick laminite**
Occurrence	Occurrence
Inner ramp Woodhurst Member. Occur as base of peritidal cycles (0.3-1.5 m) or extend seaward where they cap (<0.5 m) some shallow subtidal cycles. Also form base (<1.5 m) to some shallow subtidal cycles.	Inner ramp Woodhurst Member. Caps to peritidal cycles (0.1-4.5 m); rarely form conformable bases to shallow subtidal cycles. Rare at base of Little Bighorn Member (<5 cm).

Table 1. continued

Lithology	Lithology
Dolomitized pellet packstone/grainstone or finely crystalline dolomite (dolosiltite); may have thin interbeds (1-5 cm) of algal laminites.	Centimeter-thick graded layers (0.2-3.0 cm) of pellet grainstone/packstone to lime mudstone; commonly dolomitized.
Color	Color
Yellow gray	Yellow gray
Sedimentary structures	Sedimentary structures
Poorly laminated to burrow-homogenized. Sparse graded layers <5 cm thick.	Fining-upward layers with plane- and cross-laminations, wave- and current-ripples, scours, interbedded flat-pebble conglomerate, and sparse algal laminations.
Biota	Biota
Rare ostracodes, calcispheres, fine crinoidal debris, and abundant trace fossils.	Sparse small, vertical trace fossils.

Table 1. continued

Cryptalgal laminite	Breccias
Occurrence	**Occurrence**
Inner ramp Woodhurst Member. Common caps (0.3-3.5 m) to peritidal cycles. (Fig. 9A).	Inner ramp Woodhurst Member. Breccias (0.03-1.0 m) overlie or pass laterally into undisturbed laminites or pelleted dolomite facies. Irregular breccia surfaces are rarely veneered by cryptalgal laminite or breccia sheets are sandwiched between undisturbed laminite layers (Fig. 8A).
Lithology	**Lithology**
Millimeter-thick laminae of graded dolosiltite to dolomudstone with sparse silicified evaporite nodules.	Angular clasts (1-15 cm) of dolomudstone/dolosiltite or cryptalgal laminite.
Color	**Color**
Yellow gray	Yellow gray
Sedimentary structures	**Sedimentary structures**
Even-, crinkly-, to LLH-laminations, fining-upward layers, sparse mudcracks and tepee structures, scattered halite casts, interbedded lenses of solution-collapse breccias.	Clasts have fitted to chaotic fabrics and may have thin dolomite coatings.
Biota	**Biota**
Barren	Barren

Table 1. continued

Red fine-grained dolomite (paleosols)

Occurrence

Inner ramp Woodhurst Member.
Forms rare caps (0:03-0.30 m) caps to peritidal cycles and overlies irregular surfaces of mudcracked-cryptalgal laminite or breccia layers.

Lithology

Friable, Fe-stained dolomite composed of dolomite rhombs (>300 μm) with interstial Fe-oxides.

Color

Medium red

Sedimentary structures

Dark brown elongate mottles (≈20 mm long, few mm wide) and rare laminated caliche(?) crusts (<2 cm thick).

Biota

Barren

Table 1. continued

BASAL DOLOMITE/SILICICLASTICS

Cottonwood Canyon Member

Occurrence

Basal sheet of Lodgepole/lower Madison Formations along outer ramp and ramp-slope (0-15 m).

Lithology

Outer ramp/ramp-slope facies: shale, dolomitic silty-shale, and quartz siltstone.
Middle ramp facies: medium- to thin-bedded dolomite and silty dolomite with scattered silicified evaporite nodules.
Both facies contain glauconite grains, phosphatic nodules, and local, thin quartz conglomerate.

Color

Shale and silty shale: Black, dark gray, olive, and gray-red
Dolomite: yellow gray

Sedimentary structures

Plane-laminations.

Englewood Formation

Occurrence

Basal sheet of lower Madison Formation (0-11 m) along inner ramp.

Lithology

Thin- to medium-bedded, fine- to coarse-grained quartz arenite and quartz siltstone.

Color

Reddish brown

Sedimentary structures

Trough and herringbone cross-bedding, channel scours and lags, and plane-laminations.

Table 1. continued

Biota	Biota
Conodonts, fish, plant, and algal remains, rare crinoid fragments and brachiopods, and abundant trace fossils (*Zoophycos, Bifurgites, and Scalarituba*).	Rare braciopods.

Ramp-Slope Facies

Ramp-slope facies occur as thick, noncyclic intervals (60-79 m; Paine Member at locations LO, S, AC, and DF) of dark, rhythmically interbedded fine-grained limestone and argillite (Table1) and are locally associated with deep-water, Waulsortian-type mud mounds (Fig. 4 and Table 1). They also form thinner intervals (<15 m) at the base of deep subtidal cycles (Fig. 5A).

Rhythmically interbedded limestone-argillite (Table 1) was deposited below storm-wave base based on the lack of wave- or current-reworking features and the continuous even bedding. Water depths were likely greater than 65 m which includes 25 m of mud mound relief and at least 40 m related to the depth of storm-wave base (Fig. 6). Similar sub-storm wave base deposits and water depths are reported by Wilson (1975), Bissell and Barker, (1977), Yurewicz (1977), Read (1980), Aigner (1985), and Hanford (1986). Calcareous plankton, a major source of modern deep water deposits, did not evolve until the Mesozoic (Bathurst, 1975), therefore the limestone-argillite deposits were derived entirely from shallow carbonate ramp and from surrounding land masses.

The limestone-argillite deposits grade landward into deep ramp storm deposits. This, along with thin graded laminae, indicates they are distal storm deposits. Relatively rapid sedimentation rates for laminated limestone layers are inferred from the rare bryozoa, crinoids, and rugose corals found upright in life position. Rare skeletal and trace fossils indicate that bottom

Figure 6. Interpreted range of water depths for the major rock types estimated from Holocene analogs and stratigraphic relationships with adjacent facies (assuming a 40 m depth to storm-wave base).

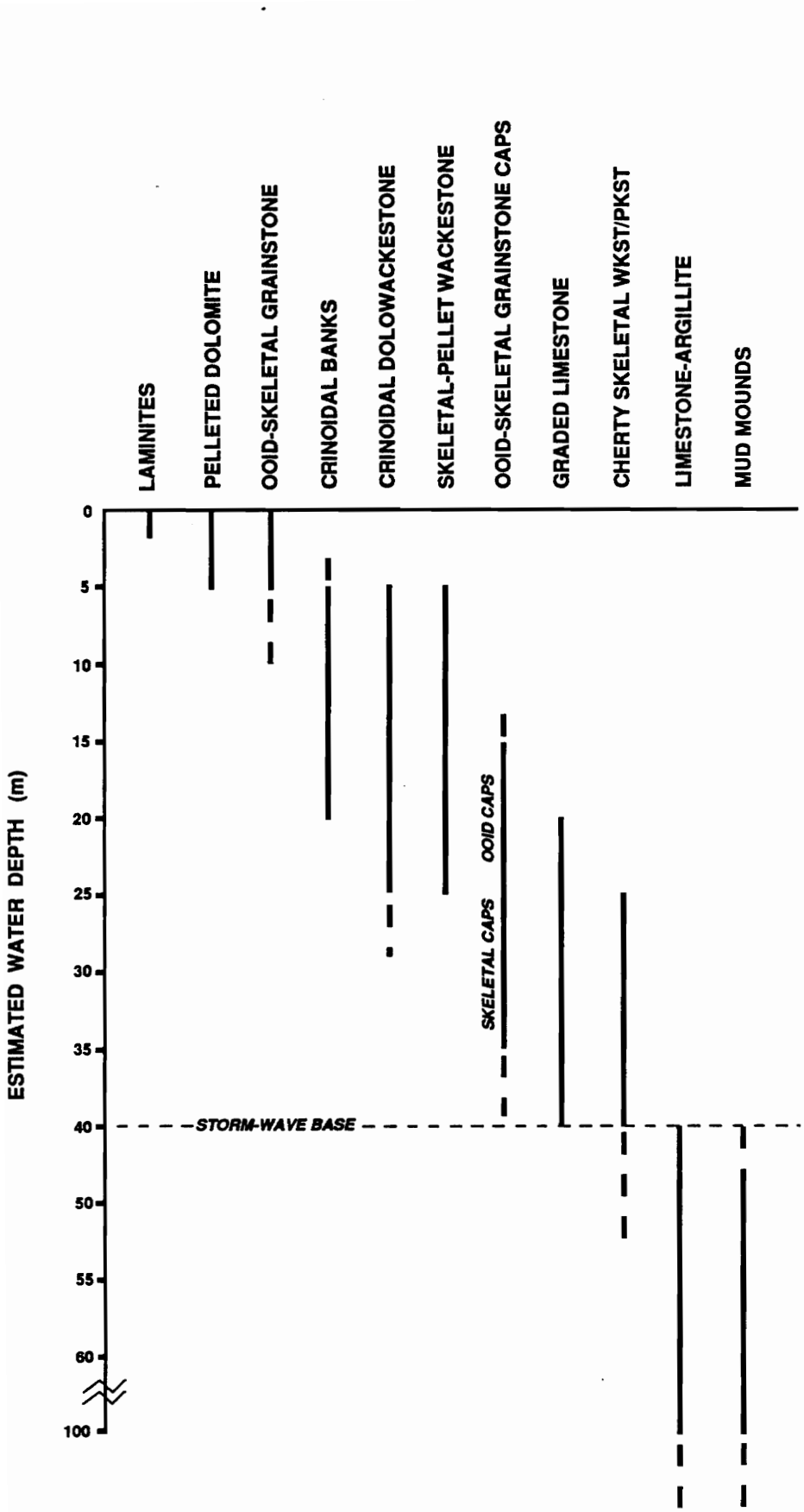
ESTIMATED WATER DEPTH (m)
0
5
10
15
20
25
30
35
40
50
55
60
100
LAMINITES
PELLETED DOLOMITE
OOID-SKELETAL GRAINSTONE
CRINOIDAL BANKS
CRINOIDAL DOLOWACKESTONE
SKELETAL-PELLET WACKESTONE
OOID-SKELETAL GRAINSTONE CAPS
GRADED LIMESTONE
CHERTY SKELETAL WKST/PKST
LIMESTONE-ARGILLITE
MUD MOUNDS
SKELETAL CAPS
OOID CAPS
STORM-WAVE BASE

waters were not fully anoxic. In contrast, fine-grained argillite layers lack textural grading and contain whole delicate fossils, suggesting deposition in quiet, well-oxygenated water. The fossil material within argillite layers lies parallel to bedding suggesting slow sedimentation rates.

The rhythmic decimeter alternation of limestone and argillite layers may be the result of 1) relatively continuous siliciclastic influx (i.e., background sedimentation) punctuated by periodic storm deposition of carbonate material (carbonate dilution), 2) storm deposition punctuated by periods of increased river-runoff which supplied siliciclastic material, or 3) periods of carbonate storm deposition alternating with periods of influx. In either of the interpretations, the rhythmicity likely results from climate fluctuations affecting the location of storm tracks and rainfall patterns (Anderson *et al.,* 1989; Chapter 2). Spectral analysis of the fluctuating siliciclastic component in the ramp-slope facies indicates a dominant 1000-3000 year periodicity to the limestone-argillite couplets and suggests that short-term paleoclimate fluctuations likely controlled ramp-slope sedimentation patterns (Chapter 2).

Deep-water mud mounds (Table 1) occur within the lower part of the Paine Member throughout west-central Montana (Fig. 4 and Table 1; Cotter, 1966; Stone, 1972; Smith, 1977; 1982; Wilson, 1975). A small mud mound (≈25 m thick) also occurs in the upper Woodhurst Member (stratigraphic section S; Fig. 4). The Paine

buildups initiated at the toe of the ramp-slope (Fig. 4; Smith, 1982). Mud mounds within the study area stood at least 25 m above the sea floor (Stone, 1972), whereas mounds in central Montana had over 50 m of syn-depositional relief (Smith, 1977; 1982). Vertical growth of the mounds was maintained by *in situ* production of lime mud and submarine cementation (Cotter, 1966; Stone, 1972; Smith, 1982). The buildups and their flanking facies were subsequently enveloped by rhythmically interbedded limestone-argillite deposits (Stone, 1972). The syn-depositional relief of the mounds suggests deposition in water depths greater than 65 m, which includes 25 m of syn-depositional relief plus at least 40 m to storm-wave base (Fig. 6).

Deep Ramp Facies

These facies include deep subtidal cycles, which are composed of calcisiltite, graded skeletal wackestone through packstone, overlain by skeletal-ooid grainstone caps (Fig. 5A), and thick (34-47 m) intervals of noncyclic cherty skeletal wackestone/packstone (Table 1; Paine Member at sections L and BM and base of Paine Member at sectons LO and S).

Cherty skeletal wackestone/packstone (Table 1) of the Paine Member grade landward into crinoidal dolowackestone and seaward into ramp-slope limestone-argillite (Fig. 4). The abundance and diversity of whole fossils and lack of wave-reworked features indicate deposition in open-marine, deep ramp environments (Wilson,

1975; Markello and Read, 1981; Aigner, 1985; Read, 1985; Dorobek and Read, 1986). Siliceous sponges were probably the major source of silica for the chert. The nodular bedding was likely caused by patchy submarine cementation and burrowing, followed by differential compaction along argillite seams and early replacement chert layers. Facies relationships and analogies with modern deep ramp deposits (Wagner and van der Togt, 1973; Logan and Cebulski, 1970) suggest deposition in 25-40 m water depths (assuming a 40 m storm-wave base; Fig. 6).

Deep subtidal cycles are 1-10 m thick (average 3 m; Fig. 7). An ideal cycle consists of rhythmically bedded limestone-argillite, overlain by graded limestone, and are capped by skeletal/ooid grainstone (Figs. 5A and 8A). Shallowing-upward trends in the cycles include an upward increase in grain size, bed thickness, storm-generated features, bioturbation, skeletal content, and biotic diversity. The most common cycle type is graded limestone overlain by a skeletal grainstone cap. Along the ramp-slope, less than 10% of the deep subtidal cycles are symmetric, i.e., basal graded limestone beds overlain by rhythmically bedded limestone-argillite, then overlain by graded limestone (Fig. 5A). Interpretation of depositional environments of specific deep subtidal facies is discussed below.

Deep water limestone-argillite facies at the base of deep subtidal cycles is similar to those in the Paine Member (discussed previously). *Graded limestone* beds (Table 1) that overlie the deeper

Figure 7. Variation in average cycle thickness of cycle types from each measured section across the ramp-to-basin transition. Peritidal cycles tend to thicken towards the basin, reflecting the increase in accommodation space. Shallow subtidal cycles show no distinct thickness trend likely due to amalgamation of stacked ooid grainstone cycles and noncylic intervals. Deep subtidal cycles thicken basinward reflecting the increase in accommodation space related to greater subsidence and initial water depths.

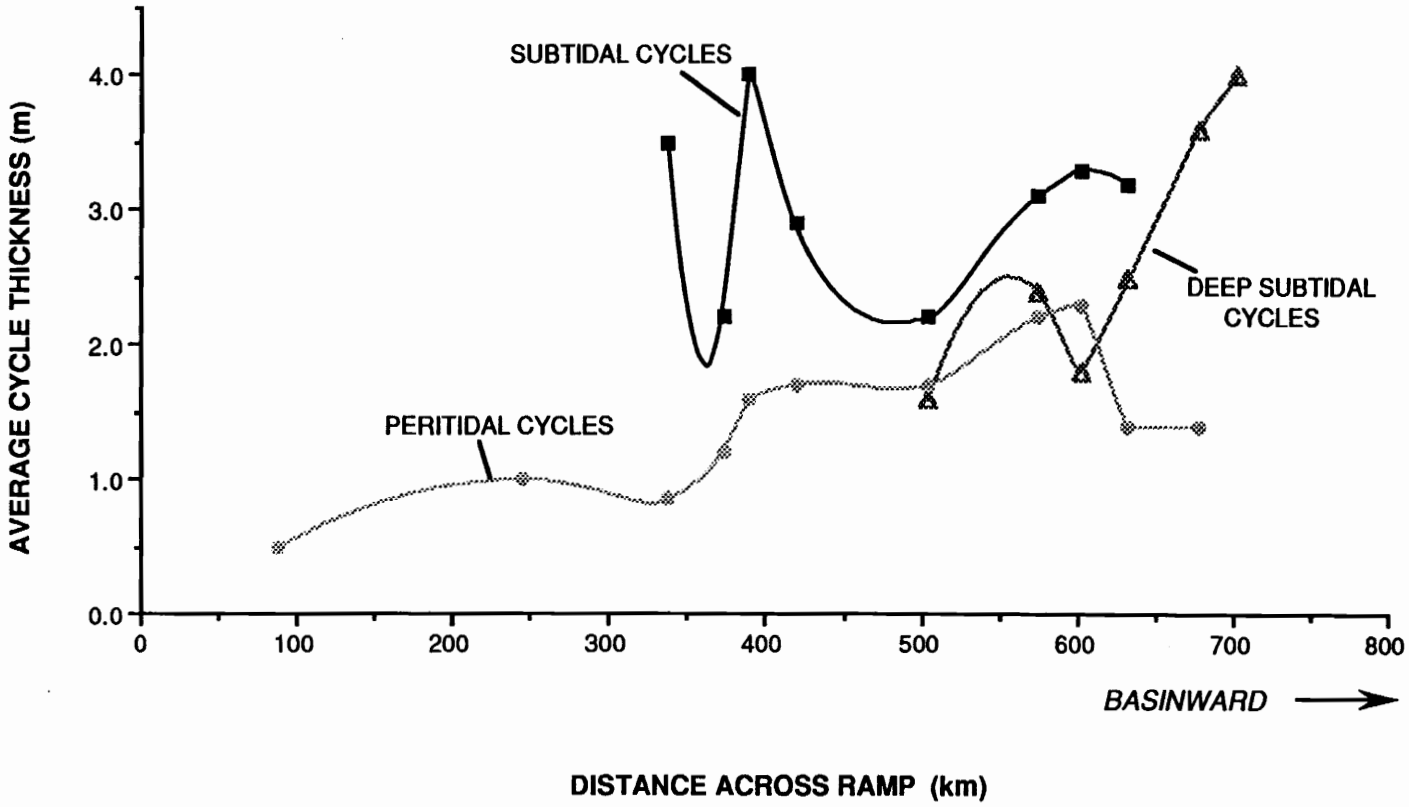
SUBTIDAL CYCLES
DEEP SUBTIDAL CYCLES
PERITIDAL CYCLES
AVERAGE CYCLE THICKNESS (m)
4.0
3.0
2.0
1.0
0.0
0
100
200
300
400
500
600
700
800
BASINWARD
DISTANCE ACROSS RAMP (km)

Figure 8.

A) Outcrop photograph of deep subtidal cycles at Dry Fork stratigraphic section (DF). Three cycles are outline with arrows. Base of cycles composed of sub-storm wave base limestone-argillite, overlain by graded limestone, and capped by skeletal-ooid grainstone.

B) Outcrop photograph of post-depositional solution collapse breccia sandwiched between undisturbed pelleted dolomite/dolosiltite.

A
B

Figure 9

A) Outcrop photograph of typical storm layers within graded limestone facies.

B) Outcrop photograph of thick laminite grading into cryptalgal laminite facies.

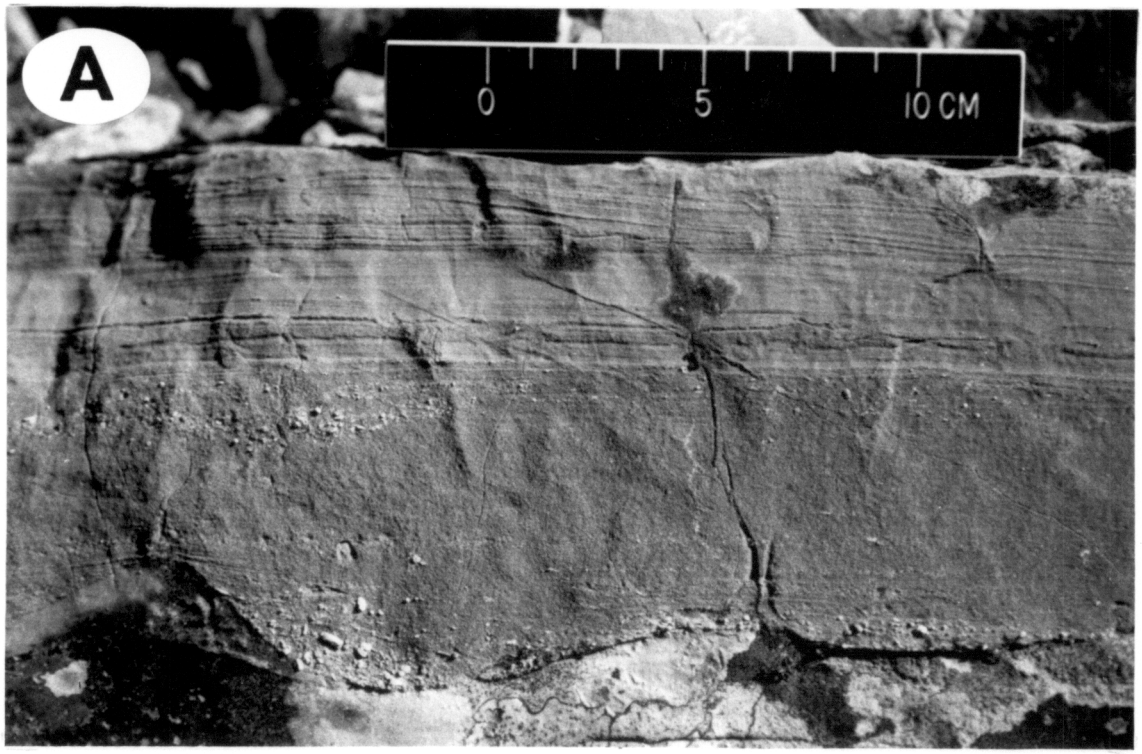
A
0
5
10 CM

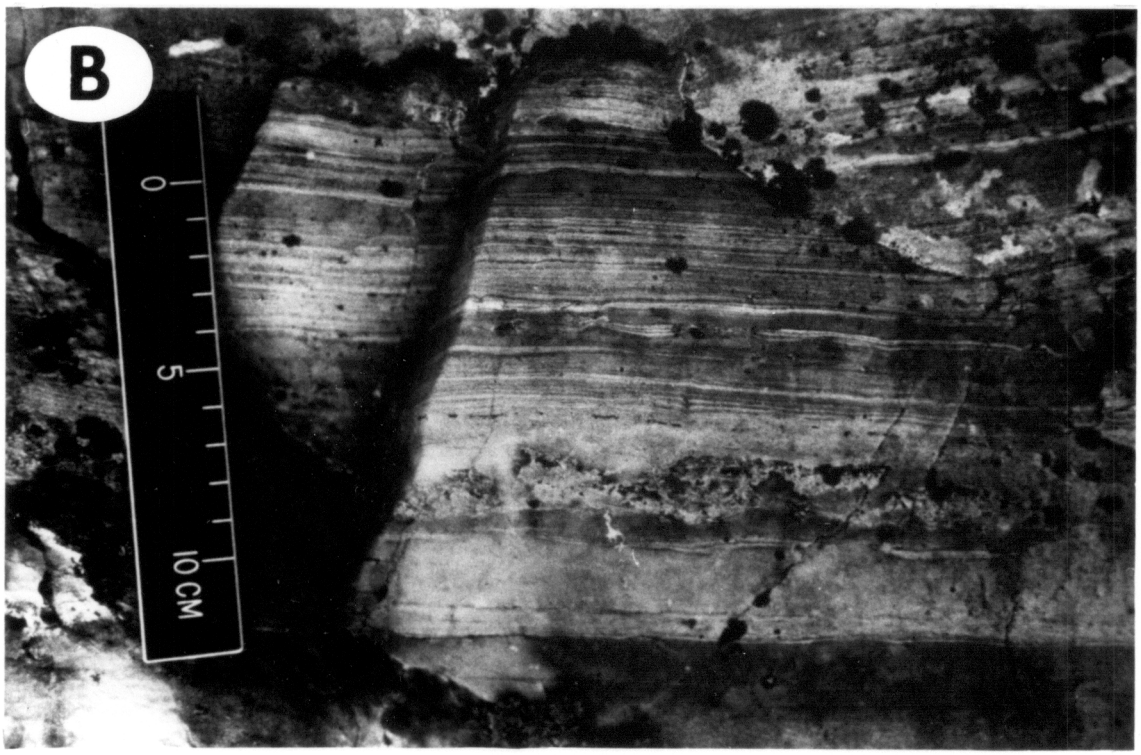
B
0
5
10 CM

water limestone-argillite are deep ramp storm deposits. Evidence for this interpretation includes graded textures, wave-ripples, and hummocky stratification (Table 1 and Fig. 9A) and by stratigraphic relationships with downslope sub-storm wave base deposits (Kriesa 1981; Walker, 1984; Handford, 1986; Aigner, 1985; Calvet and Tucker, 1988). The storm event initally eroded the sediment then redeposited it as graded (Fig. 9A), hummocky-stratified, or plane-laminated beds. During waning storm conditions, waves reworked the fine-grained material into wave-ripples (Kriesa, 1981). Laminated to burrowed lime mudstone/pellet packstone settled from suspension during fairweather conditions. The final drape of fine argillaceous limestone may represent the delayed influx of terrigenous material from storm-induced flooded rivers.

Cycles containing deep ramp storm deposits lie stratigraphically below crinoid bank and foreshoal facies, and above rhythmically bedded limestone-argillite deposits. These relationships and analogies with modern storm deposits (Aigner, 1985; Reading, 1986) suggest deposition in water depths between 20-40 m (assuming a 40m storm-wave base; Fig. 6).

Ooid-skeletal packstone/grainstone (Table 1) beds which cap some deep subtidal cycles are amalgamated proximal storm deposits that were transported downslope from ramp-margin ooid shoals. Transported ooid deposits are differentiated from *in situ* ooid shoal facies by the presence graded textures, hummocky stratification, and thin argillite interbeds and drapes. Ooid-rich grainstone caps

are most common towards the tops of depositional sequences and reflect progradation of ooid shoals towards the ramp-margin during long-term relative sea level fall. Stratigraphic relationships with adjacent facies suggest deposition in 15-25 m water depths (Fig. 6).

Hummocky-stratified and graded *skeletal packstone-grainstone* (Table 1) which cap most coarsening-upward deep subtidal cycles are amalgamated, proximal storm deposits. The paucity of ooids and the coarseness of slightly abraded, open-marine skeletal material, suggests some reworking and transport of locally derived, deep ramp material. It is unlikely each grainstone cap represents a single, large, random storm event because these cycles display gradual shallowing characteristics, and the grainstone caps are abruptly overlain by deeper water facies (Fig. 5A). Grainstone caps more likely represent multiple storm events related to shallowing during short-term sea level fall. Skeletal packstone/grainstone caps of deep subtidal cycles lie seaward of crinoidal bank deposits suggesting deposition in water depths between 20-35 m.

Foreshoal Facies

Foreshoal facies, which include intershoal (lagoonal) and interbank deposits, occur along the inner and outer ramp (Fig. 4). Rock types include noncyclic crinoidal dolowackestone (Little Bighorn Member; Fig. 4), cyclic intervals of skeletal-pellet wackestone capped by skeletal-ooid grainstone (coarsening-upward

shallow subtidal cycles; Fig. 5E), and skeletal-pellet wackestone capped by pelleted dolomite (Table 1).

Skeletal-pellet wackestone (Table 1) rich cycles lie seaward of ooid shoal deposits and commonly behind crinoidal bank facies indicating deposition in protected, slightly deeper subtidal environments. Interbedded lenses of graded skeletal debris are storm layers from adjacent crinoidal banks. Similar skeletal-pellet sands occur in 5-15 m water depths behind less restricted parts (western) of the Great Pearl Barrier of the Persian Gulf (Purser and Evans, 1973), in <10 m water depths along the interior of the Bahamas platform (Bathurst, 1975, p. 100), and 10-30 m water depths in the embayment plain of Shark Bay (Logan and Cebulski, 1970). Stratigraphic relationships with ooid shoals and crinoidal banks facies and comparisons with modern analogs suggest skeletal-pellet wackestones were deposited in water depths of 5-25 m (Fig. 6).

Crinoidal dolowackestone (Table 1) occurs seaward of ooid shoals and passes downslope into graded limestone or cherty skeletal wackestone/packstone deposits (Fig. 4). The low fossil abundance and low diversity of fauna indicate moderately restricted conditions. These stratigraphic relationships along with the paucity of wave- or current-generated features indicate deposition in protected foreshoal environments between 5-25 m water depths (Fig. 6).

Crinoidal Bank Facies

Crinoid bank facies (Table 1) occur along the outer ramp and ramp-slope (Fig. 4) and are composed of 2-15 m thick, poorly stratified crinoidal-skeletal packstone/grainstone. Cycles within the bank facies include stacked crinoid-skeletal grainstones capped by fine pelletal layers (Plate 1), or skeletal-pellet wackestone layers which coarsen-upward into crinoidal-skeletal grainstone (Fig. 5E).

The coarse packstone texture indicates mainly *in situ* skeletal accumulation that was locally reworked by waves and currents. Similar skeletal packstone/grainstone bank deposits are forming in 5-20 m water depths in Shark Bay (Hagan and Logan, 1974), the Persian Gulf (Purser, 1973) and along the seaward edge of the Pearl Barrier (Purser and Evans, 1973) and suggest the crinoidal bank facies was deposited in water depths between 5-20 m (Fig. 6).

Ooid Shoal Facies

Ooid shoal facies are composed of ooid and ooid-skeletal grainstone (Table 1) which are dolomitized on the inner ramp and are limestone along the outer ramp. Cyclic to noncyclic ooid facies are interbedded with variable amounts of coarse oolitic-intraclast grainstone, crinoidal packstone/grainstone, pelleted dolomite, and algal laminites. Three types of shallow subtidal cycles (0.5-9.0 m thick; Fig. 7) occur within the ooid shoal facies. Stacked ooid grainstone cycles are the most common type of cycle. They are

composed of cross-bedded, ooid-skeletal/oolitic intraclast grainstone which grades upward into plane-laminated or rarely herringbone cross-bedded ooid grainstone (Fig. 5B), or massive oolitic intraclast grainstone overlain by cross-bedded ooid grainstone (Fig. 5C). Fining-upward shallow subtidal cycles are characterized by cross-bedded, ooid-skeletal grainstone overlain by thin, poorly laminated, pelleted dolomite (Fig. 5D). These cycles are most common along the lateral edges of ooid shoal facies (sections CF, SH, B, and WR; Figs. 2 and 4). Coarsening-upward shallow subtidal cycles include skeletal-pellet wackestone which grades upward into ooid-skeletal grainstone (Fig. 5E). These cycles are most common along the seaward edge of the ooid shoal complex.

Ooid-skeletal grainstones (Table 1) were deposited in high energy, fringing and barrier shoal complexes. Fringing shoals passed landward into tidal flats; barrier shoals were separated from tidal flats by restricted lagoons. Coarse oolitic-intraclast grainstones are reworked clasts of early submarine cemented ooids and peloids from more inactive parts of the shoals (Harris, 1979; Hine *et al.*, 1981).

Shoals and bars composed of clean ooid sands are forming in the Persian Gulf (Loreau and Purser, 1973), the Bahamas (Ball, 1967; Harris, 1979; Hine *et al.*, 1981; Lloyd *et al.*, 1987), and Shark Bay (Hagan and Logan, 1974) in water depths less than 5 m; similar water depths are suggested ooid-skeletal grainstone shoal facies (Fig. 6).

In modern ooid shoal and beach deposits, and likely the same for ancient deposits, the width of active ooid formation is controlled by local bathymetry and energy regimes (Harris, 1979; Handford, 1986). Ooid shoals/tidal bars in the Bahamas and the Persian Gulf are less than 5-10 km wide and may be several tens of kilometers long (Ball, 1967; Purser and Evans, 1973; Bathurst, 1975; Hine, 1977; Harris, 1979). Ancient ooid shoal deposits commonly occur as broad stratigraphic belts tens to several hundreds of kilometers wide (Middle Jurassic of the Paris Basin, Upper Jurassic Smackover Formation of the Gulf Coast, and the Mississippian of Illinois Basin; in Wilson, 1975; and this study), indicating that active shoals coalesced and amalgamated during progradation to produce broad, sheet-like bodies.

Peritidal Facies

Peritidal facies occur along the inner ramp and locally within ooid grainstone facies (Fig. 4). Rock types include cyclic units of ooid grainstone, pelleted dolomite/dolosiltite, algal laminite, and thin paleosol (fine-grained red dolomite) and breccia layers (Table 1). Peritidal cycles (0.3-5 m thick; Fig. 7) may include a thin ooid grainstone base, overlain by pelleted dolomite or thick laminite, which grades into cryptalgal laminite and is rarely capped by a paleosol/breccia horizon (Fig. 5F).

Pelleted dolomite/dolosiltite (Table 1) was deposited in shallow subtidal lagoons behind ooid shoals and in ooid foreshoal

settings. Lagoonal facies are distinguished from foreshoal deposits by their stratigraphic position above ooid grainstones and below algal laminites (Fig. 5F). Thin interbeds (<5 cm) of algal laminites indicate the lagoons periodically shallowed to tidal levels. The paucity of skeletal material in both lagoonal and foreshoal facies indicates restricted conditions or elevated salinities, although there was abundant infaunal burrowing which obliterated most primary textures. In the Persian Gulf, similar poorly fossiliferous pellet sands occur in shallow (<5 m), hypersaline lagoons behind the Great Pearl Barrier (Purser and Evans, 1973); similar water depths are suggested for the pelleted dolomite facies (Fig. 6).

Thick laminites (Table 1) formed in lower intertidal flat environments where storm and tidal currents transported subtidal-derived material onto the flats and deposited the material as centimeter-thick, landward-thinning, graded layers.

Cryptalgal laminites (Table 1; Fig. 9B) were deposited in upper intertidal flat environments and reflect aggradation of the inner ramp to sea level. The gradation from centimeter- to millimeter-thick laminations in thick laminite to cryptalgal laminite facies reflects tidal flat progradation and increasing distances from subtidal source areas. Millimeter-thick laminations formed by algal-binding of thin storm layers (Fig. 9B; Hardie and Ginsburg, 1977; James, 1984). Silicified evaporite nodules, interbedded solution-collapse breccias, and the lack of bioturbation indicate an arid to semi-arid climate.

Figure 10. Depositional sequence 1 (decompacted thickness). The cross-section is oriented SW-NE to facilitate comparison with computer models. Location of measured sections shown by columns with horizontal lines indicating cycle tops. Vertical lines indicate location of portions of detailed measured sections in Figure 16. Note foreshoal facies extend into the inner ramp (probable maximum flooding surface) and are overlain by highly progradational ooid shoal and peritidal facies.

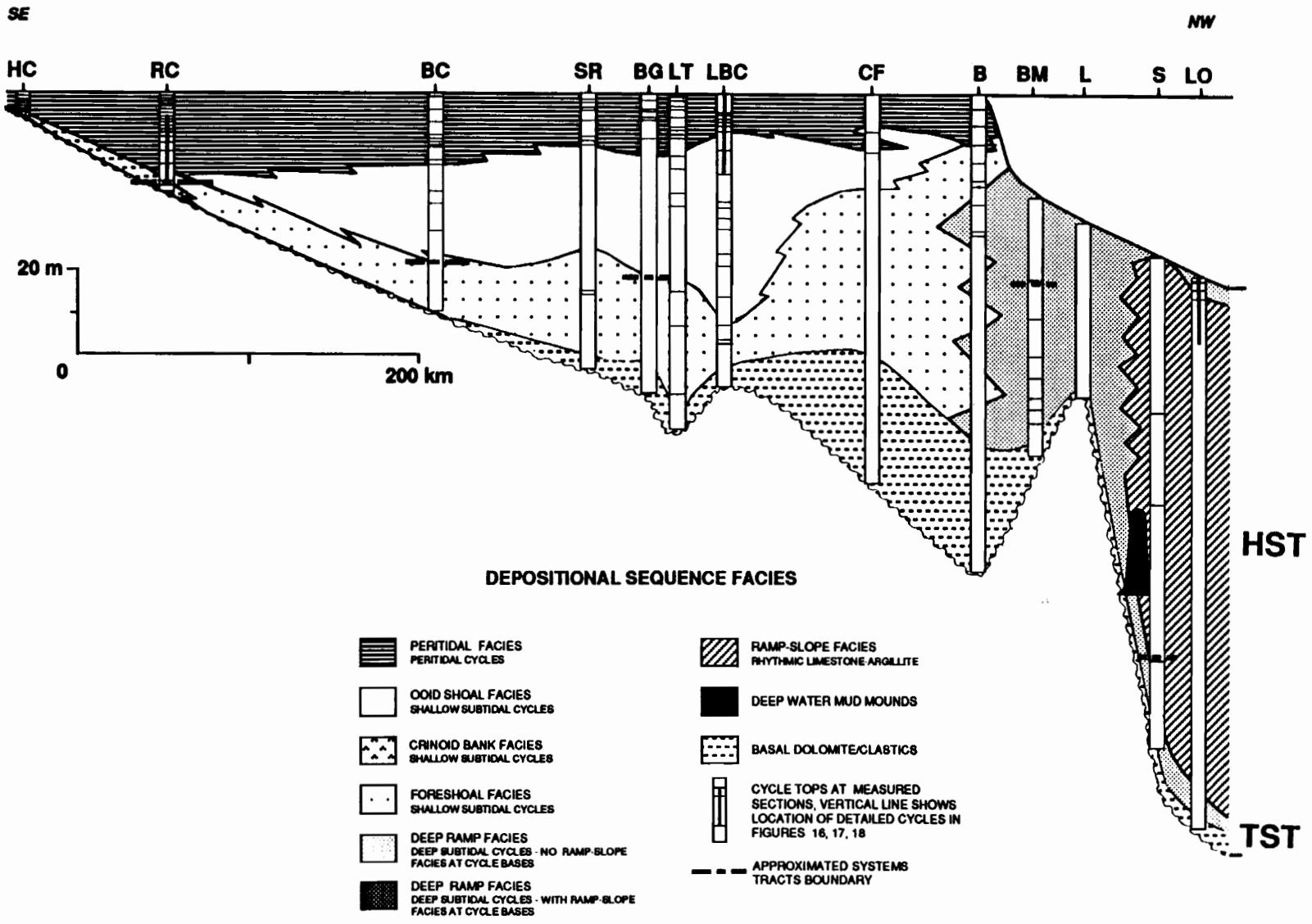
SE
NW
HC
RC
BC
SR
BG LT
LBC
CF
B
BM
L
S
LO
20 m
0
200 km
HST
TST
DEPOSITIONAL SEQUENCE FACIES
PERITIDAL FACIES
PERITIDAL CYCLES
OOID SHOAL FACIES
SHALLOW SUBTIDAL CYCLES
CRINOID BANK FACIES
SHALLOW SUBTIDAL CYCLES
FORESHOAL FACIES
SHALLOW SUBTIDAL CYCLES
DEEP RAMP FACIES
DEEP SUBTIDAL CYCLES - NO RAMP-SLOPE FACIES AT CYCLE BASES
DEEP RAMP FACIES
DEEP SUBTIDAL CYCLES - WITH RAMP-SLOPE FACIES AT CYCLE BASES
RAMP-SLOPE FACIES
RHYTHMIC LIMESTONE-ARGILLITE
DEEP WATER MUD MOUNDS
BASAL DOLOMITE/CLASTICS
CYCLE TOPS AT MEASURED SECTIONS, VERTICAL LINE SHOWS LOCATION OF DETAILED CYCLES IN FIGURES 16, 17, 18
APPROXIMATED SYSTEMS TRACTS BOUNDARY

Collapse breccias/regoliths. Solution collapse breccias (Table 1) formed by the removal of interbedded evaporites or carbonates (Middleton, 1961). Post-depositional brecciation is evident by the occurrence bedding-parallel breccia beds between undisturbed laminite or dolosiltite layers (Fig. 8B). Regolith breccias (Table 1) formed by incipient brecciation of tidal flat deposits during subaerial exposure (syn-depositional brecciation). They are distinguished from solution breccias by their irregular top surfaces which are commonly infilled by overlying facies.

Fine-grained red dolomite. Mottled, iron-stained dolomite (Table 1) occurs at the top of mudcracked tidal flat deposits and represent paleosol layers. They likely formed during periods of prolonged subaerial exposure following long-term sea level fall.

Basal Dolomite/Siliciclastics

Dolomite and fine-grained siliciclastics of the Cottonwood Canyon Member and Englewood Formation (Table 1) blanket the underlying Devonian-Early Mississippian unconformity (Figs. 4 and 10) and are composed of dark shale, siltstone and dolomite along the ramp-slope and outer ramp, and quartz sandstone/siltstone along the inner ramp.

The dark shales and siltstones of the Cottonwood Canyon Member were deposited in relatively deep, anoxic marine waters during the initial flooding of the ramp. Conodont and fish remains suggest that an oxygenated zone existed above the anoxic bottom

waters (Hayes, 1985). Suppressed sedimentation is indicated by its stratigraphic thickness (<15 m) versus estimated age range between 1-1.5 m.y. (Sandberg and Klapper, 1967; Gutschick *et al.*, 1980; Sando, 1985), by the occurrence of glauconite and phosphate grains, and by the abundance of conodonts (Sandberg and Klapper, 1967). The upper tongue of the Cottonwood Canyon is time-equivalent to the upper Bakken, Exshaw, and Leatham formations of North Dakota, southern Alberta, and Utah, respectively (Sandberg and Klapper, 1967; Hayes, 1985). These time-equivalent facies are also interpreted as relatively deep marine deposits. Bioturbated silty dolomite and dolomite of the inner ramp was deposited in well-oxygenated shallow subtidal waters.

Quartz sandstone and siltstone of the Englewood Formation (Table 1), which contains common herringbone stratification, channel scours, and flaser bedding indicating deposition in a variety of peritidal areas including tidal channels, silty tidal flats, and shallow subtidal environments.

REGIONAL FACIES RELATIONSHIPS AND SEQUENCE STRATIGRAPHY

The various meter-scale cycles within the Mississippian deposits are stacked to form three depositional sequences (Fig. 4) which are recognized by regional transgressive-regressive facies trends. Noncyclic intervals occur locally, particularly within ooid

shoal and foreshoal facies that were deposited during the transgressive phases of sequence deposition. The regional facies distributions are analyzed in an attempt to related them to sequence stratigraphic concepts and terminology, and to critically assess the ease or difficulty of defining them on the basis of lithologic rather than seismic criteria. A brief definition of sequence stratigraphic terminology is given here; detailed concepts, descriptions, and examples are given by Vail *et al.,* (1977), Haq *et al.,* (1988), Sarg (1988), and Van Wagoner *et al.,* (1988).

A depositional sequence is a relatively conformable succession of genetically related strata bounded by unconformities or their correlative conformities (Vail *et al.,* 1977, Van Wagoner *et al.,* 1988). Sequences can be subdivided into systems tracts which are genetically related intervals of strata that are interpreted to have formed during specific, though not unique, increments of a eustatic sea level cycle. Systems tracts are defined by their position within a sequence, the types of bounding surfaces, and internal stratal geometries (Van Wagoner *et al.,* 1988; Sarg, 1988).

The basal systems tract that overlies a type 2 sequence boundary (Van Wagoner *et al.,* 1988) is the shelf margin or ramp margin wedge (RMW). The RMW is characterized by weakly progradational to aggradational deposition. Strata onlaps onto the sequence boundary in a landward direction and downlaps the sequence boundary in a seaward direction; the upper boundary of the RMW is the transgressive surface (Sarg, 1988). The overlying

transgressive systems tract (TST) is characterized by retrogradational deposition, with strata onlapping the sequence boundary in a landward direction and downlapping the transgressive surface in a seaward direction (Sarg, 1988). The upper boundary of the TST is the maximum flooding surface (MFS) or downlap surface (on seismic profiles). This boundary marks the change from retrogradational to aggradational/progradational deposition. The highstand systems tract (HST) is the uppermost systems tract which is characterized by aggradational to progradational deposition. Strata within the HST onlap onto the sequence boundary in a landward direction and downlap onto the TST or RMW; the HST bounded at the top by the sequence boundary (Van Wagoner *et al.*, 1988).

Depositional Sequence 1

The present thickness of depositional sequence is 4-85 m thick (decompacted thickness of 5-135 m is shown in Figure 10). The lowstand wedge of sequence 1 does not occur within the study area, however deposits spanning the duration of the Devonian-Early Mississippian unconformity occur in central and western Utah (*cf.* Gutschick *et al.*, 1980).

The basal part of sequence 1 consists of a condensed interval of fine-grained siliciclastics and silty dolomite along the ramp-slope and outer ramp (Cottonwood Canyon Member) with quartz sandstone/siltstone along the inner ramp (Englewood Formation;

Figure 11. Depositional sequence 2 (decompacted thickness). Symbols the same as Figure 10. Vertical lines indicate location of portions of detailed measured sections in Figure 17. Note deep ramp facies onlap only onto the outer ramp, and bulk of the ramp is composed of ooid-dominated shallow subtidal cycles with peritidal cycles restricted to the innermost ramp. Crinoidal banks along outer ramp likely represent short-term progradational/lowstand events occuring during HST deposition. Also note the darker stippled pattern along the ramp-slope includes deep subtidal cycles with sub-storm wave base facies.

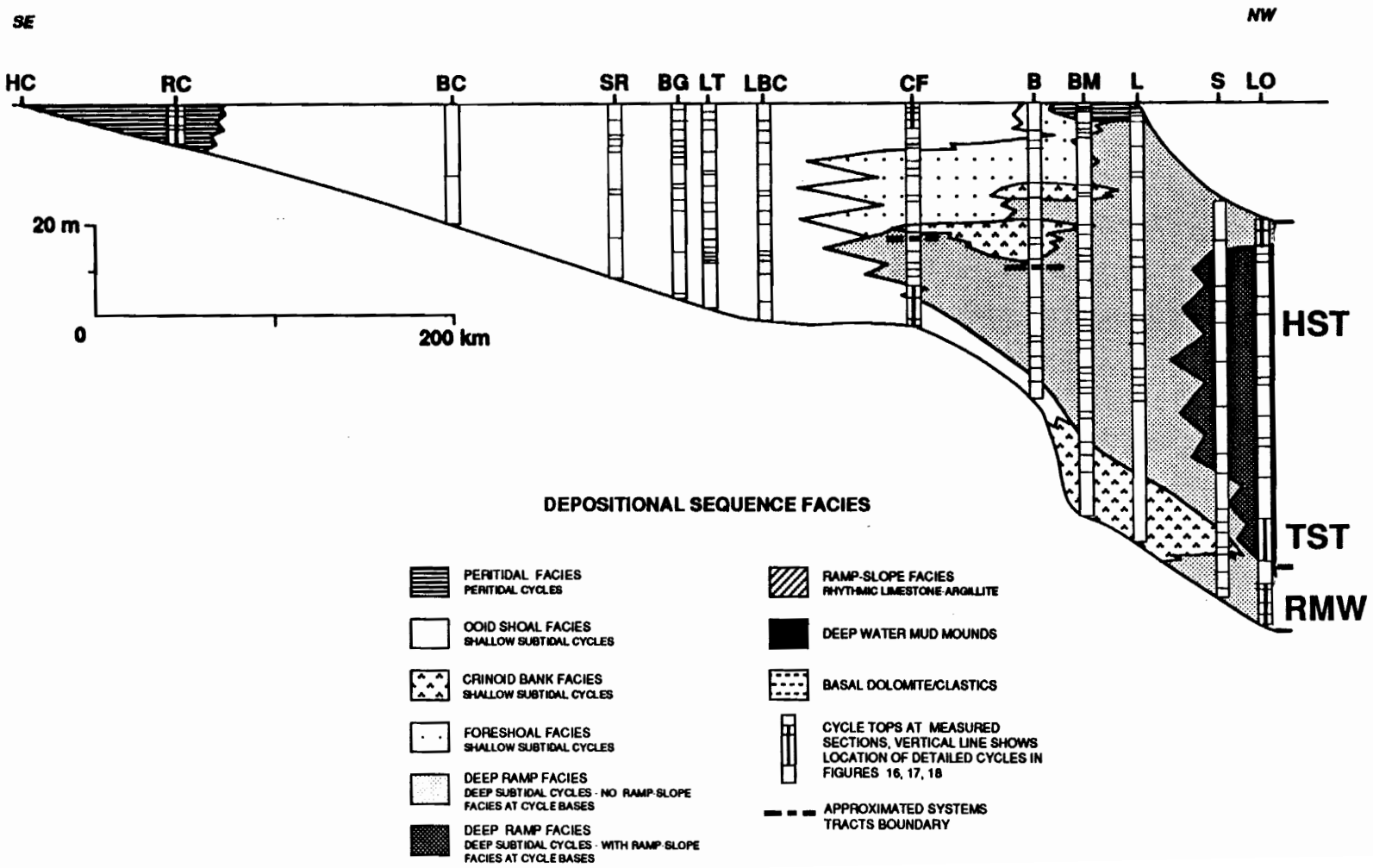
SE
NW
HC
RC
BC
SR
BG
LT
LBC
CF
B
BM
L
S
LO
20 m
0
200 km
HST
TST
RMW
DEPOSITIONAL SEQUENCE FACIES
PERITIDAL FACIES
PERITIDAL CYCLES
OOID SHOAL FACIES
SHALLOW SUBTIDAL CYCLES
CRINOID BANK FACIES
SHALLOW SUBTIDAL CYCLES
FORESHOAL FACIES
SHALLOW SUBTIDAL CYCLES
DEEP RAMP FACIES
DEEP SUBTIDAL CYCLES - NO RAMP-SLOPE FACIES AT CYCLE BASES
DEEP RAMP FACIES
DEEP SUBTIDAL CYCLES - WITH RAMP-SLOPE FACIES AT CYCLE BASES
RAMP-SLOPE FACIES
RHYTHMIC LIMESTONE-ARGILLITE
DEEP WATER MUD MOUNDS
BASAL DOLOMITE/CLASTICS
CYCLE TOPS AT MEASURED SECTIONS, VERTICAL LINE SHOWS LOCATION OF DETAILED CYCLES IN FIGURES 16, 17, 18
APPROXIMATED SYSTEMS TRACTS BOUNDARY

Fig. 4). Considerable relief on the underlying unconformity is indicated by the variable thickness of the Cottonwood Canyon Member and overlying carbonate deposits (Figs. 4 and 10). Much of the ramp thickening occurs landward of an outer ramp high on the unconformity surface at section L (Fig. 10). The basal siliciclastics and dolomite are overlain by a thin interval (3-10 m) of cherty skeletal limestone on the ramp-slope. These are overlain by a thick interval (70-79 m) of rhythmic limestone-argillite deposits with local deep-water mud mounds. The rhythmites pass landward, with a steep facies boundary, into deep ramp cherty skeletal limestone. These pass landward into noncyclic crinoidal dolowackestone foreshoal facies, then into prograding ooid shoal deposits (Fig. 10). Ooid shoal deposits contain stacked grainstone cycles that typically lack tidal flat caps. Ooid shoal facies are overlain by prograding peritidal facies (at least 300 km of seaward progradation; sections BC to B; Fig. 4). Contacts between foreshoal and overlying ooid shoal and peritidal facies are highly progradational (Fig 10). Peritidal facies pass downslope into cyclic deep ramp deposits along the outer ramp and ramp-slope.

The boundary between TST and HST deposition (maximum flooding surface; MFS) is difficult to define. It likely coincides with the most inland extent of foreshoal facies (section RC; Fig. 10 and Plate 1) and along the middle ramp where predominant retrogradational foreshoal deposition changes to strongly progradational ooid shoal deposition. The MFS may be expressed

along the outer ramp (section BM) where a thick succession of burrowed, cherty skeletal wackestone/packstone is abruptly overlain by finely laminated, dark, unfossiliferous limestone-argillite (Plate 1). Along the ramp-slope (section S), the MFS may occur at the base of the 1st or 2nd shallowing-upward subsequence, where medium-bedded, burrowed bryozoan wackestone is abruptly overlain by dark, thin-bedded, unfossiliferous limestone-argillite (Plate 1 and Fig. 10).

This possible TST to HST boundary suggests the basal shale and siltstone (Cottonwood Canyon Member) and most of the foreshoal facies (Little Bighorn Member) compose the TST, while the overlying rhythmic limestone-argillite, ooid shoal, and peritidal facies compose the HST. The TST is, therefore, approximately one-third to less than one-half the thickness of the sequence.

Sequence boundary 1, along the ramp-slope (base of overlying RMW), is difficult to define without continuous outcrop exposure or seismic data to define stratal geometries or time lines. It is arbitrarily placed at the base of the thick (15 m) crinoidal bank at sections BM and L, and along the ramp-slope where rhythmic limestone-argillite facies grade up-section into cyclic deep ramp deposits (top of first deep subtidal cycle at sections LO and S; Plate 1). Along the outer and inner ramp, the sequence boundary is defined by abrupt deepening from peritidal facies up into ooid grainstone deposits (Fig. 4 and Plate 1). There is no evidence of significant erosion along the sequence boundary (type 2 sequence boundary),

however several closely spaced paleosol layers indicate prolonged subaerial exposure (section RC; Plate 1)

Depositional Sequence 2

Although sequence boundary 2 is not recognized along the inner ramp (Fig. 4), sequence 2 is likely less than 10 m thick along the inner ramp increasing to 73 m along the ramp-slope (decompacted thickness between <10-115 m; Fig. 11). By defining the base of the ramp margin wedge (RMW) at the base of the thick crinoid bank deposits (discussed above) the RMW is 14-17 m thick and over 100 km wide (Figs. 3 and 11) and is composed of crinoidal packstone/grainstone bank facies which passes downdip into crinoidal or oolitic grainstone-capped deep subtidal cycles (Fig. 11 and Plate 1). The transgressive surface (RMW to TST boundary) at the top of the RMW is recognized by a distinct deepening above bank facies into overlying sub-storm wave base limestone-argillite or cyclic deep ramp facies (Fig. 11 and Plate 1).

Cyclic deep ramp deposits of the TST onlapped over 175 km onto the ramp during the transgression (Fig. 4). These deep ramp deposits pass landward into thick cyclic oolitic shoal deposits which are bordered on the inner ramp by a narrow peritidal facies belt. Oolitic facies become highly progradational towards the top of the sequence, passing downslope into local crinoidal bank facies, then into cyclic deep ramp deposits (Fig. 11). The two outer ramp

Figure 12. Deposition sequence 3 (decompacted thickness). Symbols the same as Figure 10. Vertical lines indicate location of portions of detailed measured sections in Figure 18. Note two ooid shoal facies belts- fringing shoals along the inner ramp and barrier shoals along the ramp-margin, and the strongly progradational peritidal facies of the late HST. Also note the darker stippled pattern along the ramp-slope includes deep subtidal cycles with sub-storm wave base facies.

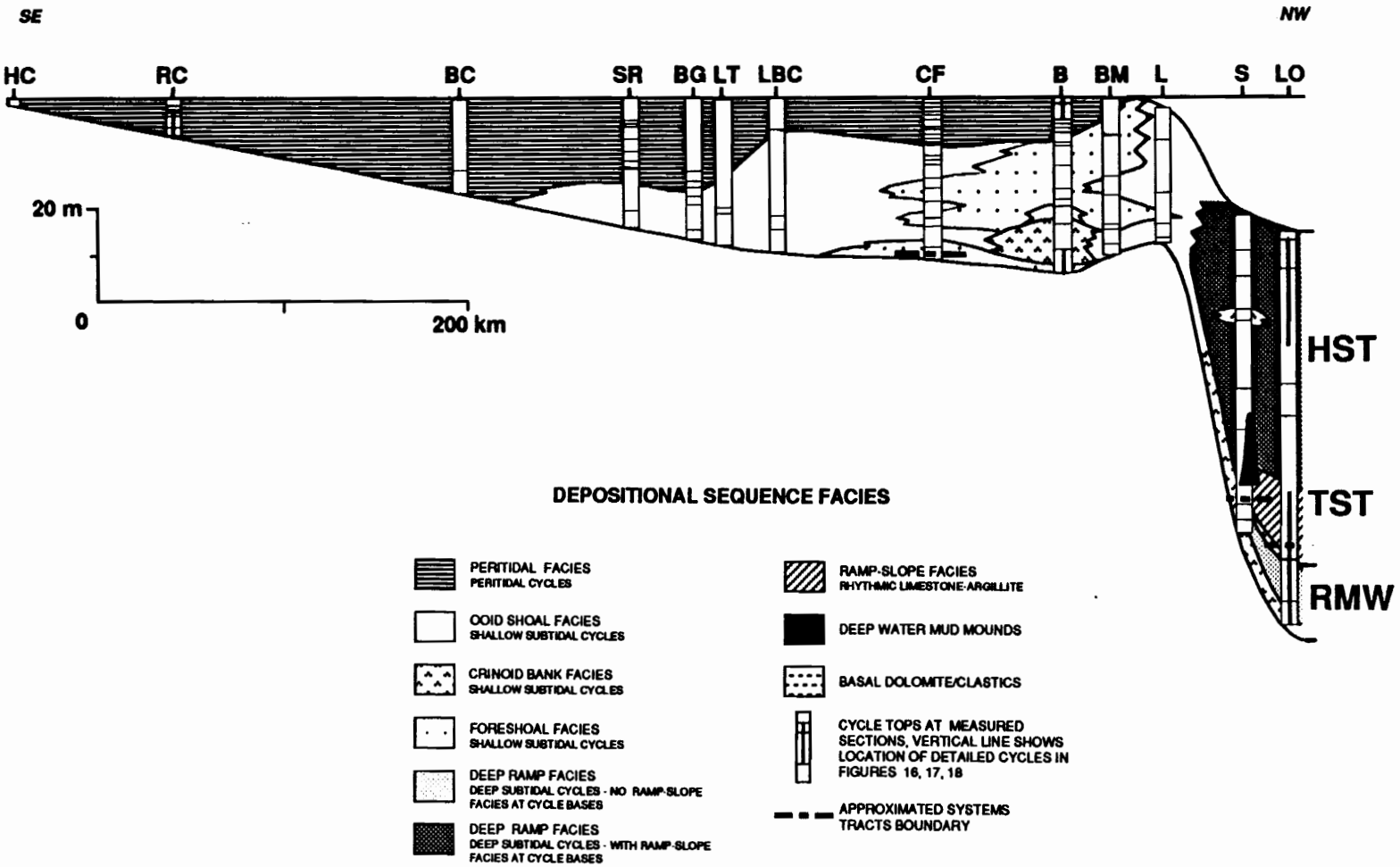
SE
NW
HC
RC
BC
SR
BG
LT
LBC
CF
B
BM
L
S
LO
20 m
0
200 km
HST
TST
RMW
DEPOSITIONAL SEQUENCE FACIES
PERITIDAL FACIES
PERITIDAL CYCLES
OOID SHOAL FACIES
SHALLOW SUBTIDAL CYCLES
CRINOID BANK FACIES
SHALLOW SUBTIDAL CYCLES
FORESHOAL FACIES
SHALLOW SUBTIDAL CYCLES
DEEP RAMP FACIES
DEEP SUBTIDAL CYCLES - NO RAMP-SLOPE FACIES AT CYCLE BASES
DEEP RAMP FACIES
DEEP SUBTIDAL CYCLES - WITH RAMP-SLOPE FACIES AT CYCLE BASES
RAMP-SLOPE FACIES
RHYTHMIC LIMESTONE-ARGILLITE
DEEP WATER MUD MOUNDS
BASAL DOLOMITE/CLASTICS
CYCLE TOPS AT MEASURED SECTIONS, VERTICAL LINE SHOWS LOCATION OF DETAILED CYCLES IN FIGURES 16, 17, 18
APPROXIMATED SYSTEMS TRACTS BOUNDARY

crinoidal banks likely reflect short-term progradational/lowstand events.

The MFS is not recognized along the inner and middle ramp because there is no lithologic change or 5th order cycle stacking pattern change that would indicate retrogradational/aggradational to progradational deposition. However, along the outer ramp, the MFS may occur where predominantly aggradational deep ramp deposition changes to progradational foreshoal and crinoidal bank deposition (sections CF, and B; Fig. 11 and Plate 1). Along the ramp-slope, the MFS cannot be distinguished from any of the deepening events related to 5th order sea level rises. The possible MFS recognized along the outer ramp suggests the TST is approximately one-half the thickness of the sequence.

Sequence boundary 2 is not evident along the middle ramp because there is no distinct lithologic break within ooid-dominated cycles (Fig. 4). However, several closely spaced paleosol/breccia layers at sections RC on the inner ramp may mark the sequence boundary (type 2 sequence boundary; Plate 1). Along the outer ramp, the sequence boundary is recognized where thin peritidal cycles at sections BM and L are abruptly overlain by oolitic grainstone, and at sections B and CF where oolitic grainstone passes upward into thick crinoidal bank facies (Plate 1). Along the ramp-slope, the sequence boundary (base of overlying RMW) is poorly defined. It may lie within or below the interval of stacked crinoidal bank facies and thick ooid-crinoid grainstone capped deep subtidal cycles (Plate 1).

It is arbitrarily placed at the base of the bank facies (section S) and at the base of the thickest ooid grainstone-capped deep subtidal cycle at section LO (Plate 1).

Depositional Sequence 3

Depositional sequence 3 is less than 5 m thick along the inner ramp and 65 m thick along the ramp-slope (<5-85 m decompacted thickness; Fig. 12). The basal RMW is approximately 10-17 m thick and over 45 km wide, although its lower boundary is arbitrarily defined (Fig. 12 and Plate 1). The RMW is composed of stacked crinoidal and oolitic bank cycles that pass downslope into deep subtidal cycles (Fig. 12). A well-defined transgressive surface separates cyclic crinoidal-oolitic bank facies of the RMW from the overlying rhythmic limestone-argillite and cyclic deep ramp facies (Fig. 12). At section S, an isolated deep-water mud mound lies on the transgressive surface (Figs. 4 and 12).

The RMW is overlain by a succession of rhythmic limestone-argillite which is in turn overlain very thick deep subtidal cycles which have thin to absent grainstone caps (Fig. 18 and Plate 1). Along the outer ramp, transgressive deposits are composed of cyclic ooid shoal, crinoidal bank, and foreshoal facies. These pass landward into cyclic oolitic grainstone which are overlain by highly progradational peritidal facies (at least 175 km of seaward progradation; Fig. 12). In the upper part of the sequence, the pertidal

Figure 12. Deposition sequence 3 (decompacted thickness). Symbols the same as Figure 10. Vertical lines indicate location of portions of detailed measured sections in Figure 18. Note two ooid shoal facies belts- fringing shoals along the inner ramp and barrier shoals along the ramp-margin, and the strongly progradational peritidal facies of the late HST. Also note the darker stippled pattern along the ramp-slope includes deep subtidal cycles with sub-storm wave base facies.

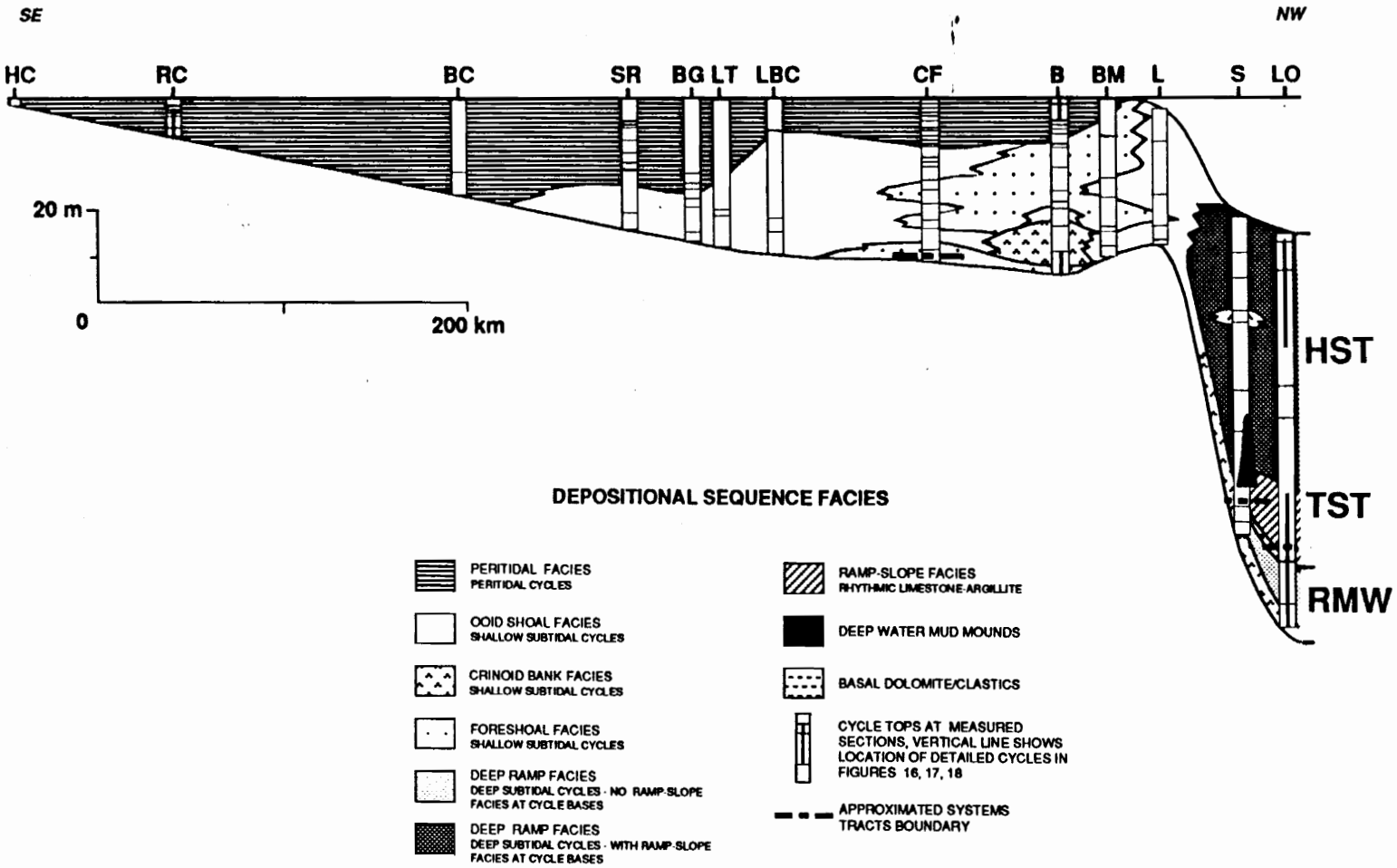
SE
NW
HC
RC
BC
SR
BG
LT
LBC
CF
B
BM
L
S
LO
20 m
0
200 km
HST
TST
RMW
DEPOSITIONAL SEQUENCE FACIES
PERITIDAL FACIES
PERITIDAL CYCLES
OOID SHOAL FACIES
SHALLOW SUBTIDAL CYCLES
CRINOID BANK FACIES
SHALLOW SUBTIDAL CYCLES
FORESHOAL FACIES
SHALLOW SUBTIDAL CYCLES
DEEP RAMP FACIES
DEEP SUBTIDAL CYCLES - NO RAMP-SLOPE FACIES AT CYCLE BASES
DEEP RAMP FACIES
DEEP SUBTIDAL CYCLES - WITH RAMP-SLOPE FACIES AT CYCLE BASES
RAMP-SLOPE FACIES
RHYTHMIC LIMESTONE-ARGILLITE
DEEP WATER MUD MOUNDS
BASAL DOLOMITE/CLASTICS
CYCLE TOPS AT MEASURED SECTIONS, VERTICAL LINE SHOWS LOCATION OF DETAILED CYCLES IN FIGURES 16, 17, 18
APPROXIMATED SYSTEMS TRACTS BOUNDARY

facies grade into a narrow region of foreshoal (lagoonal) facies, then into a thick interval of cyclic ramp-margin ooid shoal deposits.

The MFS along the ramp-slope likely occurs within the thick (15 m) interval of rhythmic limestone-argillite facies towards the base of the sequence (Fig. 4 and Plate 1). The boundary may be represented by the most landward occurrence of foreshoal (lagoonal) and ooid shoal facies at the base of the sequence (Fig. 12). Above this point, peritidal, ooid shoal, and foreshore deposition is aggradational to progradational. This boundaries suggests the TST is less than one-half the thickness of the sequence.

Sequence boundary 3 is defined along most of the ramp by the abrupt change from peritidal deposits up into ooid shoal deposits of the Mission Canyon/Upper Madison Formations (Plate 1). Along the ramp-slope, the sequence boundary is arbitrarily placed at the base of a thick (>15 m) interval of peloidal-crinoidal bank and oolitic shoal deposits at sections LO and S (RMW of overlying sequence in the Mission Canyon Formation).

ORIGIN OF SHALLOWING-UPWARD CYCLES

The possible origins of meter-scale, shallowing-upward cycles has been reviewed by numerous workers including Wilkinson (1982), James (1984), Grotzinger (1986), Wright (1986), and Koerschner and Read (1989). Briefly those mechanisms include: 1) autocyclic processes (Ginsburg, 1971; Pratt and James, 1988; Cloyd *et al.*,

1990), 2) repeated fault movements or "yo-yo" tectonics (Cisne, 1986; Atwater, 1986), and 3) eustatic sea level fluctuations (Aigner, 1985; Goodwin and Anderson, 1985; Heckel, 1986; Read *et al.,* 1986; Bova and Read, 1987; Goldhammer *et al.,* 1987; Strasser, 1988; Goldhammer and Harris, 1989; Koerschner and Read, 1989).

Autocyclic models involve mechanisms which control the rate of carbonate production in the subtidal "carbonate factory". As tidal flats prograde seaward, the area of the factory is reduced, sediment production decreases, and eventually the factory is too small in area to provide sediment to the tidal flats. At this point, sedimentation ceases and does not restart until the platform subsides to subtidal water depths (Ginsburg, 1971; Wong and Oldershaw, 1980; Wilkinson, 1982; James, 1984). The lack of tidal flat caps in the majority of Lower Mississippian cycles precludes their formation by these autocyclic mechanisms.

Repeated downdrop and uplift of the carbonate ramp ("yo-yo" tectonics) might explain the shallowing-upward cycles (Cisne, 1986; Atwater, 1986), although it is unlikely the cratonic ramp could downdrop and uplift at the frequency and consistent magnitude (1-4 m average range of cycle thickness; Fig. 7) required to form the cycles. Also, the repeated tectonic movements would have to have affected the entire ramp (>700 km) as a block to explain the correlation of depositional sequences across the ramp-to-basin transition.

The most simple and actualistic mechanism for generating meter-scale, shallowing-upward cycles is eustatic sea level fluctuations. Sea level oscillations with periods ≈20 k.y., 41 k.y., 100 k.y., and 400 k.y. are well-documented throughout the Quaternary (Hays *et al.,* 1976) and Tertiary (Matthews and Poore, 1980) are attributed to climatically forced fluctuations in glacier growth and decay (Hays *et al.,* 1976). Periods similar to Quaternary climatic changes (20-100 k.y.) have been recorded as far back as the Triassic (Olsen, 1986), Permian (Anderson, 1982), and the Middle Cambrian (Kominz and Bond, 1989 and pers. comm.). A glacio-eustatic origin for the Lodgepole/lower Madison cycles is supported by the paleogeographic position of Gondwana across polar and high latitudes during Mississippian time (Crowell, 1978; Veevers and Powell, 1987; Scotese *et al.,* 1979; Ziegler *et al.,* 1979; Witzke, 1990) and by the occurrence of Latest Devonian (≈360-367 m.y.) and Early Mississippian (≈352 m.y.) marine and nonmarine glacial deposits in South America (Veevers and Powell, 1987).

Considering the combination of geologic data, including paleosol/regolith-capped peritidal cycles, the dominance of subtidal cycles which lack tidal flat caps, and the 30-110 k.y. range of average cycle periods (discussed below), the Mississippian shallowing-upward cycles are interpreted to have formed by short-term (5th order) sea level fluctuations.

The ramp-to-basin distribution of shallowing-upward cycles is a function of accommodation space, which includes depositional

space generated by subsidence, sea level fluctuations, and initial water depths due to slope. During short-term (5th order: <100 k.y.) sea level rises, the inner ramp was only flooded to intertidal and very shallow subtidal water depths because of the low subsidence rates and initial water depths. As a result, tidal flat, lagoonal, or ooid shoal facies were deposited. Along the middle ramp, where accommodation was greater and deposition was influenced by fairweather wave-reworking, ooid and skeletal grainstone facies were deposited. Along the outer ramp, below fairweather wave base, foreshoal and graded limestone facies were deposited, while along the ramp-slope sub-storm wave base facies were deposited because of the greater initial water depths and subsidence rates.

During the short-term sea level highstands and falls, tidal flat facies along the inner ramp became exposed and were partially eroded. Along parts of the middle ramp, shallow subtidal facies were overlain by prograding tidal flats or lagoonal deposits. The absence of tidal flat-caps along the outer ramp indicates that tidal flat progradation did not keep pace with short-term sea level fall rates, or tidal flat nucleation was inhibited due to the high-energy conditions associated with the ooid shoals. As a result, cycles within these amalgamated shoal facies are often difficult to recognize. Water depths remained deep along the ramp-slope because of the steeper slopes and faster subsidence rates, consequently deeper subtidal facies were capped by prograding skeletal-ooid grainstone or by local storm-reworked facies.

COMPUTER MODELLING PARAMETERS

The Lower Mississippian sequences were numerically modeled to more quantitatively understand the variables controlling cycle and sequence development. The two-dimensional computer model generates lithologic cross-sections produced by the interaction of basin subsidence, fluctuating sea levels, and depth-dependent sedimentation (Koerschner and Read, 1989; Read *et al.,* submitted). The synthetic sequences and their component meter-scale cycles can be directly compared to observed sequences to assess the validity of input parameters and to determine how changes in individual parameters affect sequence and cycle development.

A brief outline of the model dynamics is given here; details of the model's algorithms, mechanics, and input parameters are given in Read *et al.,* (submitted). The digitized initial platform-to-basin profile is subdivided into 200 localities whose increment width is determined by the length of the profile. The program executes the the following sequences of calculations at user-specified (usually 100 to 500 yrs) time intervals. The calculated subsidence from the previous time interval occurs, then sea level is raised or lowered according to the input sea level curve and the water depth is checked. If the locality is submergent and undergoing lag, no sediment is added until the lag time has elapsed and only water load-induced subsidence for the next time interval will be added to that locality. If the locality is submerged and lag time has elapsed,

sediment is added according to the input depth-dependent sedimentation rates. If the locality is emergent, no deposition occurs or the sediment is eroded and subsidence for the next time interval will be driving subsidence only. If the locality has been emergent for a user-specified time interval (usually > 5 k.y.) a disconformity is drawn at the top of the emergent or eroded surface. The water depth is rechecked at each locality and the isostatic component of flexural subsidence due to sediment- and water-loading is calculated and is added to the driving subsidence at that locality and all adjoinging localities affected by the load. This sequence of calculations begins again until the duration of the model run has elapsed.

The models do not provide unique solutions, but illustrate how specific input variables affect sequence and cycle development. The following section discusses how the various input parameters were determined for the Lower Mississippian sequences and their likely range of values. Of the six input parameters (Table 2), subsidence rates and periods of long-term sea level curves are estimated directly from the observed geologic data. The remaining input parameters were estimated from comparisons with Holocene carbonate analogs and from modern sedimentary and oceanographic processes.

Table 2. Input parameters for computer modeling of depositional sequences 1-3.

	SEDIMENTATION RATE (m/k.y.)	INITIAL SLOPE (m/km)	LONG-TERM SEA LEVEL	SHORT-TERM SEA LEVEL	SUBSIDENCE RATES (m/k.y.)	LAG TIME
SEQUENCE 1	Water depth Rate 0-2 m 0.8-1.0 2-5 m 1.0-0.3 5-10 m 0.3-0.2 10-40 m 0.2-0.15 40-100 m 0.15-.09 100+ m 0.09	Inner-outer ramp: 0.03-0.15 Ramp-slope: 0.85	Period: 1.0 m.y. Rise: 5 m/300 k.y. Fall: 21 m/700 k.y.	Period Amplitude 100 k.y. 2 m 41 k.y. 10 m 23 k.y. 10 m	0.007-0.11	1000 yr
SEQUENCE 2	Water depth Rate 0-2 m 0.3-0.5 2-5 m 0.5-0.3 5-10 m 0.3-0.2 10-40 m 0.2-0.15 40-100 m 0.15-0.09 100+ m 0.09	Inner-outer ramp: 0.01-0.05 Ramp-slope: 0.35	Period: 0.85 m.y. Fall: 5 m/75 k.y. Rise: 15 m/50 k.y. Fall: 6 m/775 k.y.	Period Amplitude 100 k.y. 2 m 41 k.y. 10 m 23 k.y. 10 m	0.007-0.11	500 yr
SEQUENCE 3	Water depth Rate 0-2 m 0.8-1.0 2-5 m 1.0-0.3 5-10 m 0.3-0.2 10-40 m 0.2-0.15 40-100 m 0.15-.09 100+ m 0.09	Inner-outer ramp: 0.01-0.12 Ramp-slope: 0.90	Period: 0.9 m.y. Fall: 4 m/100 k.y. Rise: 28 m/100 k.y. Fall: 4 m/700 k.y.	Period Amplitude 100 k.y. 2 m 41 k.y. 10 m 23 k.y. 10 m	0.007-0.11	1000 yr

Duration of Depositional Sequences and Cycles: The duration of the Early Mississippian (Tournasian-Visean stages) from the DNAG (Palmer, 1983) and Sando (1985) time scales is 27 m.y. +/-16 m.y. This range implies any age estimates could be up to 60% in error, in the most extreme case. The duration of the three depositional sequences was estimated by:

$$D = (s/S) \times T$$

where s is the thickness of the sequence (preferably along the ramp-slope where deposition is more continuous), S is the thickness of the interval biostratigraphically tied into the DNAG time scale, and T is the absolute duration of the biostratigraphic dated interval based on the DNAG and Sando (1985) time scales. Using the maximum and minimum age range for the Lodgepole/lower Madison Formations (1.6-6.4 m.y.), depositional sequence 1 is 0.67-2.7 m.y. in duration, depositional sequence 2 is 0.36-1.4 m.y. in duration, and depositional sequence 3 is 0.37-1.5 m.y. in duration. These durations correspond to fourth order (0.1-1.0 m.y.) and third order (1-10 m.y.) sequences (Vail *et al.,* 1977).

The average duration of meter-scale cycles is calculated by:

$$D = z\ T/Z\ n$$

where z is the thickness of the cyclic interval, Z is the thickness of the interval biostratigraphically tied into the DNAG (Palmer, 1983) and Sando (1985) time scales, T is the absolute duration of the biostratigraphically dated interval, and n is the number of cycles in the cyclic interval (Koerschner and Read, 1989). Using the maximum

and minimum age range of the Woodhurst and Paine/Little Bighorn Members (1.2-4.8 m.y.), the range of average cycle periods along the outer ramp where the maximum number of cycles occur (stratigraphic section BM; Figs. 10-12) is between 30-110 k.y. The number of cycles decreases landward and seaward from the outer ramp, thus the range of average cycle periods increases accordingly.

Subsidence: The Lower Mississippian cratonic platform developed approximately 240 m.y. after Late Proterozoic/Early Cambrian rifting (Bond *et al.,* 1984), therefore subsidence was probably not thermally controlled. The most basinward stratigraphic section in the study area lies approximately 300-400 km east of the palinspastically restored leading-edge of Late Devonian/Early Mississippian Antler thrusting and approximately 100-200 km east of the eastern edge of the Antler foredeep (Fig. 1; Dover, 1980; Woodward, 1981; Speed and Sleep, 1982; Sandberg *et al.,* 1982). This suggests subsidence within the study area was probably driven by the lithosphere's flexural response to sediment infilling of the Antler foredeep (Bond, pers. comm., 1989).

Subsidence rates were calculated using decompacted sediment thicknesses (discussed below) at each stratigraphic section and range from 0.007 to 0.11 m/k.y. (Table 2). The geometry of individual depositional sequences indicates the ramp subsided differentially (Figs. 10-12), i.e., the middle ramp underwent greater subsidence than the ramp-margin, particularly during sequence 1 and 3 (Figs. 8 and 10). Differential subsidence is not incorporated into

the computer model, therefore the persistent middle ramp depression was simulated by modifying the antecedent topography of underlying synthetic sequence.

Decompaction: The computer model used does not account for burial compaction, therefore present-day rock thicknesses were decompacted using maximum burial depths for Lower Mississippian deposits (3 km in southwestern Montana; McMannis, 1965; Peterson and Smith, 1988) and maximum-minimum porosity reduction/compaction curves from Bond and Kominz (1984). The range of compaction values were applied to intervals of similar lithologies (i.e., lime mudstone, calcisiltite, grainstone, etc.). The effects of using either maximum (20%) or minimum (15%) compaction values on grainstone facies were less than 5%, whereas using maximum (60%) or minimum (20%) compaction values on highly compactible ramp-slope wackestone, mudstone, argillite, or shale facies produced up to a 25% difference in decompacted section thickness. Petrographic examination of cross-sections of circular burrows in ramp-slope limestone-argillite facies suggests limestone layers (micrite and pellet packstone) compacted less than 30-40%, while argillite layers compacted approximately 50-70%. Decompaction for the overlying post-Lower Mississippian sediments does not account for *intracycle* compaction which may have slightly increased the amount of accommodation space available during deposition of each cycle, particularly for fine-grained deep subtidal cycles.

Estimated Water Depths of Facies: The interpreted water depths of facies within cycles (Fig. 6) strongly influences estimates of initial ramp slopes and the estimates of the magnitudes of 5th order sea level fluctuations. Depth ranges were estimated from modern carbonate analogs and from stratigraphic relationships with adjacent facies.

The change from sub-storm wave base limestone-argillite deposits to storm-deposited graded limestone defines storm-wave base. In modern environments, the depth of storm-wave base is a function of climate, fetch, and basin configuration (Friedman and Sanders, 1978, p. 465). Open oceans may generate 14 to 20 second waves which correspond to wave bases between 60 to 300 meters (Friedman and Sanders, 1978). Storm-wave base in partially enclosed basins such as the Persian Gulf are >40 m (Purser and Seibold, 1973), and in the Gulf Coast are between 25-120 m, (Logan, 1969; Swift and Nummedal, 1987; Sneeden *et al.,* 1988). A range of storm-wave base depths between 20-50 m was used in the modeling; the best results were generated using a 40-50 m storm-wave base depth. Synthetic sequences with storm-wave base depths greater than 50 m require greater 5th order sea level oscillations to generate deep subtidal cycles and steeper ramp-slopes.

The placement of specific rock types into depth-dependent stratigraphic positions within the models was guided by modern carbonate analogs. In the models, intertidal facies (tidal range; 0-2 m water depths) may include algal laminites and during emergence

could include collapse breccias. Shallow subtidal facies (2-5 m) may include pelleted dolomite, ooid grainstone, and some crinoidal bank facies. Deep subtidal facies (5-40 m) may include crinoidal bank facies, skeletal-pellet wackestone, skeletal-ooid grainstone caps, graded limestone, crinoidal dolowackestone, and cherty skeletal wackestone/packstone. Very deep subtidal facies (>40 m) may include cherty skeletal wackestone/packstone, limestone-argillite, or mud mound facies.

Sedimentation Rates: Depth-dependent sedimentation rates used in the modeling range from 0.09-1.0 m/k.y. (Table 2) are based on Holocene carbonate analogs which are rates averaged over the last few thousand years (Stockman *et al.*, 1967, Neumann and Land, 1975; Olsen, 1978; Schlager, 1981; and Scholle *et al.*, 1983). These rates include the effects of sediment redistribution into and out of the depositional environments, periods of nondeposition, short-term erosion, and geologically instantaneous storm events. Sedimentation rates differ from production rates which are measured over several years and do not include the effects of redistribution. Sedimentation rates are typically an order of magnitude greater than long-term accumulation rates which are averaged over millions of years and include the major effects of subaerial erosion, marine diastems, and burial compaction. These accumulation rates approach subsidence rates in shallow water environments where sea level forms the upper limit of accommodation space for carbonates.

Platform Morphology: Relatively rapid lateral facies changes along the Lower Mississippian ramp and the geometry of individual sequences (Figs. 13-15) suggests distinct slope changes (Fig. 4), in particular, at the base of sequence 1, which lies on the Late Devonian-Early Mississippian unconformity. Ramp slopes were estimated from the change in water depths of equivalent facies across the ramp. For example,

$$\text{slope} = Z_2\text{-}Z_1/L$$

where Z_2 is the estimated water depth of the deepest water facies in outer ramp shallow subtidal cycles, Z_1 is the estimated water depth of the deepest water facies of time-equivalent inner ramp peritidal cycles, and L is the distance between the inner and outer ramp sections. Similar calculations were made along all segments of the ramp-to-basin transition.

Initial slopes on the shallow ramp were less than 0.08 m/km (Table 2 and Figs. 13-15). This is similar to those reported for ancient peritidal-dominated carbonate ramps (Lohmann, 1976; Grotzinger, 1986; Bova and Read, 1987; Handford, 1986; Koerschner and Read, 1989). The inclination of the ramp-slope ranged from 0.4-0.9 m/km (less than 0.1°; Table 2).

Using this slope estimate method, it is apparent that the greater the differences in estimated water depths, the greater the slope. Likewise, if there are little or no facies changes across the ramp (tops of sequence 1 and 3), the calculated slope will be very low.

Long-term Sea Level Curves: The specific periods of 3rd to 4th order sea level curves used in the modeling were chosen by taking the approximate mid-point of the estimated age range of individual depositional sequences. Sequence 1 was modeled using a 1.0 m.y. duration (excluding the age range of the basal dolomite/siliciclastic facies), sequence 2 a 0.85 m.y. duration, and sequence 3 was modeled using a 0.9 m.y. duration (Table 2).

Steckler and Watts (1978), Bond and Kominz (1984), and Moore *et al.*, (1987) utilized equations incorporating decompacted sediment thicknesses, mantle and sediment densities, and tectonic subsidence (determined from backstripping) to estimate the magnitude of long-term sea level change. The modeling was used to test the validity of the equations by comparing the magnitudes calculated from the equations to actual input values. The calculated values were consistently less than the input sea level magnitudes because sediment thickness varied markedly across the ramp. As a consequence, the effects of flexural isostatic loading were not uniform, particularly across the ramp-margin (Fig. 4).

Fischer plots (Fischer, 1964; Read and Goldhammer, 1988) of the Lower Mississippian sequences were not used to estimate magnitudes of long-term sea level oscillations (*cf.* Read and Goldhammer, 1988) because the stratigraphic sections are composed of subtidal or mixed subtidal and peritidal cycles. Subtidal cycles do not shallow to sea level, therefore cycle thicknesses may not reflect changes in accommodation space. Furthermore, there are too

few cycles within the total interval (20-50 cycles) to make reasonable comparisons of Fischer plots between stratigraphic sections.

The approximate magnitude of long-term sea level change was estimated by dividing the decompacted ramp-slope sediment thickness (above the shallow water ramp margin wedge) by 3. This estimation assumes roughly 70% of the sediment thickness is the result of space created by sediment and water loading (isostatic loading), while the remaining 30% of sediment thickness was the result of long-term sea level change (Matthews, 1984, p. 138). These initial approximations were subsequently refined by repeated model runs until a reasonable thickness of sediment was produced across the ramp-to-basin profile.

The three long-term sea level curves used to model the depositional sequences are not directly comparable with the eustatic sea level curves published by Ross and Ross (1987, 1988) because the duration of the Sando (1985) foraminiferal zones, which have been used to biostratigraphically tie the stratigraphic sections into the DNAG radiometric time scale, are shorter than the durations of foraminiferal zones used by Ross and Ross (1987). However, regardless of the foraminiferal zone boundaries, the Lodgepole/lower Madison Formations are Kinderhookian to lower Osagean in age, and the Ross and Ross sea level curve indicates three long-term eustatic sea level oscillations occurred during that time

interval suggesting the three depositional sequences identified in this study may correlate with these eustatic events.

Fifth Order Sea Level Curves: Fifth order sea level fluctuations with periods between ≈20 k.y., 41 k.y., and 100 k.y. (Milankovitch-type sea level curves) were used in the modeling to test whether the cycles could have formed by orbitally forced, glacio-eustatic sea level fluctuations. Minimum magnitudes of these 5th order sea level oscillations were determined from the estimated water depths of facies within deep subtidal cycles on the ramp-slope. Amplitude estimations using water depths of shallow subtidal or peritidal cycles determines minimum amplitudes because only the upper part of the 5th order sea level oscillations or highstands affect the shallow ramp, while both highstands (depositing deepest water facies) and lowstands (depositing shallowest water facies) affect the deep ramp and ramp-slope. Estimated water depths of facies within deep subtidal cycles (Fig. 5A) range from >40 m (limestone-argillite facies) to <20 m (ooid or skeletal packstone/grainstone cap). This requires at least a 20 m sea level change to shallow through these lithologies. Sediment aggradation accounts for less than 6 m of decompacted average cycle thickness. If the range of estimated water depths is greater, say 70 m for limestone-argillite facies, then at least 50 m of sea level change is necessary. Water depth estimates for the sub-storm wave base limestone-argillite facies, therefore, strongly influence what magnitudes of sea level oscillations are used in the modeling.

The form of the sea level curve is dependent on which of the three quasi-periods dominates the signal. For example, Pleistocene sea level fluctuations were dominated by asymmetric 100 k.y. periods (Hays *et al.*, 1976). The asymmetry (i.e., approximately 15% of the period taken up on the rise while approximately 85% of the period is taken up in the fall) resulted in several of the shorter-term oscillations (≈20 and 41 k.y.) being missed along the south Florida and Bahamian platforms (Enos, 1977). In contrast, modeling studies of Triassic cycles in the Italian Dolomites indicate that the 100 k.y. and 41 k.y. oscillations were supressed, resulting in dominant ≈20 k.y. cycles recorded (Goldhammer *et al.*, 1987, 1990; Goldhammer and Harris, 1989).

The form of the Lower Mississippian sea level curve was estimated from 5th order cycle stacking patterns observed in shallow through deep ramp stratigraphic sections. Several amplitude combinations add to produce a total amplitude of approximately 20 m (minimum amplitude assumed to reproduce the Lower Mississippian deep subtidal cycles). Computer models using each of the possible amplitude combinations (while holding all other parameters constant) generated distinct cycle stacking patterns which were compared to observed stacking patterns.

Models run with dominant 23 k.y. oscillations (23 k.y. = 16 m, 41 k.y. = 2 m, and 100 k.y. = 2 m) produce cycle lithologies and thicknesses similar to those observed in the field; however, there are too many cycles generated across most of the ramp and ramp-

slope, resulting in shorter average cycle periods than observed. This is particularly evident along the ramp-slope where each 23 k.y. lowstand event was recorded resulting in average periods around 23 k.y (versus between 50-70 k.y. in the observed ramp-slope cycles).

Models run with dominant 41 k.y. oscillations (23 k.y. = 2 m, 41 k.y. = 16 m, and 100 k.y. = 2 m) generate too few and too thick of cycles across the entire ramp-to-basin profile and thick (>3 m) intertidal cycle caps prograde across the ramp during each 41 k.y. oscillation. Thick intertidal caps developed because input intertidal sedimentation rates (≈1 m/k.y.) kept pace with 5th order sea level fall rates (<1.0 m/k.y.).

Synthetic sequences run with asymmetric 100 k.y. oscillations as the dominant signal (23 k.y. = 2 m, 41 k.y. = 2 m, and 100 k.y. = 16 m) generated very few and very thick (>15 m) cycles along the entire ramp. Fewer cycles were generated because several of the shorter-term oscillations (23 and 41 k.y.) were missed on the shallow ramp. In addition, thick intertidal cycle caps (>3 m) developed along the entire ramp, which is not observed in the actual sequences.

Synthetic sequences run with the same amplitudes for the 23 k.y., 41 k.y., and 100 k.y. period oscillations (7 m) generated too few cycles along the entire ramp-to-basin profile. Deep subtidal cycles were not generated along the ramp-slope because alternating very deep subtidal (>40 m water depths) and deep subtidal water depths were not attained.

The sea level curve that best simulated the observed cycle stacking patterns, average cycle periods, and sequence geometry was composed of equal 23 k.y. and 41 k.y. period oscillations, both with 10 m amplitudes and supressed 100 k.y oscillations 2 m (Table 2; Figs. 13-15). Suppressed 100 k.y. oscillations allowed nearly each of the 41 k.y. oscillations and some of the 23 k.y. oscillations to affect the ramp, as well as the ramp-slope. However, because it is difficult to accurately constrain the 5th order sea level curves, it is likely that several different sea level curves may simulate the data if they are coupled with different combinations of sedimentation rates.

Lag Time or Lag Depth is the time or water depth required following initial submergence of the depositional surface until the onset of substantial carbonate sedimentation or accumulation (Enos, 1989). Lag time/depth is critical to the development of asymmetric shallowing-upward cycles that were generated from relatively low amplitude (<10 m) sea level oscillations (Koerschner and Read, 1989). This is because rapid carbonate sedimentation rates can keep pace with sea level rise rates, which precludes the generation of deeper water facies at the base of the cycle.

Inner ramp peritidal cycles were best simulated using lag times between 500-1000 years (0.25-2 m lag depths), however these shorter lag times resulted in the development of symmetric subtidal cycles along the outer ramp. For the input sea level curve and sedimentation rates, lag times of about 2000 years generated

asymmetric outer ramp subtidal cycles. This likely difference in lag times or lag depths across the ramp and even within a single deposition environment (Enos and Perkins, 1979) is discussed in Read *et al.,* (submitted). Because the model utilizes a constant lag time across the ramp, the sequences were modeled with lag times between 500-1000 years to best simulate the inner ramp peritidal cycles (Table 2).

COMPUTER MODELING RESULTS

Each sequence and its component meter-scale cycles was modeled separately using a range of geologically constrained variables (Table 2). For each of the sequences, the amplitudes and periods of 5th order sea level oscillations and basinward increasing subsidence rates were held constant. Depth-dependent sedimentation rates were similar for each of the sequences, except in sequence 2, where intertidal sedimentation rates were decreased. Lag time was also decreased from 1000 yrs to 500 yrs for sequence 2. Long-term sea level curves and initial ramp morphologies were varied for each of the sequences (Table 2).

The computer model generates lithofacies that correspond only to changes in water depth. The model does not account for energy changes across the ramp, nutrient and oxygen supply, salinity, and variable substrates which also influence carbonate rock types in nature. The synthetic sequences in Figures 13, 14, and 15 illustrate

Figure 13. Synthetic sequence 1 (excluding basal dolomite/siliciclastics facies) generated using initial ramp-to-basin topography and sea level curve shown; additional input parameters shown in Table 2. Dotted portion of sea level curve indicates the general shape of the transgressive phase of the long-term sea level curve represented by the basal siliciclastic deposits. Systems tract boundaries are shown and tied into the sea level curve by time lines generated by the model. Vertical lines indicate location of portions of synthetic stratigraphic sections in Figure 16.

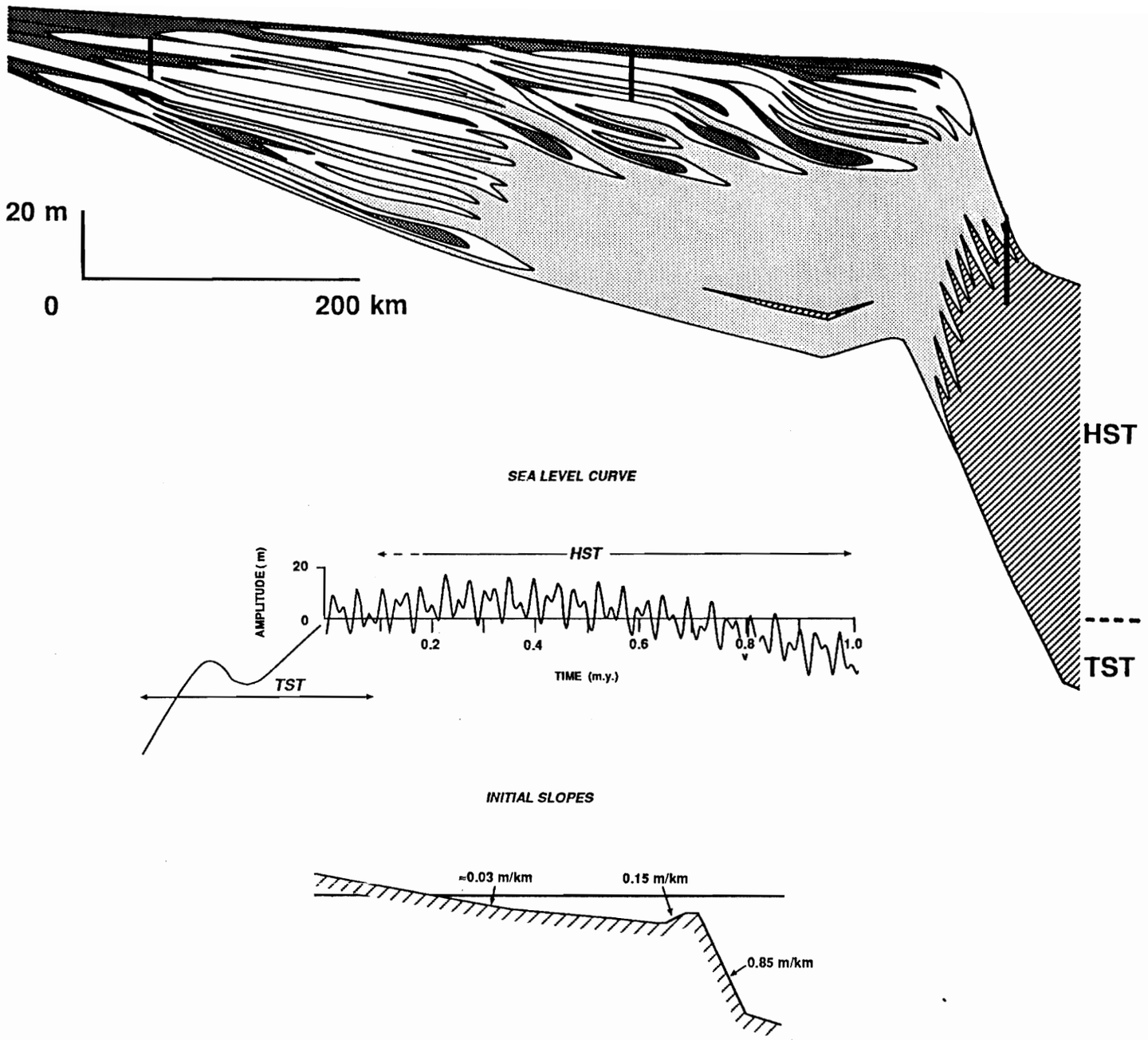

SYNTHETIC SEQUENCE FACIES

- INTERTIDAL FACIES — 0-2 m WATER DEPTHS
- SHALLOW SUBTIDAL FACIES — 2-10 m WATER DEPTHS
- DEEP SUBTIDAL FACIES — 10-40 m WATER DEPTHS
- VERY DEEP SUBTIDAL FACIES — >40 m WATER DEPTHS
- LOCATION OF SYNTHETIC SECTIONS SHOWN IN FIGURES 16, 17, 18
- SYSTEMS TRACT BOUNDARIES
- DISCONFORMITY (>5 k.y. DURATION)

Figure 14. Synthetic sequence 2 generated using initial ramp-to-basin topography and sea level curve shown; additional input parameters shown in Table 2. Vertical lines indicate location of portions of synthetic stratigraphic sections in Figure 17.

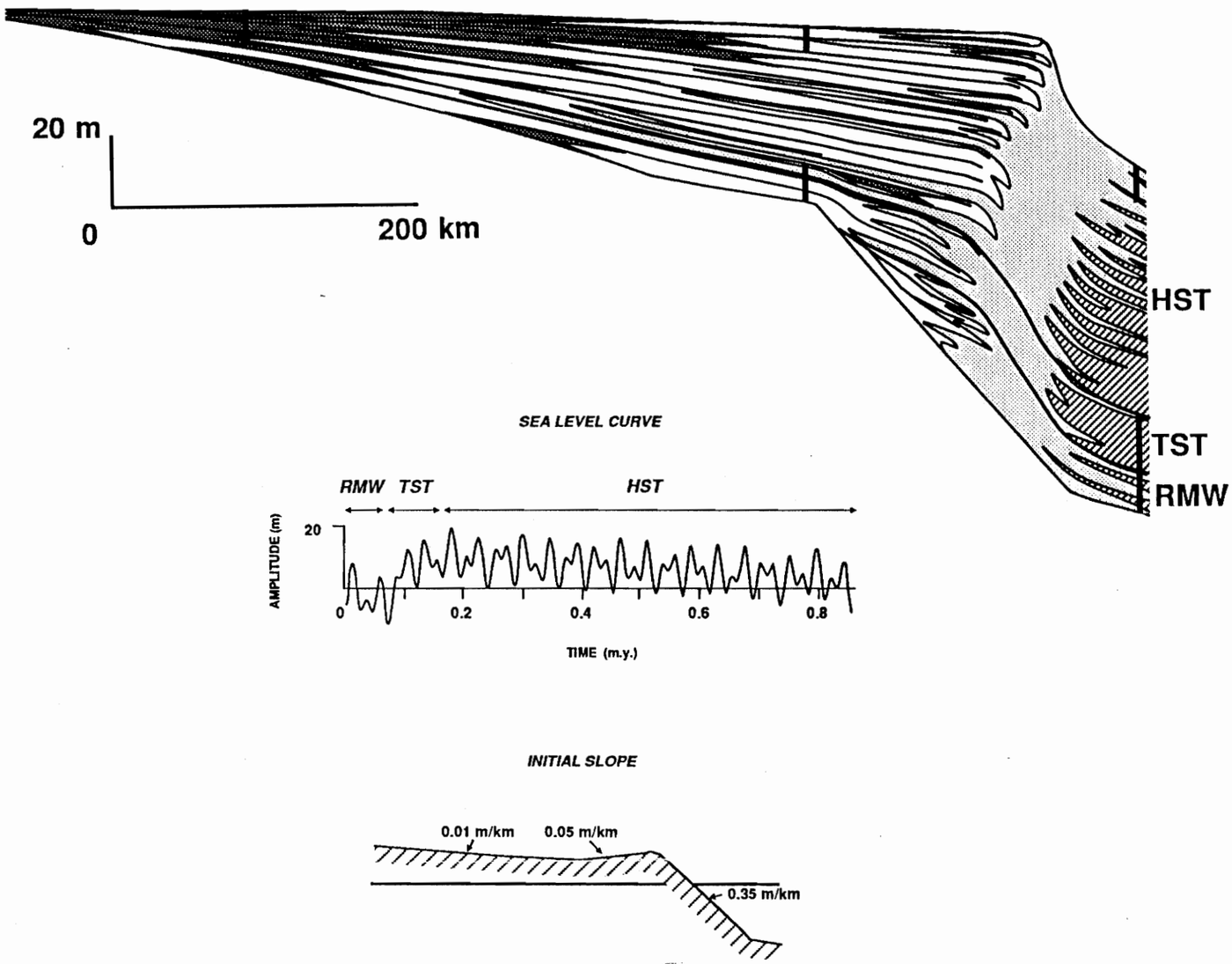

SYNTHETIC SEQUENCE FACIES

- INTERTIDAL FACIES — 0-2 m WATER DEPTHS
- SHALLOW SUBTIDAL FACIES — 2-10 m WATER DEPTHS
- DEEP SUBTIDAL FACIES — 10-40 m WATER DEPTHS
- VERY DEEP SUBTIDAL FACIES — >40 m WATER DEPTHS

- LOCATION OF SYNTHETIC SECTIONS SHOWN IN FIGURES 16, 17, 18
- SYSTEMS TRACT BOUNDARIES
- DISCONFORMITY (>5 k.y. DURATION)

Figure 15. Synthetic sequence 3 generated using initial ramp-to-basin topography and sea level curve shown; additional input parameters shown in Table 2. Vertical lines indicate location of portions of synthetic stratigraphic sections in Figure 18.

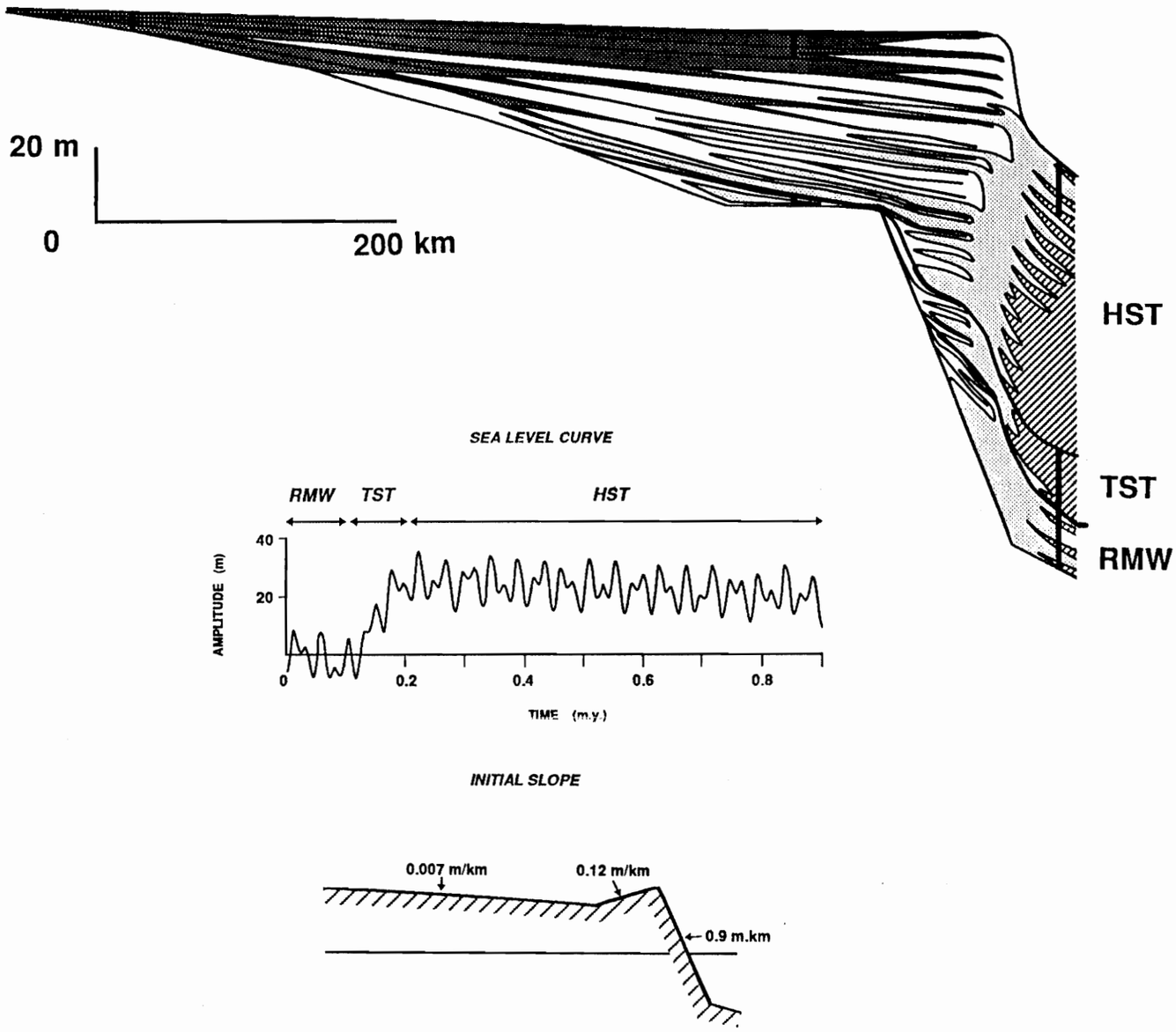

SYNTHETIC SEQUENCE FACIES

- INTERTIDAL FACIES, 0-2 m WATER DEPTHS
- SHALLOW SUBTIDAL FACIES, 2-10 m WATER DEPTHS
- DEEP SUBTIDAL FACIES, 10-40 m WATER DEPTHS
- VERY DEEP SUBTIDAL FACIES, >40 m WATER DEPTHS
- LOCATION OF SYNTHETIC SECTIONS SHOWN IN FIGURES 16, 17, 18
- SYSTEMS TRACT BOUNDARIES
- DISCONFORMITY (>5 k.y. DURATION)

the results of one of *several* possible combinations of input variables that reproduce sequences and cycles similar to those observed in the field. Modeling solutions are not unique, however most of the input variables are justified by the observed geologic data.

Ramp Margin Systems Tract

The ramp margin systems tract (RMW) of sequence 1 does not occur within the study area. The RMW of depositional sequences 2 and 3 occur along ramp-slope and consist of stacked ooid or crinoidal bank cycles along the landward edges which pass downdip into deep subtidal cycles (Figs. 11, 12, 17 and 18). The increase in skeletal diversity and abundance in RMW deposits suggests more open-marine conditions prevailed near the long-term sea level lowstand because most of the inner and outer ramp was subaerially exposed, therefore slightly hypersaline or nutrient-poor waters were not flowing off the ramp.

Synthetic RMW facies of sequences 2 and 3 were simulated using ramp-slopes of 0.3 m/km and 0.9 m/km, respectively (Figs. 14 and 15). Both RMWs were generated during late long-term sea level fall (5 m fall), lowstand, and very early rise (rise rates less than 0.3 m/k.y.; Table 2). The deposits are confined to the ramp-slope and consist of peritidal and shallow subtidal cycles along the landward edge which pass downdip into deep subtidal cycles (Figs. 14, 15, 17

and 18). Disconformities capping the peritidal cycles indicate >5 k.y. exposure durations.

Exposure features are not evident in the observed RMW deposits nor are they observed in the majority of subtidal cycles that occur within the sequences. The absence of these features (microkarst surfaces, paleosol/regolith caps, meteoric diagenesis) may be the result of not recognizing the subtle features in outcrop, or more likely the arid climate during Mississippian time (Middleton, 1961; Sando, 1988) may have limited the effects of dissolution or meteoric diagenesis. For example, there is little evidence of meteoric cementation or leaching associated with small-scale cycle diconformities in the Mississippian of Kentucky, probably because of the arid climate (Niemann and Read, 1988).

The absence of tidal flat caps cycles in actual RMW deposits suggests tidal flat nucleation may have been inhibited by high-energy conditions along the ramp-slope, or perhaps the upper parts of cycles, including thin intertidal caps or microkarst surfaces, were eroded during emergence and the ensuing 5th order transgression. Alternatively, 5th order sea level oscillations may have been less than the assumed 20 m, which would have prevented the RMW deposits being exposed during short-term sea level lowstands. However, assuming a 40 m storm wave base, amplitudes less than about 10 m would not generate the deep subtidal cycles that occur downdip from the shallow subtidal cycles.

Time lines generated by the model indicate that the upper boundary of both RMWs (transgressive surfaces) developed during the maximum rate of long-term sea level rise, before sea level flooded the outer ramp.

Transgressive Systems Tract

The TST of sequence 1 consists mainly of a thin (<15 m thick) condensed interval of fine siliciclastics and silty dolomite (Cottonwood Canyon Member; Fig. 10). This initial phase of transgression was not included in the modeling of depositional sequence 1 because accumulation of the fine siliciclastics was likely a function of siliciclastic poisoning and oxygen depletion rather than changes in water depth. Deposition of the fine clastics and overlying deep ramp facies indicates rapid flooding of the Devonian-Early Mississippian unconformity, followed by a slight shallowing event or a deepening of the oxygen minimum zone, followed by continued sea level rise and inner ramp flooding. Thus, modeling of synthetic sequence 1 was begun after the initial rapid flooding of the ramp (*cf.* Figs. 4 and 13). TST deposits of observed sequences 2 and 3 are characterized by shallow through deep subtidal cycles which onlap the underlying sequence boundaries; peritidal cycles are restricted to the inner ramp (Figs. 11 and 12).

The synthetic TSTs of sequences 2 and 3 were generated during long-term sea level rise (maximum rise rates of approximately 0.3 m/k.y.; Table 2). The increase in accommodation space is reflected

in the dominance of shallow through deep subtidal cycles which onlap the underlying sequence boundary; peritidal cycles occur mainly along the inner ramp (Figs. 14, 15, 17 and 18).

In contrast to the observed TSTs, the synthetic TSTs do not abruptly deepen above the underlying RMWs. Instead, a relatively wide region of interbedded shallow and deep subtidal facies overlies the RMW with shallow subtidal facies extending as far seaward as the ramp-slope (Fig. 14). The extent of intertonguing may be reduced by decreasing the amplitudes of 5th order sea level oscillations. However, amplitudes less than 10 m do not generate deep subtidal cycles along the ramp-slope. The inland extent of deep subtidal facies may be reduced by increasing shallow subtidal sedimentation rates to greater than or equal to 5th order sea level rise rates (>1-2 m/k.y.), and by decreasing lag times to less than 1000 yrs. This would result in shallow subtidal sedimentation rates keeping pace with the generation of accommodation space, therefore deeper subtidal water depths would not be generated along the shallow ramp. This effect could be argued for dominately ooid grainstone deposits, which in modern environments, have relatively high production rates (1-2 m/k.y.; Harris, 1979; Schlager, 1981), and likely do not require significant lag times before the onset of carbonate production after subaerial exposure because ooid generation is maximized in <2 m water depths (Bathurst, 1975). The negative side effect to these increased sedimentation rates is that they increase the amount of shallow subtidal facies progradation

Figure 16. Comparison of detailed stratigraphic columns from depositional sequence 1 and synthetic section 1 (locations indicated by vertical lines in Figs. 10 and 13). Observed stratigrahic columns are present day thicknesses, while synthetic columns have not been corrected for burial compaction.

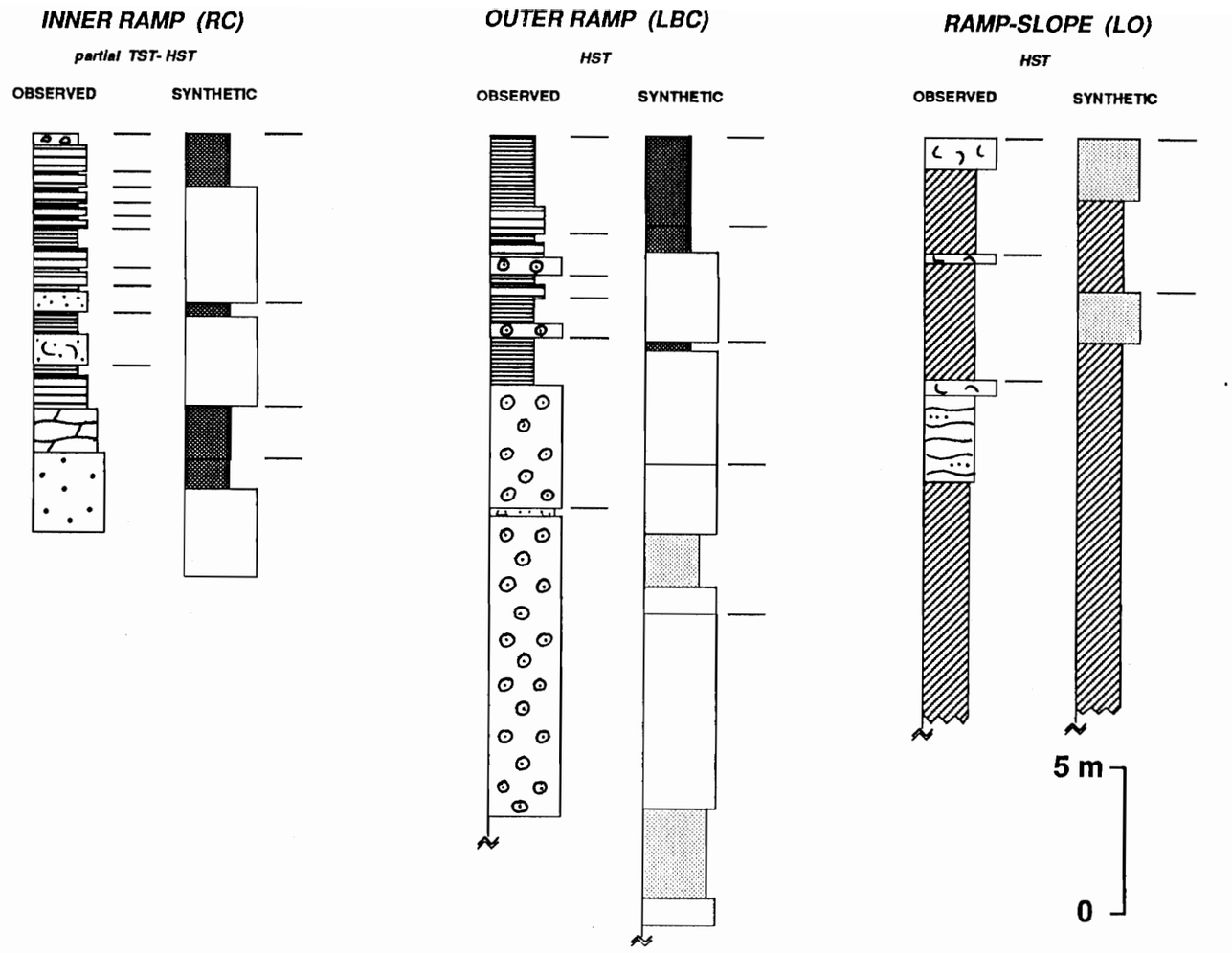
INNER RAMP (RC)
partial TST- HST
OBSERVED
SYNTHETIC
OUTER RAMP (LBC)
HST
OBSERVED
SYNTHETIC
RAMP-SLOPE (LO)
HST
OBSERVED
SYNTHETIC
5 m
0

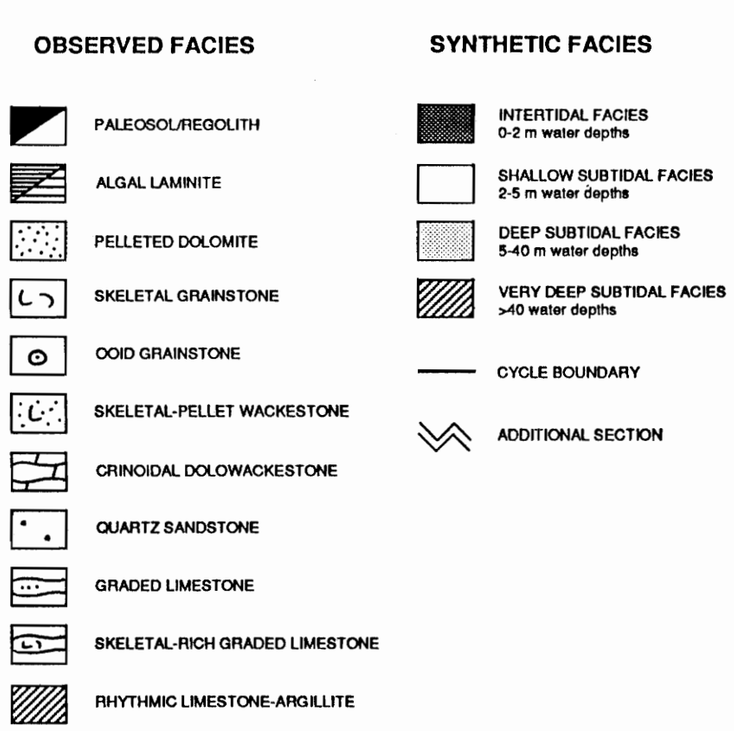
OBSERVED FACIES
SYNTHETIC FACIES
PALEOSOL/REGOLITH
ALGAL LAMINITE
PELLETED DOLOMITE
SKELETAL GRAINSTONE
OOID GRAINSTONE
SKELETAL-PELLET WACKESTONE
CRINOIDAL DOLOWACKESTONE
QUARTZ SANDSTONE
GRADED LIMESTONE
SKELETAL-RICH GRADED LIMESTONE
RHYTHMIC LIMESTONE-ARGILLITE
INTERTIDAL FACIES
0-2 m water depths
SHALLOW SUBTIDAL FACIES
2-5 m water depths
DEEP SUBTIDAL FACIES
5-40 m water depths
VERY DEEP SUBTIDAL FACIES
>40 water depths
CYCLE BOUNDARY
ADDITIONAL SECTION

Figure 17. Comparison of detailed stratigraphic columns from depositional sequence 2 and synthetic section 2 (locations indicated by vertical lines in Figs. 11 and 14). Observed stratigrahic columns are present day thicknesses, while synthetic columns have not been corrected for burial compaction.

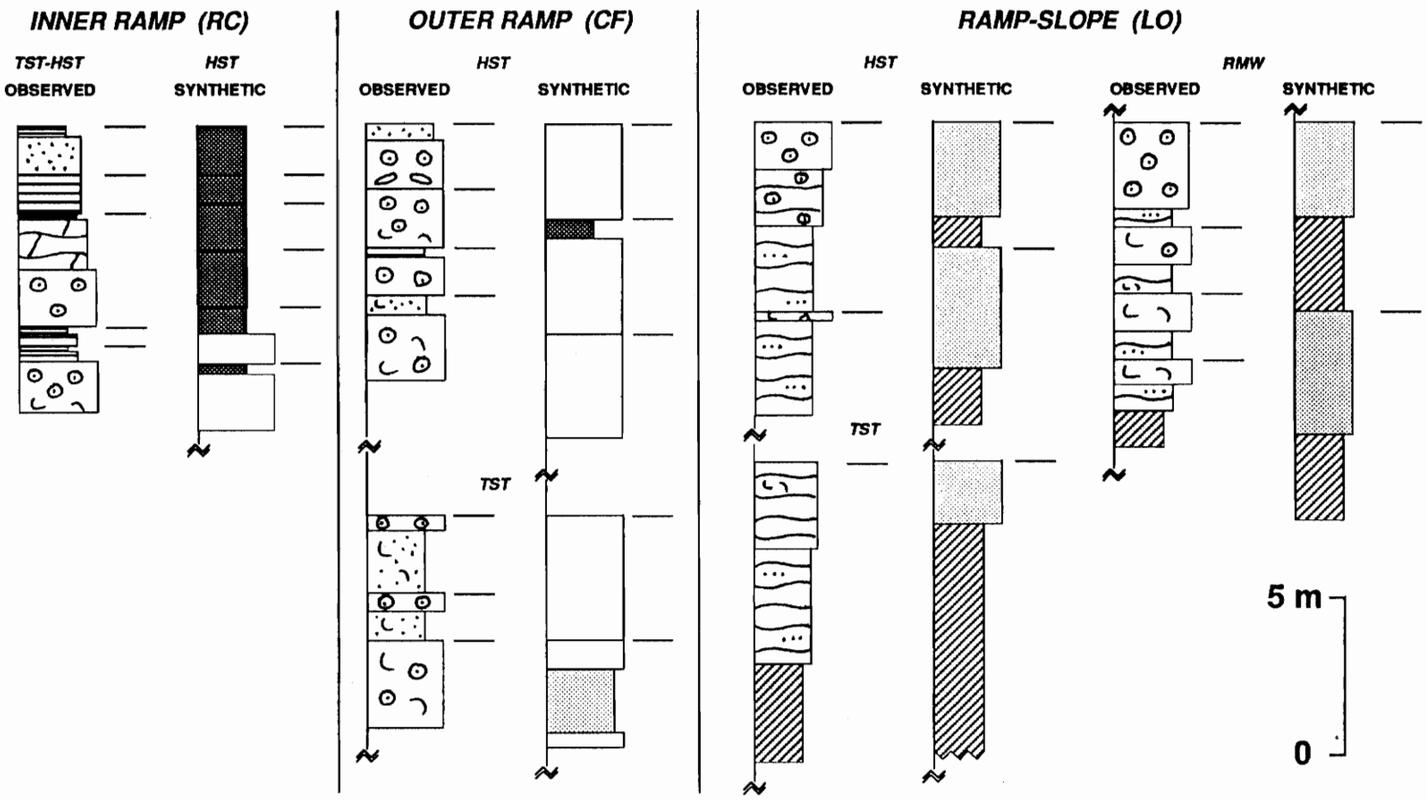
INNER RAMP (RC)
TST-HST
OBSERVED
HST
SYNTHETIC
OUTER RAMP (CF)
HST
OBSERVED
SYNTHETIC
TST
RAMP-SLOPE (LO)
HST
OBSERVED
SYNTHETIC
TST
RMW
OBSERVED
SYNTHETIC
5 m
0

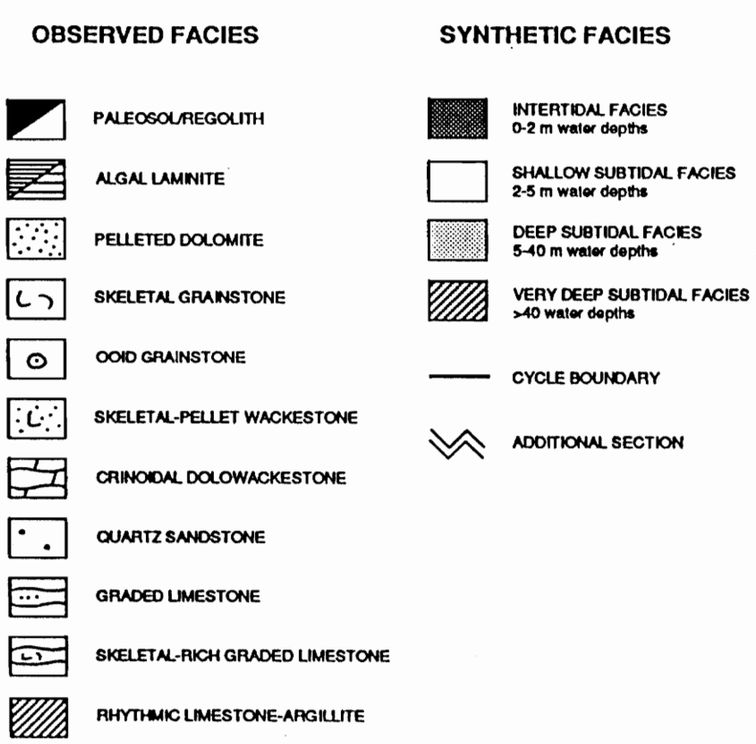
OBSERVED FACIES
PALEOSOL/REGOLITH
ALGAL LAMINITE
PELLETED DOLOMITE
SKELETAL GRAINSTONE
OOID GRAINSTONE
SKELETAL-PELLET WACKESTONE
CRINOIDAL DOLOWACKESTONE
QUARTZ SANDSTONE
GRADED LIMESTONE
SKELETAL-RICH GRADED LIMESTONE
RHYTHMIC LIMESTONE-ARGILLITE
SYNTHETIC FACIES
INTERTIDAL FACIES
0-2 m water depths
SHALLOW SUBTIDAL FACIES
2-5 m water depths
DEEP SUBTIDAL FACIES
5-40 m water depths
VERY DEEP SUBTIDAL FACIES
>40 water depths
CYCLE BOUNDARY
ADDITIONAL SECTION

Figure 18. Comparison of detailed stratigraphic columns from depositional sequence 3 and synthetic section 3 (locations indicated by vertical lines in Figs. 12 and 15). Observed stratigrahic columns are present day thicknesses, while synthetic columns have not been corrected for burial compaction.

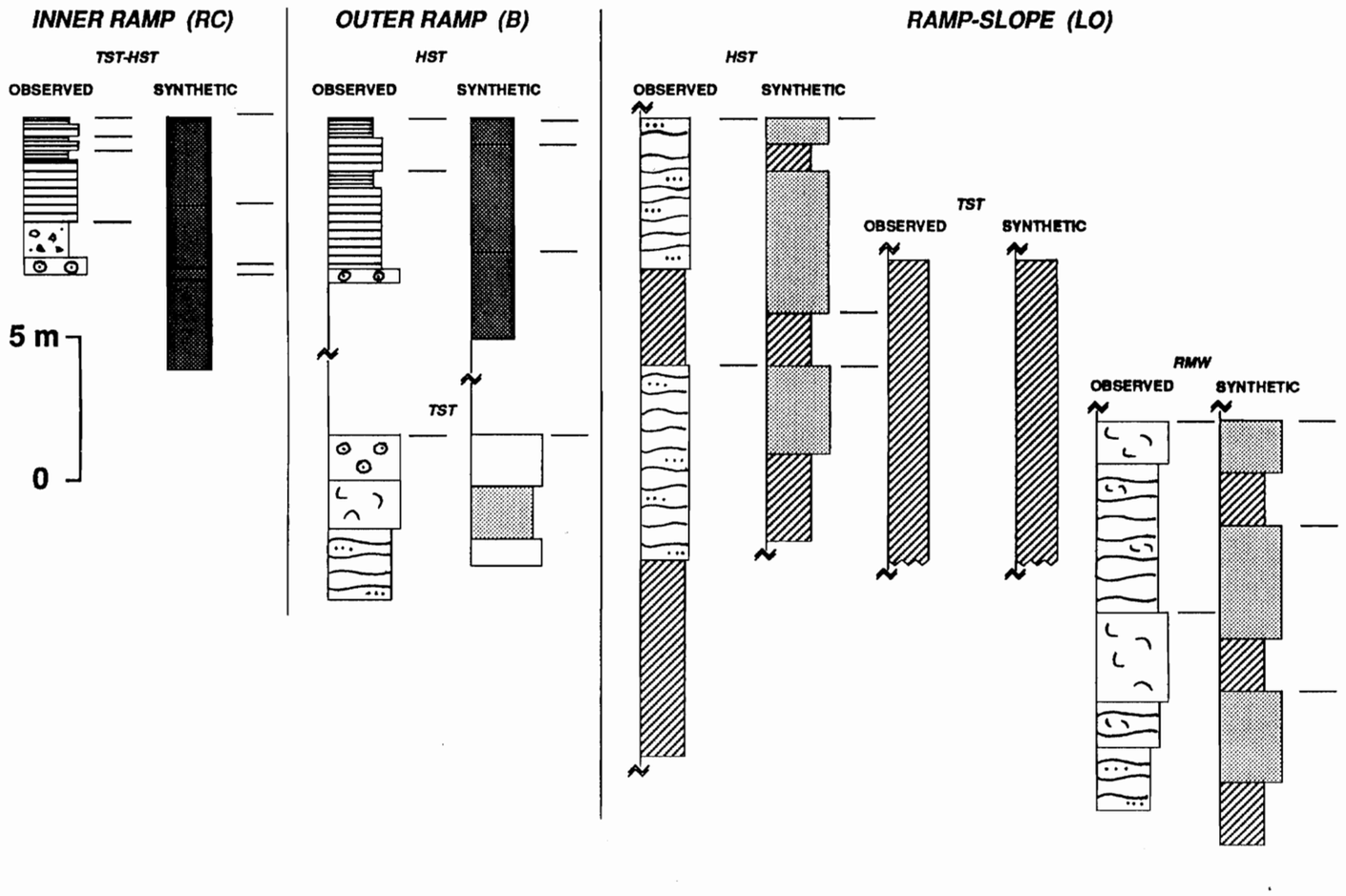
INNER RAMP (RC)
TST-HST
OBSERVED
SYNTHETIC
5 m
0
OUTER RAMP (B)
HST
OBSERVED
SYNTHETIC
TST
RAMP-SLOPE (LO)
HST
OBSERVED
SYNTHETIC
TST
OBSERVED
SYNTHETIC
RMW
OBSERVED
SYNTHETIC

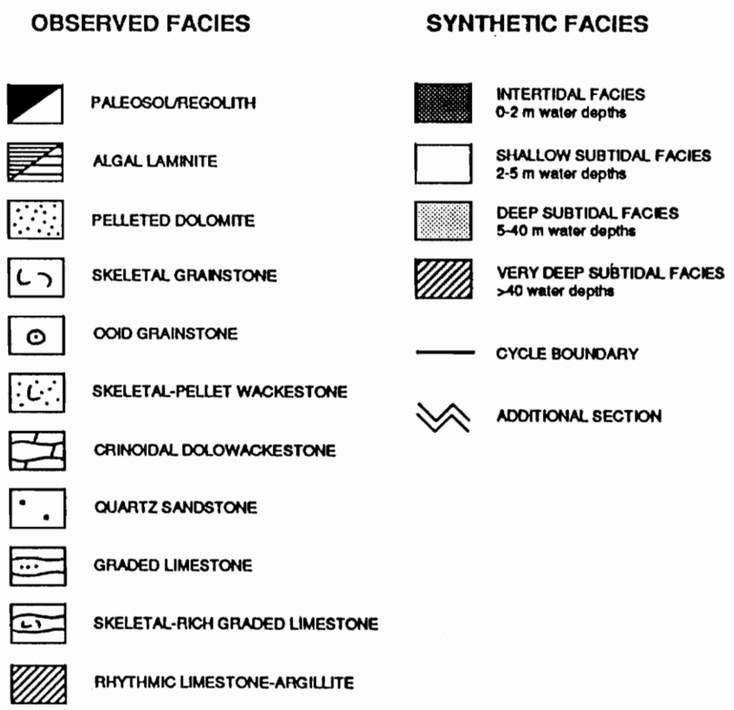
OBSERVED FACIES
PALEOSOL/REGOLITH
ALGAL LAMINITE
PELLETED DOLOMITE
SKELETAL GRAINSTONE
OOID GRAINSTONE
SKELETAL-PELLET WACKESTONE
CRINOIDAL DOLOWACKESTONE
QUARTZ SANDSTONE
GRADED LIMESTONE
SKELETAL-RICH GRADED LIMESTONE
RHYTHMIC LIMESTONE-ARGILLITE
SYNTHETIC FACIES
INTERTIDAL FACIES
0-2 m water depths
SHALLOW SUBTIDAL FACIES
2-5 m water depths
DEEP SUBTIDAL FACIES
5-40 m water depths
VERY DEEP SUBTIDAL FACIES
>40 water depths
CYCLE BOUNDARY
ADDITIONAL SECTION

during 5th order falls and lowstands. Furthermore, the increased sedimentation rates have the affect of decreasing the number of cycles generated along the shallow ramp (with the given 5th order sea level curve; Table 2) because the shallow ramp stays aggraded to sea level, resulting in less accommodation space available for the next 5th order flooding event.

Lastly, the inclination of the ramp-slope could be steepened to narrow the region affected by 5th order oscillations and therefore the extent of shallow and deep subtidal intertonging. However ramp-slopes substantially steeper than those used in the model (0.3-0.9 m/km) are not supported by the lateral variations in sequence thicknesses and lateral facies relationships.

The difference between the observed and synthetic sequences indicates some factor not included in the modeling controlled the abrupt deepening at the base of the TST and the seaward extent of ooid shoal progradaton. The deepening above RMWs (transgressive surfaces) may be the result of a deep water lag time/depth which would occur during the relatively rapid long-term sea level rise. The affect of the lag time would be to supress shallow subtidal accumulation until deep subtidal water depths were attained. This deep water lag time/depth may have been due to slower sedimentation rates in deeper water either from slower production, continuous wave-sweeping, or due to off-ramp flow of turbid, slightly hypersaline, or nutrient-poor water from the shallow ramp during the early transgression (Lighty *et al.*, 1978).

Maximum Flooding Surfaces

In the synthetic sequences the upper boundary of both TSTs (maximum flooding surface) occurs just before the long-term sea level highstand position when sea level had flooded the ramp and accommodation space was still being generated (Read *et al.*, submitted). Maximum flooding did not occur during the maximum rate of long-term sea level rise (*cf.* Goldhammer *et al.,* 1990) because at that time, sea level had not yet flooded the outer ramp.

The modeling points out possible reasons why the MFSs are difficult to define in outcrop. In synthetic sequences 2 and 3, the MFSs along the ramp-slope are difficult to define because the rise rates of moderate amplitude 5th order sea level oscillations overpower long-term sea level rise rates, consequently each 5th order sea level rise generates a significant deepening event that is difficult to distinguish from a single maximum flooding surface. Along the inner and middle ramp of the synthetic sequences, the MFS occurs at the base of the cycle that contains the deepest water facies; this location also coincides with the change from retrogradation to aggradation/progradation (Figs. 13-15). In the observed sequences, it is this change from retrogradation to progradation that is used to identify the TST to HST transition.

Highstand Systems Tracts

HST deposits of depositional sequences 1 and 3 are characterized along the inner and outer ramp by ooid-dominated

subtidal cycles overlain by a thick succession of late HST peritidal cycles (Figs. 10, 12, 16, and 18). Depositional sequence 2 lacks the thick interval of late HST peritidal cycles, instead the sequence is capped by ooid-dominated shallow subtidal cycles and cyclic foreshoal deposits (Fig. 11). The loss of accommodation space during HST deposition is reflected in the highly progradation nature of the ooid shoal and peritidal facies.

The synthetic HSTs were generated during late long-term sea level rise, highstand, and early fall (maximum fall rates between 0.01-0.03; Table 2). The majority of synthetic sequence 1 represents HST deposits consisting of deeper subtidal facies extenting into the inner ramp overlain by aggradational to progradational deeper subtidal and minor peritidal facies. The model generates seaward prograding tongues and topographic buildups during 5th order falls and lowstands. The 1-5 m thick intervals of intertidal facies within the predominantly deeper subtidal succession were generated during the 5th order lowstands. These features are not observed in the actual sequence suggesting energy conditions were too high to allow tidal flat deposition, or intertidal ooid facies were not recognzied in outcrop.

The main problems with the model runs of synthetic sequences 1 and 3, are that an insufficient amount of intertidal facies (peritidal cycles) was generated during the HST. This is because the rate of accommodation loss during 5th order sea level falls was greater than the generation of intertidal facies (compare Figs. 10

and 12 with 13 and 15). Decreasing lag times to less than about 500 yrs and keeping intertidal sedimentation rates relatively high (≈1.0 m/k.y.) would allow intertidal sedimentation rates to keep pace with most 5th order fall rates, resulting in regionally extensive peritidal cycles. Similarly, intertidal sedimentation rates could be increased to >2 m/k.y. so as to keep pace with short-term sea level fall rates (1-2 m/k.y.) or the tidal range could be increased to >3 m (mesotidal). The drawback to these modifications is that thick peritidal cycles would also form during RMW and TST deposition, a feature not observed in the actual sequences, and the shorter lag times result in symmetric shallow subtidal cycles developed along the outer ramp, which also is not observed. These modifications also would result in the shallow ramp staying aggraded to sea level during each 5th order flooding event, therefore fewer cycles are generated because there is less accommodation space available during the next 5th order rise. The number of cycles could be increased by changing the form of the 5th order sea level curve to a ≈20 k.y. dominated signal rather than the ≈20 k.y. and 40 k.y. dominant signal that was used in the models. However, the dominant ≈20 k.y. signal would result in too many cycles that were too thin generated along the outer ramp and ramp-slope.

A thicker succession of HST peritidal cycles could be generated if 5th order sea level oscillations were less than 10 m (fall rates <1.0 k.y.). However, anomalously thick peritidal cycles would also form during RMW and TST deposition, and a storm-wave

base depth less than 25 m would be required to generate deep subtidal cycles along the ramp-slope. Such shallow depths to storm-wave base is unlikely for the open-ramp setting of the Lower Mississippian. A 25 m storm-wave base depth also would imply that the tops of ramp-slope mud mounds grew within < 5m water depths. This is unlikely because they lack any evidence of wave- or current-reworking and they lack photosynthetic algae indicative of shallow subtidal water depths (Stone, 1972; Smith, 1977).

Sequence Boundaries

Inner to outer ramp sequence boundaries of observed sequences 1 and 3 are well-defined by the abrupt change from thin peritidal cycles to overlying ooid grainstone-dominated shallow subtidal cycles (Fig. 4 and Plate 1). The middle to outer ramp sequence boundary of observed sequence 2 is not recognized because there is no distinct lithologic break within ooid-dominated cycles (Figs. 4 and 11). Sequence boundary 2, along the inner ramp, is difficult to differentiate from any of the disconformity-capped 5th order peritidal cycles (Plate 1). Ramp-slope sequence boundaries in each of the observed sequence is not well-defined, and have been arbitrarily placed where cyclic deep ramp facies are overlain by crinoidal bank/ooid shoal facies or at the base of deep subtidal cycles with the thickest grainstone caps (Plate 1).

In the models, sequence boundaries were initiated when long-term sea level fall rates exceeded inner ramp subsidence rates.

Along the ramp-slope, the rates of long-term sea level fall did not exceed the combined effects of driving subsidence and isostatic flexural subsidence due to sediment- and water-loading; i.e., type 2 sequence boundary (Vail *et al.,* 1977; Van Wagoner *et al.,* 1988).

Time lines generated by the model suggest the durations of the sequence-bounding unconformities were greatest along the inner ramp (0.1-0.5 m.y.) decreasing to conformable boundaries along the ramp-slope. This time loss along the inner ramp may be reflected in the closely spaced paleosol and regolith breccia layers observed within peritidal facies of depositional sequences 1 and 3 (Plate 1).

Time lines generated by the model illustrate why sequence boundaries along the ramp-slope (base of RMW) are difficult to recognize in outcrop. During development of the sequence boundary along the inner and middle ramp, there was continuous deeper water sedimentation along the ramp-slope, consequently there are no facies changes along the ramp-slope which correspond in time to the shallow ramp sequence boundary. It is only during the long-term sea level lowstand that shallower water facies are deposited along the ramp-slope; i.e., shallow water facies of the RMW (Read *et al.*, submitted).

Discussion

Sequence stratigraphic concepts and terminolgy were initially defined on the basis of stratal geometries observed within seismic cross-sections (Vail *et al.,* 1977). Sequence and systems tracts

boundaries are defined as surfaces, however when considering the resolution or vertical scale of typical seismic data, these surfaces actually represent zones that may be several 10's meters thick. By realizing the scale difference between typical seismic data and meter-scale outcrop data, it is understood why single surfaces are difficult to recognize in outcrop, particularly without the aid of precise time lines between stratigraphic sections or without continuous outcrop exposure.

The modeling illustrates the change in ramp-slope inclination during sequence develoment. The ramp-slope flattens during RMW deposition because the locus of shallow water sedimentation (relatively fast sedimentation rates) shifts basinward and the ramp-slope surface aggrades (Figs. 14 and 15). During the TST, when the generation of accommodation space is greatest, relatively fast shallow water sedimentation along the ramp keeps pace with the accommodation change, while deeper water ramp-slope sedimentation lags behind the increase in accommodation space. As a result, the ramp-slope steepens (Figs. 14 and 15). During HST deposition, the ramp-slope once again flattens because the decrease in accommodation space during long-term sea level highstand and fall results in the seaward progradation of shallow water facies towards the the ramp-slope (Figs. 13-15).

The modeling results suggest that the initial inclination along the ramp-slope, which was likely inherited from the Late Devonian-Early Mississippian unconformity (Fig. 4), persisted throughout

Lower Mississippian time because of the difference in sedimentation rates between shallow and deeper water facies. Models run with more uniform ramp-to-basin sedimentation rates generated homoclinal ramp morphologies, whereas models run with contrasting shallow to deep water sedimentation rates generated steep ramp-slopes to rimmed shelf morphologies (Read *et al.,* submitted).

The modeling points out the paradox of generating thick, laterally extensive intertidal-capped cycles (5th order sea level oscillations <10 m) while generating deep subtidal cycles along the ramp-slope (oscillations ≥20 m). Perhaps storm-wave base was oscillating at a greater rate than sea level due to water density stratification (fluctuating pycnocline), or due to fluctuations in long-term climate-induced wind stress which would influence the depth to storm-wave base. Both processes may be related to orbitally forced climatic changes (Arthur *et al.,* 1984; Rossignol-Strick, 1983).

Alternatively, the amplitudes of 5th order sea level oscillations may fluctuate during a single long-term (3rd to 4th order) sea level cycle. If the long-term sea level oscillations are, in fact, a result of glacio-eustacy (Williams, 1988; Vail *et al.,* 1989), then long-term sea level highstands reflect times of ice melting and high latitude warming, and it would follow that 5th order glacio-eustatic sea level oscillations would also reflect this warming, therefore smaller amplitudes. This difference between 5th order sea level amplitudes during the TST versus the HST would explain

many of the problems pointed out by the modeling, in particular, the predominance of subtidal cycles occurring during the TST with mainly peritidal cycles occurring during the HST.

CONCLUSIONS

1) The Lower Mississippian Lodgepole/lower Madison Formations (20-225 m thick) developed along a broad (>700 km), storm-dominated, cratonic ramp which bordered the Antler foredeep. Subsidence rates (from decompacted sediment thicknesses) across the ramp range between 0.007-0.11 m/k.y. Slopes along the inner and outer ramp were less than 0.08 m/km, while the ramp-slopes were between 0.35-0.9 m/km (less than 0.1°).

2) The ramp-to-basin transition includes thin peritidal cycles consisting of very shallow subtidal deposits overlain by algal-laminated tidal flat facies, which are rarely capped by paleosol/breccia layers. These grade seaward into a broad region of ooid-dominated shallow subtidal cycles which are characterized by stacked ooid shoal deposits or by deeper subtidal facies overlain by ooid-skeletal grainstone caps. Noncyclic intervals within the ooid shoal facies are common. Deep subtidal cycles consist of sub-storm wave base limestone-argillite, overlain by thin-bedded graded limestone, and are capped by storm-deposited skeletal-ooid

grainstone. These cycle types pass basinward into ramp-slope facies which consist of rhythmically interbedded limestone and argillite with local deep-water mud mounds.

3) Average cycle periods, calculated along the outer ramp where the maximum number of cycles occur, range from 30-110 k.y. The cycles likely formed in response to 5th order sea level oscillations with estimated amplitudes of at least 20-25 m, superimposed on long-term (3rd to 4th order) sea level fluctuations. Peritidal cycles developed behind the protection of ooid shoal barriers where accommodation space was lowest. In front of the tidal flats, ooid-dominated shallow subtidal cycles formed over most of the ramp. Deep subtidal cycles developed downslope of ooid shoals, where accommodation was greatest, and were capped by local, reworked skeletal-ooid grainstone facies during 5th order sea lowstands. Ramp-slope rhythmites formed in deeper water below storm-wave base and lack any evidence of facies changes related to 5th order sea level oscillations.

4) The meter-scale cycles are arranged into three depositional sequences (3rd to 4th order) which are recognized by regional-scale, transgressive-regressive facies trends. The ramp margin wedge (RMW), confined to the ramp-slope, consists of shallow and deep subtidal cycles. It developed during 3rd to 4th order lowstand conditions. The transgressive systems tract (TST) which onlapped

the ramp during long-term sea level rise, is dominated by thick deep subtidal and shallow subtidal cycles with peritidal cycles restricted to the inner ramp. The highstand systems tract (HST) developed during the long-term sea level highstand and fall, and on the inner and outer ramp consists of early HST shallow subtidal cycles overlain by thick successions of late HST peritidal cycles; shallow through deep subtidal cycles occur along the ramp-slope.

5) Two-dimensional computer modeling of the cyclic sequences suggests long-term sea level rises were relatively rapid (0.3 m/k.y.), which resulted in RMW drowning and rapid flooding of the outer ramp. This was followed by relatively slow long-term sea level fall rates (0.01-.03). These slow fall rates are suggested by the absence of significant erosion along sequence boundaries (type 2 sequence boundary).

For the assumed depth to storm-wave base (>40 m), 5th order amplitudes of at least 20-25 m were required to generate deep subtidal cycles along the ramp-slope. However, these amplitudes generated poorly developed peritidal cycles during the HST. Alternatively, models run with <10 amplitudes generated peritidal-dominated HSTs, but unreasonably shallow depths to storm-wave base (<25 m) were required to generate deep subtidal cycles along the ramp-slope. The <10 m amplitude oscillations also generated regional intertidal caps during RMW and TST deposition, which is not observed in the actual sequences. Other factors, in addition to 5th

order sea level fluctuations, played a role in the generation of synchronous peritidal and deep subtidal cycle deposition during the HST. These factors may include long-term climatic changes which influenced the depths to storm-wave reworking, or variations in 5th order sea level amplitudes during a single long-term sea level cycle. The likely 10-25 m 5th order amplitudes suggested by the Lower Mississippian cycles are greater than those thought responsible for peritidal cycle-dominated platforms (Bova and Read, 1987; Koerschner and Read, 1989; Goldhammer *et al.*, 1987) but are significantly less than Pleistocene glacio-eustatic oscillations (Shackleton, 1982; Matthews, 1984). These moderate amplitudes may reflect the initial effects of Carboniferous glaciation occuring in Gondwanaland (Crowell, 1978; Veevers and Powell, 1987).

REFERENCES

Aigner, T., 1985, Storm Depositional Systems: *in* Freidman, G. M., Neugebauer, H. J., and Seilacher, A., eds., Springer-Verlag, New York, 173 p.

Anderson, R. Y., Gardner, J. V. and Hemphill-Haley, E., 1989, Variability of the Late Pleistocene-Early Holocene oxygen-minimum zone off northern California: Geophysical Monograph. v. 55, p. 75-84.

Anderson, R. Y., 1982, A long geoclimatic record from the Permian: Jour. Geophys. Research, v. 87, p. 7285-7294.

Arthur, M. A., Dean, W. E., Bottjer, D. J. and Scholle, P. A., 1984, Rhythmic bedding in Mesozoic-Cenozoic pelagic carbonate sequences: The primary and diagenetic origin of Milankovitch-like cycles: *in* Berger, A. L. and others, eds., Milankovitch and Climate: Dordrecht, Netherlands, D. Reidel, p. 191-222.

Atwater, B. F., 1986, Evidence for great Holocene earthquakes along the outer coast of Washington state: Science, v. 236, p. 942-944.

Ball, M. M., 1967, Carbonate sand bodies of Florida and the Bahamas: Jour. Sed. Petrology, v. 37, p. 556-591.

Bathurst, R. G. C., 1975, Carbonate Sediments and Their Diagenesis: Elsevier, Amsterdam, 658 p.

Bissell, H. J. and Barker, H. K., 1977, Deep-water limestones of the Great Blue Formation (Mississippian) in the eastern part of the Cordilleran miogeosyncline in Utah: *in* Enos, P. and Cook, H. E., eds., S.E.P.M. Spec. Pub. 25, p. 171-186.

Bond, G. C. and Kominz, M. A., 1984, Construction of tectonic subsidence curves for the early Paleozoic miogeocline, southern Canadian Rockies: Implications for subsidence mechanisms, age of breakup, and crustal thinning: Geol. Soc. Amer. Bull., v. 95, p. 155-173.

Bond, G. C., Nickeson, P. A. and Kominz, M. A., 1984, Breakup of a supercontinent between 625 Ma and 555 Ma: New evidence and implications for continental histories: Earth and Planetary Science Letters, v. 98, p. 325-345.

Bova, J. A. and Read, J. F., 1987, Incipiently drowned facies within a cyclic peritidal ramp sequence, Early Ordovician Chepultepec interval, Virginia Appalachians: Geol. Soc. Amer. Bull., v. 98, p. 714-727.

Calvet, F. and Tucker, M. E., 1988, Outer ramp cycles in the Upper Muschelkalk of the Catalan Basin, NE Spain: Sed. Geology, v. 57, p. 185-198.

Cisne, J. L., 1986, Earthquakes recorded stratigraphically on carbonate platforms: Nature, v. 323, p. 320-322.

Cloyd, K. C., Demicco, R. V. and Spencer, R, J., 1990, Tidal channel, levee, and crevasse-splay deposits from a Cambrian tidal channel system: A new mechanism to produce shallowing-upward sequences: Jour. Sed. Petrology, v. 60, p. 73-83.

Cotter, E. J., 1966, Waulsortian-type carbonate banks in the Mississippian Lodgepole Formation of central Montana: Jour. Geol., v. 73, p. 881-888.

Crowell, J. C., 1978, Gondwanan glaciation, cyclothems, continental positioning and climate change: Amer. Jour. Science, v. 278, p. 1345-1372.

deBoer, P. L. and Wonders, A. A., 1984, Astronomically induced rhythmic bedding in Cretaceous pelagic sediments near Moria (Italy): *in* Berger, A. L. and others eds., Milankovitch and Climate: Dordrecht, Netherlands, D. Riedel, p. 177-190.

Dorobek, S. L. and Read, J. F., 1986, Sedimentology and basin evolution of the Siluro-Devonian Helderberg Group, central Appalachians: Jour. Sed. Petrology, v. 56, p. 601-613.

Dover, J. H., 1980, Status of the Antler orogeny in central Idaho-clarifications and contraints from the Pioneer Mountains; *in* Fouch, T. D. and Magathan, E. R., eds., Rocky Moutain section, S.E.P.M., Paleozoic Paleogeography of the West-Central United States, Rocky Mountain Paleogeography Symposium 1, p. 371-386.

Enos, P., 1977, Holocene sediment accumulations of the south Florida shelf margin: in Enos, P. and Perkins, R. D., eds., Quaternary Sedimentation in South Florida: Geol. Soc. Amer. Memoir 147, p. 1-130.

Enos, P., 1989, Lag time- is it simply storm-wave base?, *in* Franseen, E.K. and Watney, W.L., eds., Sedimentary Modeling: Computer Simulations of Depositional Systems, Subsurface Geology Series 12, Kansas Geol. Survey, p. 41-42.

Enos, P. and Perkins, R. D., 1979, Evolution of Florida Bay from island stratigraphy: Geol. Soc. Amer. Bull, v. 90, p. 59-83.

Eriksson, K. A. and Simpson, E. L., 1990, Recognition of high-frequency sea-level fluctuations in Proterozoic siliciclastic tidal deposits, Mount Isa, Austrlia: Geology, v. 18, p. 474-477.

Fischer, A. G., 1964, The Lofer cyclothems of the Alpine Triassic: Kansas Geol. Surv. Bull., v. 169, p. 107-149.

Fischer, A. G., Herbert, T. and Premoli-Silva, I., 1985, Carbonate bedding cycles in Cretaceous pelagic and hemipelagic sediments: S.E.P.M. Guidebook 4, p. 1-10.

Friedman, G. M. and Sanders, J. E., 1978, Principles of Sedimentology: Wiley, New York, 792 p.

Ginsburg, R. N., 1971, Landward movement of carbonate mud: New model for regressive cycles in carbonates (abstr.): Amer. Assoc. Petrol. Geol. Bull, v. 55, p. 340.

Goldhammer, R. K., Dunn, P. A. and Hardie, L. A., 1987, High frequency glacio-eustatic sea-level oscillations with Milankovitch characteristics recorded in Middle Triassic platform carbonates in northern Italy: Amer. Jour. Science, v. 287, p. 853-892.

Goldhammer, R. K. and Harris, M. T., 1989, Eustatic controls on the stratigraphy and geometry of the Latemar Buildup (Middle Triassic) the Dolomites of northern Italy: *in* Crevello, P. D. and others eds., Controls on Carbonate Platform and Basin Development, p. 323-338.

Goldhammer, R. K., Dunn, P. A. and Hardie, L. A., 1990, Depositional cycles, composite sea-level changes, cycle stacking patterns, and the hierarchy of stratigraphic forcing: Examples from Alpine Triassic platform carbonates: Geol. Soc. Amer. Bull., v. 102, p. 535-562.

Goodwin, P. W. and Anderson, E. A., 1985, Punctuated aggradational cycles: A general hypothesis of stratigraphic accumulation: Jour. Geology, v. 93, p. 515-533.

Gutschick, R. C., Sandberg, C. A. and Sando, W. J., 1980, Mississippian shelf margin and carbonate platforms from Montana to Nevada: *in* Fouch, T. D. and Magathan, E. R., eds., Rocky Mountain Section, S.E.P.M. Paleozoic Paleogeography of the West-Central United States, Rocky Mountain Paleogeography Symposium 1, p. 111-128.

Gutschick, R. C. and Sandberg, C. A., 1983, Mississippian continential margins of the conterminous United States: *in* S.E.P.M. Spec. Pub. 33, p. 79-96.

Grotzinger, J. P., 1986, Cyclicity and paleoenvironmental dynamics, Rocknest platform, northwest Canada: Geol. Soc. Amer. Bull., v. 97, p. 1208-1231.

Hagan, G. M. and Logan, B. W., 1974, Development of carbonate banks and hypersaline basins, Shark Bay, Western Australia, *in* Evolution and Diagenesis of Quaternary Carbonate Sequences, Shark Bay, Western Australia: A.A.P.G. Memoir 22, p. 61-139.

Handford, C. R., 1986, Facies and bedding sequences in shelf-storm-deposited carbonates; Fayetteville Shale and Pitkin Limestone (Mississippian), Arkansas: Jour. Sed. Petrolgy, v. 56, p. 123-137.

Handford, C. R., 1988, Review of carbonate sand-belt deposition of ooid grainstones and application to Mississippian reservior, Damme Field, southwestern Kansas: Amer. Assoc. Petrol. Geol. Bull. v. 72, p. 1184-1199.

Hardie, L. A. and Ginsburg, R. N., 1977, Layering: the origin and environmental significance of lamination and thin bedding: Baltimore, Maryland, Johns Hopkins University Press, p. 42-76.

Hardie, L. A. and Shinn, E. A., 1986, Carbonate depositional environments, modern and ancient, Part 3: Tidal Flats: Colorado School of Mines Quarterly, v. 81, p. 59-74.

Harris, C. W. and Eriksson, K. A., 1990, Allogenic controls on the evolution of storm to tidal shelf sequences in the Early Proterozoic Uncompahgre Group, southwest Colorado, U.S.A.: Sedimentology, v. 37, p. 189-214.

Harris, P. M., 1979, Facies anatomy and diagenesis of a Bahamian ooid shoal: *in* Sedimenta VII, Ginsburg, R. N., ed., The Comparative Sedimentology Lab, Miami, Florida, 164 p.

Haq, B. U., Hardenbol, J. and Vail, P. R., 1988, Mesozoic and Cenozoic chronostratigraphy and eustatic cycles: *in* Wilgus, C.K. and others, eds., Sea-Level Changes: An Integrated Approach: S.E.P.M. Spec. Pub. 42, p. 71-108.

Hayes, M. D., 1985, Conodonts of the Bakken Formation (Devonian and Mississippian), Williston Basin, North Dakota: The Mountain Geologist, v. 22, p. 64-77.

Hays, J. D., Imbrie, J. and Shackleton, J. J., 1976, Variations in the Earth's orbit: Pacemaker of the ice ages: Science, v.194, p. 1121-1132.

Heckel, P. H., 1986, Sea-level curve for Pennsylvanian eustatic marine transgressive-regressive depositional cycles along mid-continent outcrop belt, North Amrica: Geology, v. 14, p. 330-334.

Herbert, T. D. and Fischer, A. G., 1986, Milankovitch climatic origin of mid-Cretaceous black shale rhythms in central Italy: Nature, v. 321, p. 739-743.

Hine, A. C., 1977, Lily Bank, Bahamas: history of an active oolite sand shoal: Jour. Sed. Petrolgy. v. 47, p. 1554-1581.

Hine, A. C., Wilber, R. J. and Neumann, A. C., 1981, Carbonate sand-bodies along contrasting shallow-bank margins facing open seaways, northern Bahamas: Amer. Assoc. Petrol. Geol. Bull., v. 65, p. 261-290.

James, N. P., 1984, Shallowing-upward sequences in carbonates: *in* Walker, R. G., eds., Facies Models, Second edition: Geoscience Canada, Reprint Series 1, p. 213-228.

Johnson, J. G., Klapper, G. and Sandberg, C. A., 1985, Devonian eustatic fluctuations in Euramerica: Geol. Soc. Amer. Bull., v. 96, p. 567-587.

Kominz, M. A. and Bond, G. C., 1989, Are cyclic sediments periodic?: Subsurface Geology Series 12, Kansas Geol. Survey, p. 35.

Koerschner, W. F. III and Read, J. F., 1989, Field and modelling studies of Cambrian carbonate cycles, Virginia Appalachians: Jour. Sed. Petrology, v. 59, p. 654-687.

Kreisa, R. D., 1981, Storm-generated sedimentary structures in subtidal marine facies with examples from the Middle and Upper Ordovician of southwestern Virginia: Jour. Sed. Petrology, v. 51, p. 823-848.

Lighty, R. G., Macintyre, I. G. and Strinkenrath, R., 1978, Submerged early Holocene barrier reef, southeast Florida shelf: Naure, v. 275, p. 59-60.

Lloyd, R. M., Perkins, R. D. and Derr, S. D., 1987, Beach and shoreface ooid deposition on shallow interior banks, Turks and Caicos islands, British West Indies: Jour. Sed. Petrology, v. 67, p. 976-982.

Logan, B. W., 1969, Carbonate Sediments and Reefs, Yucatan Shelf, Mexico, A.A.P.G. Memoir 11, p. 1-198.

Logan, B. W. and Cebulski, D. E., 1970, Sedimentary environments of Shark Bay, western Australia: *in* Logan, B. W., and others, eds., Carbonate Sedimentation and Environments, Shark Bay, western Australia, A.A.P.G. Memoir 13, 1-37.

Lohmann, K. C., 1976, Lower Dresbachian (Upper Cambrian) platform to deep-shelf transition in eastern Nevada and western Utah: An evaluation through lithologic cycle correlation: in Robison, R. A. and Rowell, A. J., eds., Paleontology and depositional environments: Cambrian of western North America: Brigham Young Univ. Geol. Studies, v. 23, p. 111-122.

Loreau, J. P. and Purser, B. H., 1973, Distribution and ultrastructure of Holocene ooids in the Persian Gulf, *in* Purser, B. H., ed., The Persian Gulf: Springer-Verlag, New York, p. 279-328.

Markello, J. R. and Read, J. F., 1981, Carbonate ramp-to-deeper shale shelf transitions of an Upper Cambrian intrashelf basin, Nolichucky Formation, southwest Virginia Appalachians: Sedimentology, v. 28, p. 573-597.

Matthews, R. K., 1984, Dynamic Stratigraphy: An Introduction to Sedimentation and Stratigraphy: Second edition: Englewood Cliffs, New Jersey, Prentice-Hall Inc.

Matthews, R. K. and Poore, R. Z., 1980, Tertiary $\partial^{18}O$ record and glacio-eustatic sea-level fluctuations: Geology, v. 8, p. 501-504.

McMannis, W. J., 1965, Resume of depositional and structural history of western Montana: Amer. Assoc. Petrol. Geol. Bull., v. 49, p. 1801-1823.

Middleton, G. V., 1961, Evaporite solution breccias from the Mississippian of southwestern Montana: Jour. Sed. Petrology, v. 31, p. 189-195.

Milliman, J. D., 1974, Marine Carbonates: Springer-Verlag, New York, 375 p.

Moore, T. C., Loutit, T. S. and Greenlee, S. M., 1987, Estimating short-term changes in sea level: Paleoceanography, v. 2., p. 625-637.

Neumann, A. C. and Land, L. S., 1975, Lime mud deposition and calcareous algae in the Bight of Abaco, Bahamas: a budget: Jour. Sed. Petrology. v. 45, p. 763-786.

Niemann, J. C. and Read, J. F., 1988, Regional cementation from unconformity-recharged aquifer and burial fluids, Mississippian Newman Limstone, Kentucky: Jour. Sed. Petrology, v. 58, p. 688-705.

Olsen, C. R., 1978, Sedimentation rates: *in* Fairbridge, R. W. and Bourgeois, J., eds., The Encyclopedia of Sedimentology, Dowden Hutchinson and Ross, Inc., Stroudsburg, Pa., p. 687-692.

Olsen, P. E., 1986, A 40-million-year lake record of Early Mesozoic orbital climatic forcing: Science, v. 234, p. 842-848.

Palmer, A. R., 1983, The Decade of North American Geology 1983 geologic time scale: Geology, v. 11, p. 503-504.

Peterson J. A. and Smith, D. L., 1988, Rocky Mountain paleogeography through geologic time: *in* Peterson, J. A., ed., Paleotectonics and Sedimentation in the Rocky Mountain Region, U.S., A.A.P.G. Memoir 41, p. 3-19.

Poole, F. G. and Sandberg, C. A., 1977: Mississippian paleogeography and tectonics of the western United States: *in* Stewart, J. H. and others, eds., Paleozoic Paleogeography of the Western United States, S.E.P.M. Pacific Coast Paleogegraphy Symposium 1, p. 67-86.

Pratt, B. R. and James, N. P., 1988, The St. George Group (Lower Ordovician) of western Newfoundland: tidal flat island model for carbonate sedimentation in shallow epeiric seas: Sedimentology, v. 33, p. 313-343.

Purser, B. H., 1973, Sedimentation around bathymetric highs in the southern Persian Gulf: *in* Purser, B. H., ed., The Persian Gulf: Springer-Verlag, New York, p. 157-178.

Purser, B. H. and Evans, G.,1973, Regional sedimentation along the Trucial Coast, SE Persian Gulf: *in* Purser, B. H., ed., The Persian Gulf: Springer-Verlag, New York, p. 211-231.

Purser, B H. and Seibold, E.,1973, The principal environmental factors influencing Holocene sedimentation and diagenesis in the Persian Gulf: *in* Purser, B. H., ed., The Persian Gulf: Springer-Verlag, New York, p. 1-10.

Read, J. F., 1980, Carbonate ramp-to-basin transitions and foreland basin evolution, Middle Ordovician, Virginia Appalachians: Amer. Assoc. Petrol. Geol. Bull., v. 64, p. 1575-1612.

Read, J. F., 1985, Carbonate platform facies models: Amer. Assoc. Petrol. Geol. Bull., v. 66, p. 860-878.

Read, J. F., Grotzinger, J. P., Bova, J. A. and Koerschner, W. F., 1986, Models for generation of carbonate cycles: Geology, v. 14, p. 107-110.

Read, J. F. and Goldhammer, R. K., 1988, Use of Fischer plots to define 3rd order sea level curves in peritidal cyclic carbonates, Ordovician, Appalachians: Geology, v. 16, p. 895-899.

Read, J. F., Osleger, D. A and Elrick, M., Two-dimensional modelling of carbonate ramp sequences and component cycles (submitted).

Reading, H. G., 1986, Sedimentary Environments and Facies: Blackwell, London, 615 p.

Rodriguez, J. and Gutschick, R.C., 1970, Late Devonian-Early Mississippian ichnofossils from western Montana and northern Utah: *in* Crimes, T.P. and Harper, J.C. eds., Trace Fossils: Seel House Press, Liverpool, p. 407-438.

Ross, C. A. and Ross, J. R. P., 1987, Late Paleozoic sea levels and depositional sequences: *in* Ross, C. A. and Haman, D., eds., Timing and Depositional History of Eustatic Sequences: Constraints on Seismic Stratigraphy: Cushman Foundation for Foraminiferal Research, Spec. Pub. 4, p. 137-149.

Ross, C. A. and Ross, J. R. P., 1988, Late Paleozoic transgressive regressive deposition, *in* Wilgus, C.K. and others, eds., Sea-Level Changes: An Integrated Approach: S.E.P.M. Spec. Pub. 42, 156-181.

Rossignol-Strick, M., 1983, African monsoon, an immediate climate response to orbital insolation: Nature, v. 304, p. 46-49.

Sandberg, C. A. and Klapper, G., 1967, Stratigraphy, age and paleotectonic significance of the Cottonwood Canyon Member of the Madison Limestone in Wyoming and Montana: U.S.G.S. Bull. 1251-B, 70 p.

Sandberg, C. A. and Gutschick, R. C., 1983, Early carboniferous conodont biofacies and paleoecologic models: Geol. Soc. Amer. Abst. with Prog., v. 15, p. 221.

Sandberg, C. A., Gutschick, R. C., Johnson, J. G., Poole, F. G. and Sando, W. J., 1983, Middle Devonian to Late Mississippian geologic history of the Overthrust belt region, western United States: *in* Powers, R. B., ed., Geologic Studies of the Cordilleran Thrust Belt, v. 2: Denver, Rocky Mountain Assoc. Geol., p. 691-719.

Sando, W. J., 1976, Mississippian history of the northern Rocky Mountains region: Jour. Research U. S. Geological Survey, v. 4, p. 317-338.

Sando, W. J., 1982, New members of the Madison Limestone (Devonian and Mississippian), north-central Wyoming and southern Montana: Contributions to stratigraphy, U.S.G.S. Bull. 1529-H, p. H125-H130.

Sando, W. J., 1985, Revised Mississippian time scale, western interior region, conterminous United States: U. S. Geological Survey Bull. 1605-A p. A15-A26.

Sando, W. J., 1988, Madison Limestone (Mississippian) Paleokarst: a geologic synthesis: *in* James, N. P. and Choquette, P. W., Paleokarst, Springer-Verlag, New York, p. 256-277.

Sarg, J. F., 1988, Carbonate sequence stratigraphy: *in* Wilgus, C.K. and others, eds., Sea-Level Changes: An Integrated Approach: S.E.P.M. Spec. Pub. 42, p. 56-181.

Schlager, W., 1981, The paradox of drowned reefs and carbonate platforms: Geol. Soc. Amer. Bull., v. 92, p. 197-211.

Scholle, P. A., Arthur, M. A. and Ekdale, A. A., 1983, Pelagic environment: *in* Scholle, P. A., and others eds., Carbonate Depositional Environments, A.A.P.G. Memoir 33, p. 619-691.

Scotese, C. R., Bambach, R. K., Barton, C., Van der Voo, R. and Ziegler, A. M., 1979, Paleozoic base maps: Jour. Geology, v. 87. p. 217-227.

Shackleton, D. F., 1982, The deep-sea record of climate variablility: Progress in Oceanography, v. 199-218.

Smith, D. L., 1977, Transition from deep- to shallow-water carbonates, Paine Member, Lodgepole Formation, central Montana: *in* Enos, P. and Cook, H. E., eds., S.E.P.M. Spec. Pub. 25, p. 87-201.

Smith, D. L., 1982, Waulsortian bioherms in the Paine Member of the Lodgepole Limestone (Kinderhookian) of Montana, U.S.A., *in* Symposium on the Paleoenvironmental Setting and Distribution of the Waulsortian Facies: El Paso, University of Texas, p. 51-64.

Sneeden, J. W., Nummendal, D. and Amos, A. F., 1988, Storm- and fair-weather combined flow on the central Texas continental shelf: Jour. Sed. Petrolgy., v. 58, p. 580-595.

Speed, R. C. and Sleep, N. H., 1982, Antler orogeny and foreland basin: A model: Geol. Soc. Amer. Bull., v. 93, p. 815-828.

Steckler, M. S. and Watts, A. B., 1978, Subsidence history and tectonic evolution of Atlantic-type continental margins: *in* Scrutton, R. A., ed., Dynamics of passive margins: American Geophysical Union Geodynamics Series, p. 184-196.

Stockman, K. W., Ginsburg, R. N. and Shinn, E. A., 1967, The production of lime mud in south Florida: Jour. Sed. Petrolgy. v. 37, p. 633-648.

Stone, R. A., 1972, Waulsortian-type bioherms (reefs) of Mississippian age, central Bridger Range, Montana: *in* Montana Geol. Soc. Guidebook, p. 37-55.

Strasser, A., 1988, Shallow-upward sequences in the Purbeckian peritidal carbonates (lowermost Cretaceous, Swiss and French Jura Mountains): Sedimentology, v. 35, 369-383.

Swift, K. J. P. and Nummedal, D. 1987, HCS, tropical hurricanes, and intense winter storms: Sedimentology, v. 34, p. 338-344.

Vail, P. R., Mitchum, R. M. and Thompson, S., 1977, Seismic stratigraphy and global changes of sea level, Part 4-Global cycles of relative changes of sea level: *in* Seismic Stratigraphy-Applications to Hydrocarbon Exploration: A.A.P.G. Memoir 26, p. 83-97.

Vail, P. R., Bowman, S. A. and Ross, M. I., 1989, Sedimentary systems: Amer. Geophy. Union Conf. on Long-term Sea Level Changes: abstracts, Snowbird, Utah.

Van Wagoner, J. C., Posamentier, H. W., Mitchum, R. M., Vail, P. R., Sarg, J. F., Loutit, T. S. and Hardenbol, J., 1988, An overview of the fundamentals of sequence stratigraphy and key definitions: *in* Wilgus, C.K. and others, eds., Sea-Level Changes: An Integrated Approach: S.E.P.M. Spec. Pub. 42, p. 39-45.

Veevers, J. J. and Powell, McA. C., 1987, Late Paleozoic glacial episodes in Gondwandaland reflected in transgressive-regressive depositional sequences in Euramerica: Geol. Soc. Amer. Bull., v. 98, p. 475-487.

Wagner, C. W. and van der Togt, C., 1973, Holocene sediment types and their distribution in the southern Persian Gulf: *in* Purser, B. H., ed., The Persian Gulf: Springer-Verlag, New York, p. 123-156.

Walker, R. G., 1884, Shelf sands and shallow marine sands: *in* Walker, R.G., ed., Facies Models, Second edition: Geoscience Canada, Reprint Series 1, p. 141-170.

Weedon, G. P., 1986, Hemipelagic shelf sedimentation and climatic cycles: the basal Jurassic (Blue Lias) of south Britian: Earth Planetary Sci. Letters., v. 76, p. 321-335.

Wilkinson, B. R., 1982, Cyclic cratonic carbonates and Phanerozic calcite seas: Jour. Geologic Education, v. 30, p. 180-203.

Williams, D. F., 1988, Evidence for and against sea level changes from the stable isotopic record of the Cenozoic: *in* Wilgus, C.K. and others, eds., Sea-Level Changes: An Integrated Approach: S.E.P.M. Spec. Pub. 42, p. 31-36.

Wilson, J. L., 1975, Carbonate Facies in Geologic History: Springer-Verlag, New York, 470 p.

Witzke, B. J., 1990, Palaeoclimatic constraints for Palaeozoic Palaeolatitudes of Laurentia and Euroamerica: *in* McKerrow, W.

S. and Scotese, C. R., eds., Palaezoic Palaeogegraphy and Biogeography, Geo. Soc. Amer. Memoir 12, p. 57-73.

Wong, P. K. and Oldershaw, A. E., 1980, Causes of cyclicity in reef interior sediments, Kabob Reef, Alberta: Bull. Can. Petrol. Geol. v. 28, p. 411-425.

Woodward, L. A., 1981, Tectonic framework of the disturbed belt of west-central Montana: Amer. Assoc. Petrol. Geol. Bull., v. 65, p. 291-302.

Wright, R., 1986, Cycle stratigraphy as a paleogeographic tool: Point Lookout Sandstone, southeastern San Juan Basin, New Mexico: Geol. Soc. Amer. Bull., v. 96, p. 661-673.

Wright, V. P., 1986, Peritidal carbonate facies: a review: Geol. Jour. v. 19, p. 309-325.

Yurewicz, D. A., 1977, Sedimentology of MIssissippian Basin-facies carbonates, New Mexico and west Texas- the Rancheria Formation: *in* Enos, P. and Cook, H. E., eds., S.E.P.M. Spec. Pub. 25, p. 203-219.

Ziegler, A. M., Scotese, C. R., McKerrow, W. S., Johnson, M. E. and Bambach, R. K., 1979, Paleozoic Paleogegraphy: Ann. Review Earth Science, v. 7, p. 473-502.

SHORT-TERM PALEOCLIMATIC FLUCTUATIONS IN RHYTHMICALLY BEDDED RAMP-SLOPE DEPOSITS, LOWER MISSISSIPPIAN OF SOUTHWESTERN MONTANA

ABSTRACT

Ramp-slope deposits of the Lower Mississippian Paine Member of the Lodgepole Formation (60-80 m thick) are characterized by thin, rhythmically interbedded limestone and argillaceous limestone (argillite). Limestone-argillite couplets (10-40 cm thick) are bundled into fourth-order (<1.0 m.y.) shallowing-upward sequences (8-39 m thick). Poorly fossiliferous limestone layers, which consist of spiculitic lime mudstone to laminated pellet packstone are interpreted as distal storm deposits. Argillite layers, which consist of burrowed, bryozoan-crinoid argillaceous limestone were deposited in quiet-water. The rhythmic interbedding of these contrasting rock types suggests periodic fluctuations in storm activity alternating with times of little or no storm activity. Time-equivalent shallow and deep ramp deposits of Wyoming and southwestern Montana consist of meter-scale, shallowing-upward cycles which are stacked into larger scale (3rd to 4th order) depositional sequences.

Spectral analysis of the fluctuating siliciclastic component (HCl insoluble residues) indicate a dominant 0.7-2.9 k.y. periodicity in the deep-water deposits. Similar ≈2.5 k.y. periodicities are recorded in Quaternary continental and alpine glaciers, Quaternary deep-sea deposits, Holocene tree rings, and in Permian deep-water evaporite varves. This short-term paleoclimatic signal may represent one of several harmonics of the periods of the Earth's

changing orbital parameters or it may be due to fluctuations in solar activity.

Typical Milankovitch-type periods (≈20-100 k.y.) were not recorded in the insoluble residue data suggesting that the contrasts in storm activity were not intensified by orbitally forced climatic changes. However, the range of thicknesses of the 4th order shallowing-upward sequences suggest that longer term sea level fluctuations affected the depositional patterns along the ramp-slope.

INTRODUCTION

Rhythmic interbedding of limestone and siliciclastic-rich layers is a common feature in many basinal and deep-sea settings. The decimeter-scale rhythmicity has been attributed to climatic (Arthur *et al.,* 1984; deBoer and Wonders, 1984; Herbert and Fischer, 1986; Weedon, 1986), eustatic (King, 1990), and diagenetic changes (Hallam, 1964; Eder, 1982; Ricken, 1986). These types of deep-water deposits preserve a relatively continuous record of sedimentation, thus they may be utilized to estimate the periodicity and ultimately the origin of the rhythmic interbedding. Many studies of Mesozoic-Cenozoic pelagic deposits suggest the periods of the rhythms are between 20-100 k.y. (deBoer and Wonders, 1984; Fischer and Schwarzacher, 1984; Herbert and Fischer, 1986; Weedon, 1986; Kate and Sprenger, 1989) and were the result of climatic fluctuations related to the Earth's changing orbital parameters (Milankovitch climatic forcing; Hays *et al.,* 1976). This paper discusses the results of spectral analysis of a finely sampled interval of rhythmically interbedded deep-water deposits of Mississippian age which record very short-term periodicities distinct from typical Milankovitch-type periods.

SETTING AND STRATIGRAPHY

Ramp-slope deposits of the Lower Mississippian (Kinderhookian) Paine Member of the Lodgepole Formation occur central Montana, western Wyoming, and eastern Idaho (Fig. 19). The ramp-slope was bordered on the east by a cratonic ramp and on the west by the Antler foredeep and orogenic highlands (Fig. 19). The Paine Member was deposited during a third order (≈1 m.y.) sea level rise that is recognized throughout the western U. S. (Sando, 1976; Sandberg *et al.,* 1983) and worldwide by Ross and Ross (1987, 1988). Laterally equivalent shallow ramp and overlying deep ramp deposits are characterized by 1-10 m thick shallowing-upward cycles which are stacked within 3rd and 4th order depositional sequences (Fig. 20).

The section sampled for this study is located in the Bridger Range, approximately 30 km north of the town of Bozeman, Montana (Fig. 19). At this location, the Paine Member is 80 m thick and composed of dark, rhythmically interbedded limestone and argillaceous limestone (argillite) which is bundled into four shallowing-upward sequences which are recognized by upsection increases in limestone and argillite bed thickness, and abundance and diversity of skeletal and trace fossils (Fig. 20). Deep-water mud mounds (18-20 m tall) occur 35 m from the base of the section (Fig. 20; Stone, 1972; Smith, 1977).

Figure 19. Major paleogeographic and tectonic features of the northern Rocky Mountains during Mississippian time as well as the Mesozoic-Cenozic Sevier thrust belt. The sampled stratigraphic section indicated by star. Cyclic shallow and deep ramp cyclic ramp deposits occur along cratonic ramp.

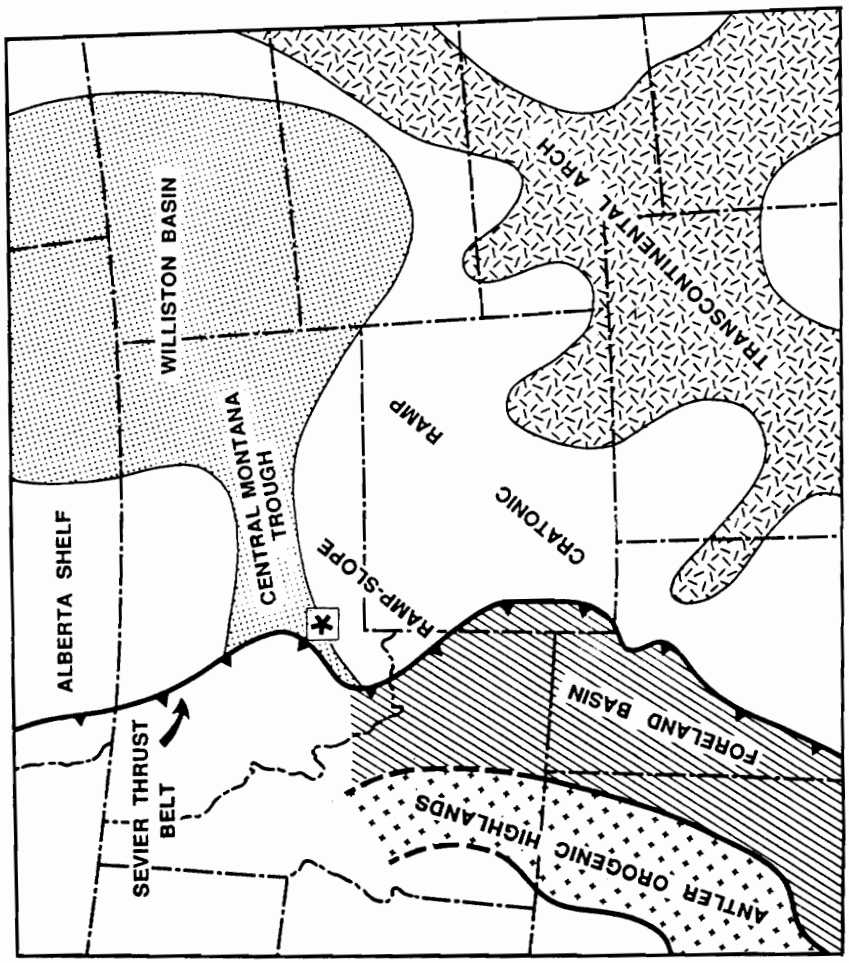
WILLISTON BASIN
TRANSCONTINENTAL ARCH
CENTRAL MONTANA TROUGH
RAMP
CRATONIC
ALBERTA SHELF
RAMP-SLOPE
FORELAND BASIN
SEVIER THRUST BELT
ANTLER OROGENIC HIGHLANDS

Figure 20. Lower depositional sequence (decompacted thicknesses) of the Lodgepole/lower Madison Formations from southeastern Wyoming to southwestern Montana (down-dip cross-section; >700 km). Shown to left is enlarged stratigraphic column of sample section with four shallowing-upward sequences (labeled 1-4) and sampled interval.

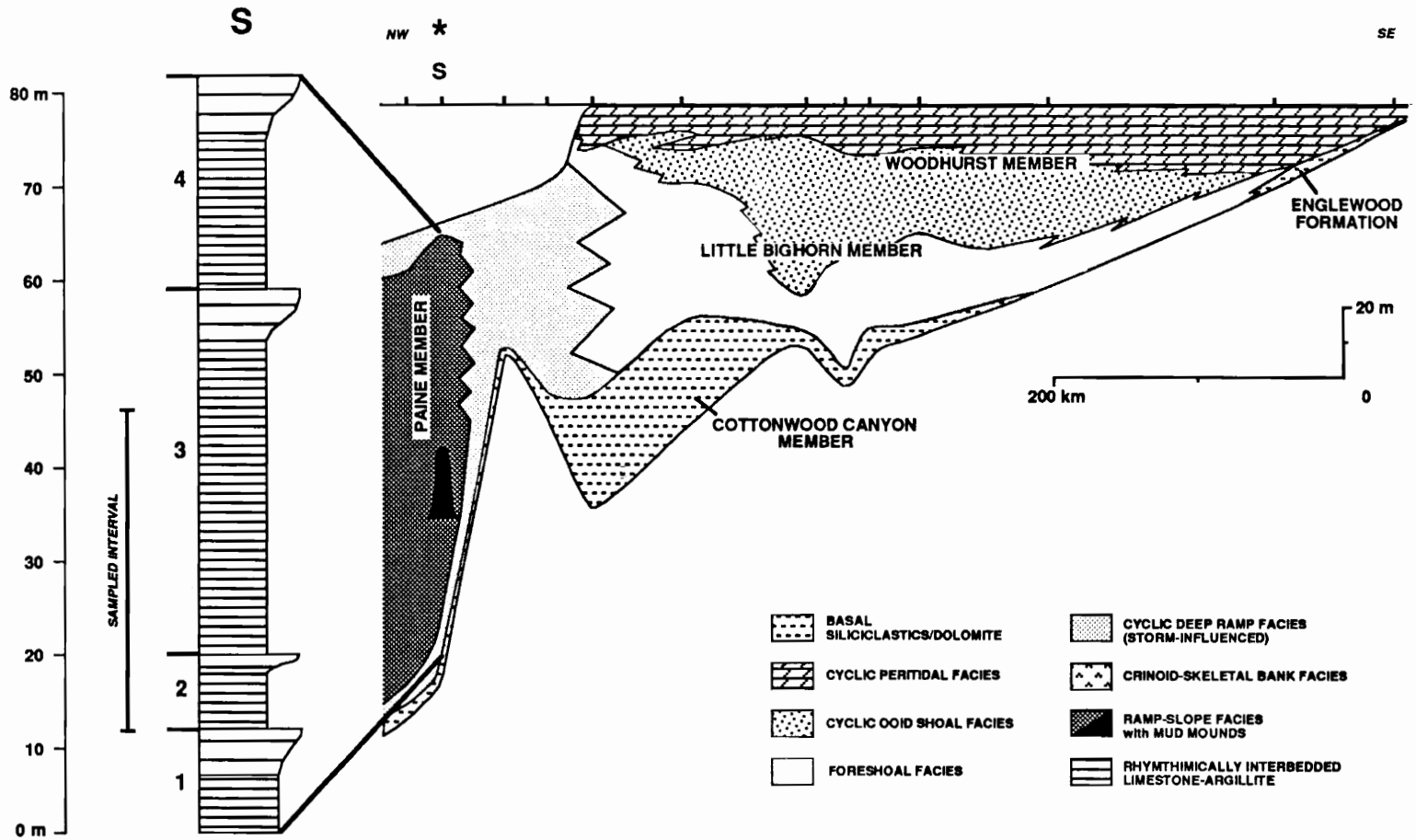
S
NW
S
SE
80 m
70
60
50
40
30
20
10
0 m
4
3
2
1
SAMPLED INTERVAL
PAINE MEMBER
WOODHURST MEMBER
LITTLE BIGHORN MEMBER
ENGLEWOOD FORMATION
COTTONWOOD CANYON MEMBER
20 m
0
200 km
BASAL SILICICLASTICS/DOLOMITE
CYCLIC PERITIDAL FACIES
CYCLIC OOID SHOAL FACIES
FORESHOAL FACIES
CYCLIC DEEP RAMP FACIES (STORM-INFLUENCED)
CRINOID-SKELETAL BANK FACIES
RAMP-SLOPE FACIES with MUD MOUNDS
RHYMTHIMICALLY INTERBEDDED LIMESTONE-ARGILLITE

METHODS

The section was sampled for spectral analysis to determine if a climatic signal was preserved in the deposits and to compare the deep-water signal with those recorded in laterally equivalent shallowing-upward cycles within cratonic ramp deposits (Fig. 20). A 3 cm sampling interval was chosen so that each argillite layer was represented. Samples were collected over 36 m of section by drilling into fresh outcrop with a battery powered handrill, equipped with a 0.6 cm masonry drill bit. Powdered samples (≈1.0 grams) were weighed, and dissolved in 0.5N HCl for 24 hours. The remaining insoluble residues were filtered through pre-weighed 1.5 μm filter papers, dried for 24 hours, and reweighed to calculate the weight percent (wt%) insoluble residues. Calculated errors on this technique were less than 5%.

The insoluble residue time-series was analyzed by Maximum Entropy Spectral Estimation (MESE) and Fast Fourier Transform (FFT) methods (Kanasewich, 1981) on a VAX computer; both methods produced similar results.

LITHOLOGIES

Limestone-argillite couplets are between 10-40 cm thick and average 10 cm in thickness (Figs. 21A and 21B). *Limestone layers* (5-30 cm thick) are gray-brown in color consist of spiculitic lime mudstone and poorly fossiliferous laminated pellet packstone. The insoluble residue content ranges from 3-16 wt% and consists of quartz silt, muscovite/illite (<100 μm), (determined from x-ray diffraction analysis) and organic matter. Rare fossils include fenestrate bryozoan, crinoids, and rugose corals which are found upright, in life position. Spiculitic mudstone layers are moderately bioturbated with rare preservation of fine laminations. The laminae in pelleted beds are millimeter-thick, planar to wavy graded layers composed of pellet silt and mud (Fig. 22B). Upper and lower contacts of limestone layers are gradational (over 10-15 mm) and are laterally continuous over the width of the outcrop (>50 m).

Argillite layers (1-10 cm thick) are yellow gray in color and composed of bryozoan-crinoid wackestone (matrix composed of argillaceous microspar with sparse <100 μm dolomite rhombs; Fig. 22B). The insoluble residue content ranges from 5-60 wt% and consists of quartz silt, muscovite/illite (<100 μm), and organic matter. Skeletal material includes large fragments of fenestrate bryozoan, articulated crinoid stems and caylxes, thin-walled brachiopods, and abundant trace fossils (*Zoophycus, Chondrites, Cosmoraphe(?), and Scalarituba*; Rodriguez and Gutschick, 1970). No

Figure 21.

A) Photograph of rhythmically interbedded limestone and argillite ramp-slope deposits. Scale bar is approximately 1 meter.

B) Close-up photograph of interbedded limestone and argillite.

A
B
0
5
10 CM

Figure 22.

A) Photomicrograph of finely laminated limestone layer. Fining-upward laminae consist of pellets and very fine skeletal debris (light layers) which grade into pelletal-calcisiltite (dark layers). Scale bar represents 0.5 mm.

B) Photomicrograph of bryozoan-crinoidal argillite layer. Note the absence of textural grading and large, unabraded skeletal material lacking evidence of significant pressure solution dissolution. Scale bar represents 0.5 mm.

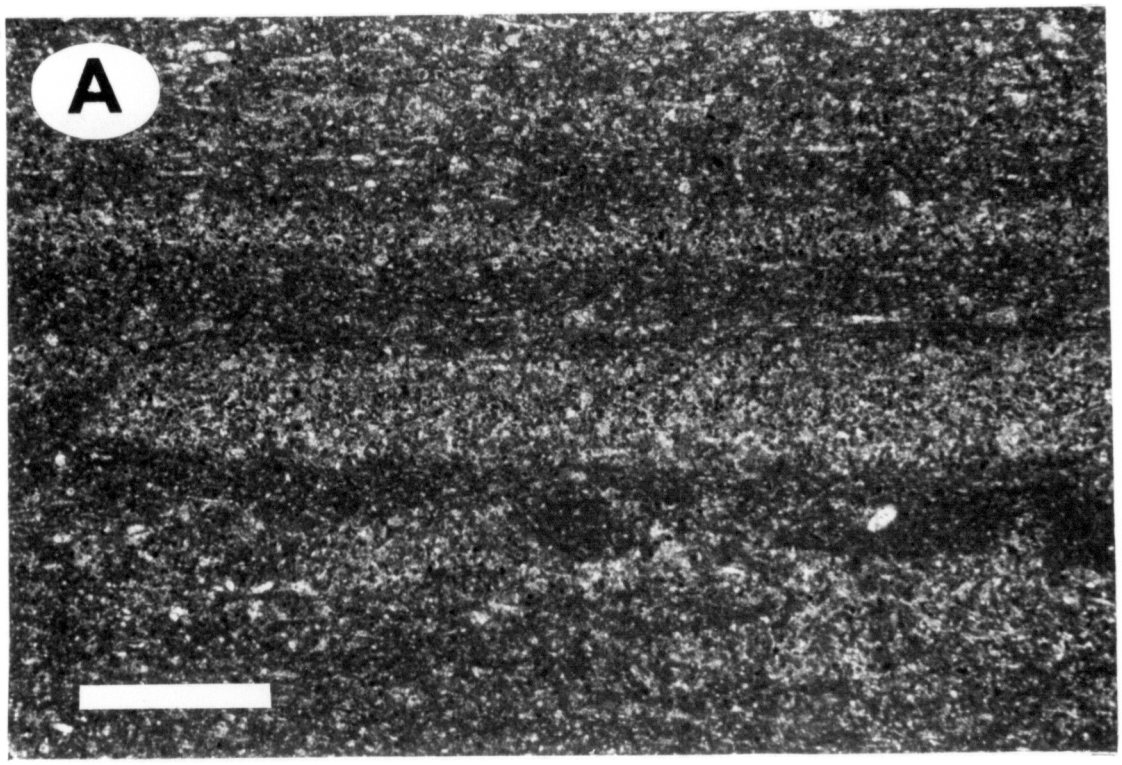
A

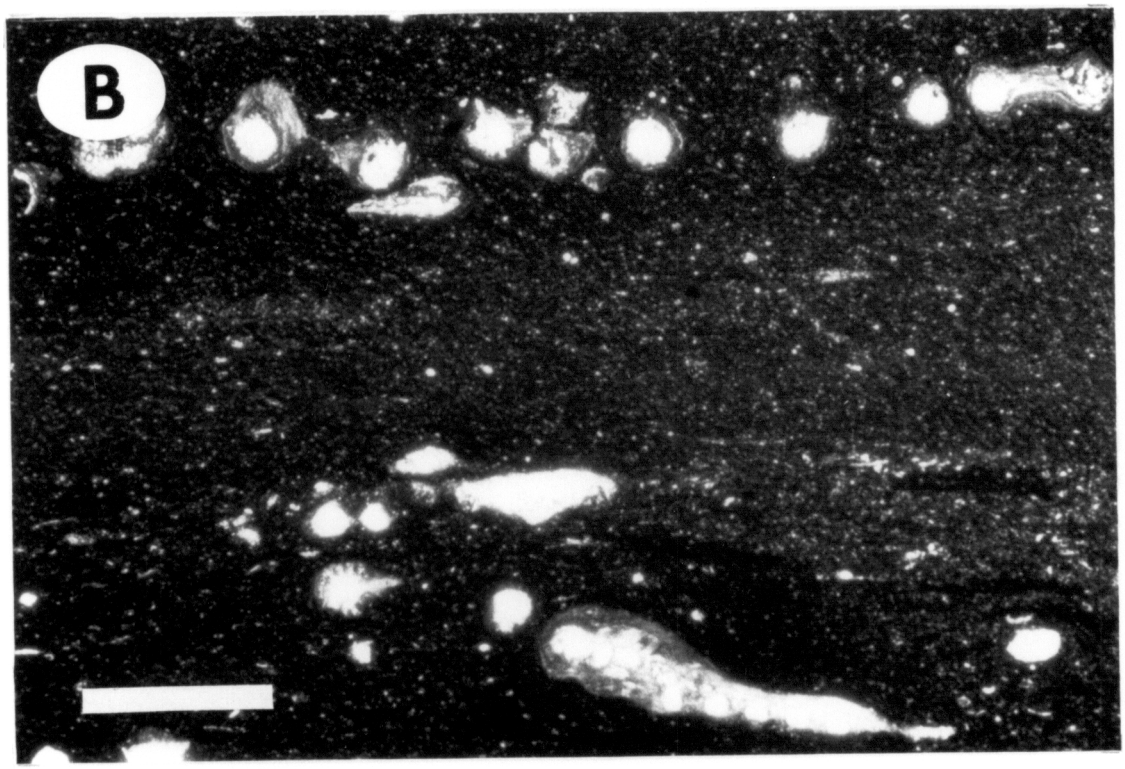
B

sedimentary structures or textural grading was observed. Argillite layers average 3 cm in thickness; layers >3 cm thick are laterally continuous over the entire width of the outcrop; layers less than 1-2 cm thick commonly pinch-out or coalesce with thicker argillite layers.

Interbedding of limestone and argillite is a primary depositional feature. This is in contrast to "diagenetic unmixing" processes (Hallam, 1964; Ricken, 1986) in which originally homogeneous argillaceous limestone is separated into calcareous and argillaceous rich layers during compaction and pressure solution. Primary interbedding is indicated by 1) burrows in argillite layers are commonly filled with limestone from the overlying bed, 2) delicate fossils within argillite layers show little evidence of dissolution (Fig. 22B), 3) thin, graded layers are preserved, and 4) the lateral continuity of bedding. Post-depositional compaction and pressure solution have enhanced primary differences in layering. Petrographic examination of burrow fabrics within limestone-argillite layers suggest limestone beds compacted less than 30-40%, whereas argillite layers compacted approximately 50-70%.

DEPOSITIONAL INTERPRETATION

The fine-grained, limestone-argillite deposits lack evidence of current- or wave-reworking, and are locally associated with mud mounds whose syn-depositional relief above the sea floor was >20 m (Stone, 1972). This suggests the rhythmic limestone-argillite facies was deposited below storm-wave base in water depths >60 m (assuming a 40 m storm-wave base; Purser and Evans, 1973; Friedman and Sanders, 1978; Sneeden *et al.*, 1988). These water depths preclude their formation as a result of fluctuations in the calcium carbonate compensation depth, CCD (Einsele, 1982; Arthur *et al.,* 1986). Calcareous plankton, a major source of modern deep water deposits, did not evolve until the Mesozoic (Bathurst, 1975); therefore, the Lower Mississippian deep-water deposits were derived entirely from shallow-water carbonate and terrigenous sources. The rhythmic interbedding cannot be attributed to fluctuating deep sea carbonate productivity or dissolution (Einsele, 1982), thus must be related to the availability and transport of the calcareous and terrigenous material.

The difference in color, fossil abundance, and sedimentary structures in limestone and argillite layers indicates contrasting depositional conditions.

Limestone layers: The fine, graded laminae within pelleted limestone layers and less commonly within spiculitic mudstone layers represent suspension deposition from dilute storm-generated currents. A storm origin is supported by the occurrence of overlying cyclic deep ramp deposits which are composed of hummocky stratified, wave-rippled, and graded deposits (Chapter 1). Storm-generated waves and currents suspended deep ramp lime muds and silts and transported the material basinward (>70 km) and perhaps parallel to isobaths; i.e., geostrophic currents (Swift and Nummedal, 1987; Sneeden *et al.,* 1988). Moderate bioturbation and rare skeletal material indicates the bottom waters were not fully anoxic. Preservation of fine laminae may be the result of relatively rapid sedimentation rates which is supported by the in life position of bryozoan, crinoids, and corals. Similar finely laminated distal storm deposits are described by Kreisa (1981), Pedersen (1985), Aigner (1985), Handford (1986), and Calvet and Tucker (1988).

Argillite layers: Argillite layers lack current- or wave-transport features and contain large, unabraded skeletal fragments indicating deposition in well-oxygenated, quiet-water. The siliciclastic material was derived from the Transcontinental Arch or the Antler orogenic highlands (Fig. 19) and was likely transported into the ramp-slope environment by very weak storm-generated or nephaloid currents (Dean *et al.,* 1981). Presumably an increase in river discharge would increase the density of nephaloid layers resulting in greater transport distances (Dean *et al.,* 1981).

The rhythmic alternation of limestone (storm) and argillite (quiet-water) layers may be the result of relatively continuous siliciclastic influx with fluctuating carbonate storm deposition (carbonate dilution). This is supported by the occurrence of siliciclastic material in both limestone and argillite layers and the abundance of large, unabraded fossil material in argillite layers which indicates little or no storm activity occurred during argillite intervals. The interbedding may also be a result of continuous carbonate storm deposition with fluctuating siliciclicastc influx (siliciclastic dilution), presumably from increased river discharge during wetter climates. This is supported by the fact that it would require large magnitudes of carbonate fluctuation (with constant siliciclastic influx) to produce the limestone-argillite interbeds, whereas much smaller magnitudes of siliciclastic fluctuation would produce similar limestone-argillite interbeds (Einsele, 1982). Alternatively, the interbedding may be the result of carbonate storm deposition alternating with siliciclastic deposition. This interpretation implies both components fluctuated out of phase with respect to each other, however increased storm activity would presumably correspond to greater rainfall and increased river discharge. Without separate measurements of a third component common to both layers (i.e., organic matter; Ricken, 1989), it is not possible to determine which of the components was fluctuating to produce the rhythmic interbedding.

Regardless of which specific mechanism might have occurred, the rhythmicity is likely the result of periodic climate fluctuations which affected storm tracks and rainfall patterns, i.e., periods of intensified storm activity alternating with periods of little or no storm activity.

SPECTRAL ANALYSIS

The wt% insoluble residues were plotted as a function of stratigraphic thickness (Figs. 23 and 24). Figure 23 is an enlarged segment of the insoluble time series illustrating the difference in wt% insoluble residues in limestone versus argillite layers. Limestone layers have relatively low and constant wt% insoluble residues, whereas argillite layers have relatively high and variable wt% insoluble residues and plot as distinct peaks (Fig. 23).

To interpret the result of the spectral analysis, stratigraphic thickness was converted to time using long-term accumulation rates (present-day stratigraphic thickness divided by the age duration of the interval). The Lower Mississippian (Tournasian-Visean stages) is 27 m.y. +/- 16 m.y. in duration (DNAG time scale; Palmer, 1983; Sando, 1985). Using these maximum and minimum age durations, the Paine Member at the sampled section is between 0.44-1.8 m.y. in duration, which corresponds to accumulation rates between 0.04-0.18 m/k.y. These values are average rates for both limestone

Figure 23. Enlarged portion of the insoluble residue time-series data. Horizontal axis is stratigraphic thickness with 3 cm sampling interval. Stippled pattern represents argillite layers; plain pattern represents limestone layers. Note limestone layers have relatively low and constant insoluble residue values, while argillite layers have variable values and plot as distinct peaks.

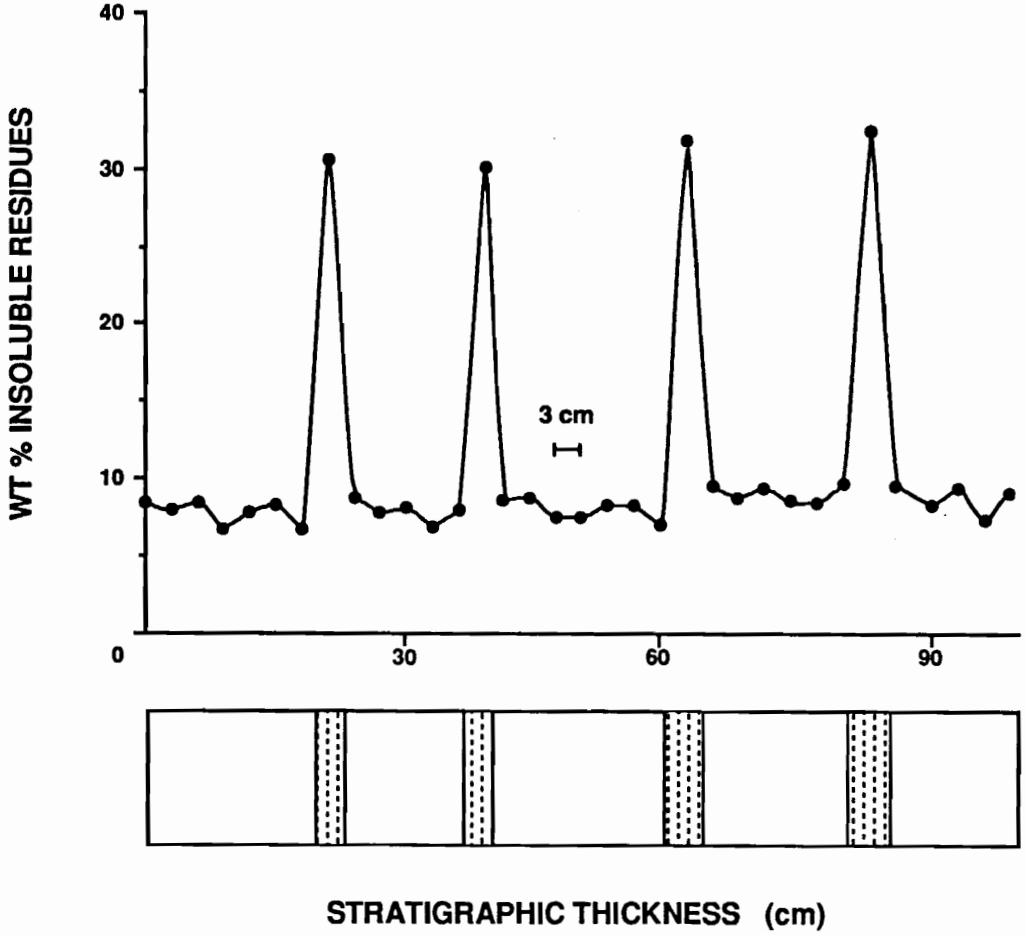
WT % INSOLUBLE RESIDUES
40
30
20
10
0
3 cm
30
60
90
STRATIGRAPHIC THICKNESS (cm)

Figure 24. Complete insoluble residue time-series representing 36 m of sampled section (raw time-series data, not debiased).

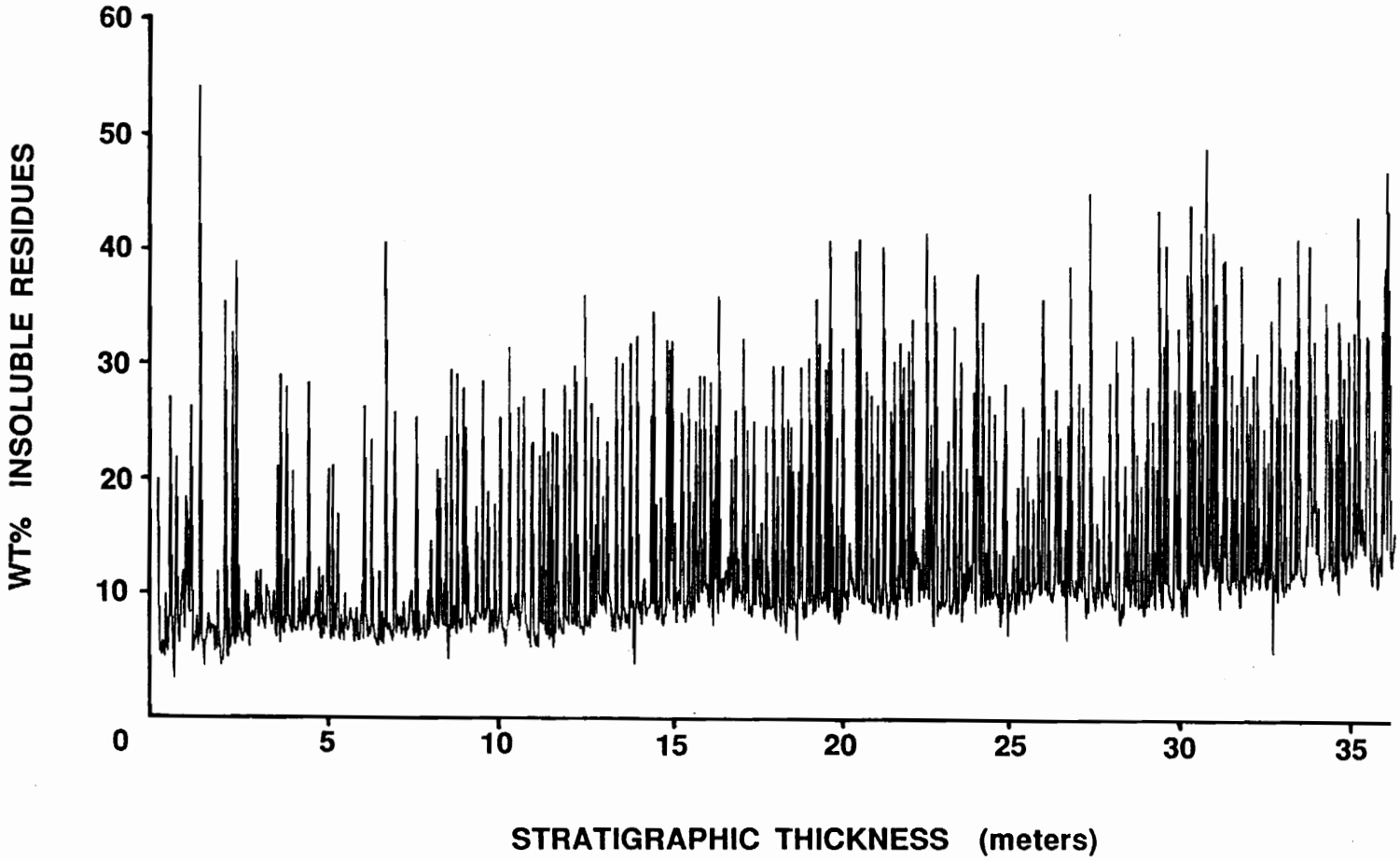
WT% INSOLUBLE RESIDUES
60
50
40
30
20
10
0
5
10
15
20
25
30
35
STRATIGRAPHIC THICKNESS (meters)

and argillite layers, however it is likely the accumulation rates of the individual rock types were different and the rates may have varied during the duration of the sampled interval.

The dominant peak in the 36 m insoluble residue time-series occurs at 8.7 cycles/meter or 0.11 m thick cycles (Fig. 25). Using the maximum and minimum range of long-term accumulation rates for this stratigraphic section, the 0.11 m thick cycle converts to a period between 0.7-2.9 k.y. (Table 3). The subordinate peaks convert to periods between 0.75-7.0 k.y. (Fig. 25 and Table 3).

DISCUSSION

The rhythmically bedded ramp-slope deposits are time-equivalent to cyclic shallow and deep ramp deposits in Wyoming and southwestern Montana (Fig. 19). The shallowing-upward cycles (1-10 m thick) are characterized by subtidal bases which grade upsection into very shallow subtidal or tidal flat facies. Thin paleosol or regolith layers cap some of the inner ramp tidal flat-capped cycles indicating prolonged subaerial exposure of the flats during sea level falls and lowstands. The average periods of the cycles range from 30-110 k.y. (using maximum and minimum age range of the Lodgepole Formation). The meter-scale cycles are stacked into 3rd to 4th order depositional sequences whose

Figure 25. Power spectrum of the debiased insoluble residue time-series. Wavenumbers between 0.02 and 10.0 were analyzed. A 67 m thick cycle (0.37-1.6 m.y.) occurs in the power spectrum (0.015 cycles/meter), which may relate to the observed long-term increase in the insoluble residue content within the time-series.

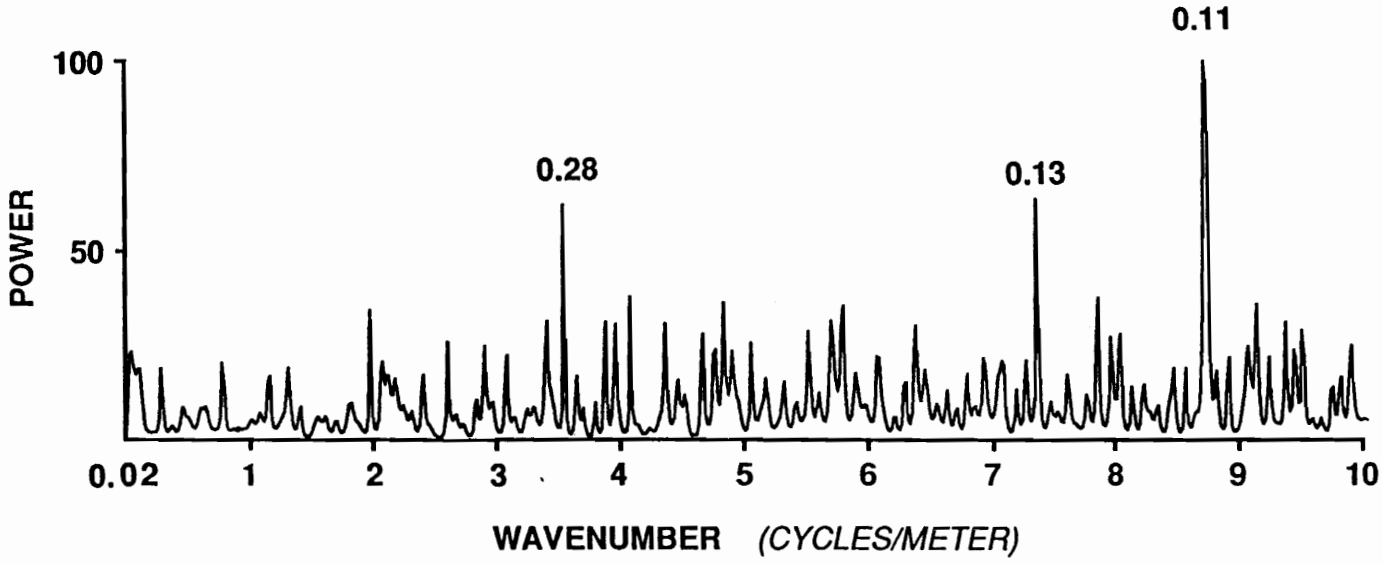
0.11
100
0.28
0.13
POWER
50
0.02
1
2
3
4
5
6
7
8
9
10
WAVENUMBER (CYCLES/METER)

Table 3. Significant cycle thicknesses within power spectrum.

WAVENUMBER (cycles/meter)	THICKNESS (m)	PERIOD* (k.y.)
8.75	0.11	0.6-2.85
7.35	0.13	0.75-3.4
3.55	0.28	1.5-7.0

* assuming a 0.04-.18 m/k.y. accumulation rate, respectively. All peaks above the 40 power level.

estimated durations range from 0.36-2.7 m.y. (determined from the thickness of the sequence divided by the subsidence rate; Koerschner and Read, 1989). Combined field and computer modeling studies of the cyclic ramp-to-basin deposits suggest the cycles and sequences were likely formed by 5th order (20-100 k.y.) sea level fluctuations, with amplitudes between 20-25 m, superimposed on 3rd to 4th order oscillations (Chapter 1).

The lack of meter-scale cycles in the ramp-slope facies indicates they were deposited in water depths too great to record the effects of 5th order sea level oscillations. However, converting the thickness of the 4th order shallowing-upward sequences (8-39 m thick) to time using the calculated accumulation rates, suggests that the ramp-slope was affected by long-term (0.04-1.0 m.y.) sea level oscillations similar to those recorded in the depositional sequences of the cyclic shallow ramp deposits.

There are no significant spectral peaks corresponding to typical Milankovitch-type periods (≈20-100 k.y.; Fig. 25). This implies that orbitally forced climatic fluctuations did not intensify the processes controlling the input of terrigenous and carbonate components along the ramp-slope. In other words, the contrasts in storm activity were greatest at the <3 k.y. time scale.

The 0.7-2.9 k.y. (<3 k.y.) period which dominates Paine Member sedimentation appears to be climatically induced. Periods of intensified storm activity alternating with periods of little or no storm activity suggest fluctuating storm tracks or changing rainfall

patterns which affected the relative amounts of terrigenous material reaching the ramp-slope. Paleoclimatic fluctuations with periods between 1-3 k.y. are recognized in a variety of terrestrial and marine systems. For example, Quaternary ice cores from Antarctica and Greenland contain a strong ≈2.5 k.y. periodicity (as well as other distinct periods between 2-15 k.y.) in the oxygen isotope (Dansgaard *et al.,* 1984; Benoist *et al.,* 1982) and deuterium isotopes record (Yiou *et al.,* 1989). The oxygen and deuterium isotope records reflect fluctuations in surface air temperature. A similar ≈2.5 k.y. periodicity is recognized in the advance and retreat patterns of North American and European alpine glaciers (Denton and Karlen, 1973), which reflects changes in air temperature and precipitation. Quaternary deep sea cores preserve a ≈2.5 k.y. periodicity in the oxygen isotope record of planktonic and benthic foraminifera (Pestiaux *et al.,* 1987), the paleotemperature record derived from foraminiferal assemblages, and from variations in sediment composition (Pisias *et al.,* 1973), which result from changes in ocean salinity and circulation. A 1-2 k.y. periodicity is reported in varved slope sediments off the northern California coast which preserve a record of fluctuations in the oxygen-minimum zone related to wind-controlled upwelling (Anderson *et al.,* 1989). A similar short-term periodicity can be traced back to the Permian where spectral analysis of deep-water evaporite varves indicate a strong 2.7 k.y. periodicity related to freshening of the evaporitic basin (Anderson, 1982). The common link between these various

systems is climatic change, in particular, changes in sea water temperature, salinity and circulation, air temperature, wind patterns, and rainfall.

The cause of these paleoclimatic fluctuations is not well understood; however, two theories have been suggested (Anderson, 1982; Pestiaux *et al.,* 1987; Yiou *et al.,* 1989). Most recently, Pestiaux *et al.,* (1987) and Yiou *et al.,* (1989) have suggested the ≈2.5 k.y. periodicity (as well as other distinct periods between 2-15 k.y.) in the Quaternary deep-sea record and Antarctica ice core data is one of several harmonics or combination tones of the 19-23 k.y. and 41 k.y. orbital forcing periods (precession and obliquity, respectively). The presence of these harmonics was predicted by nonlinear climatic oscillator models of LeTreut and Ghil (1983) and LeTreut *et al.,* (1988) which were forced by periods of the Earth's changing orbital parameters and include components of the climatic system acting at the 10^4-10^5 time scale (equations connecting global temperature, ice volume, and bedrock deflections under ice sheet loading).

The <3 k.y. periodicity has also been attributed to changes in solar activity (Bray, 1971; Denton and Karlen, 1973; Anderson, 1982, Anderson *et al.,* 1989). The link between solar activity and climate has been suggested by Anderson (1982) and Anderson *et al.,* (1989) because known solar cycle periods (≈82 yr and ≈200 yr; Cole, 1973) have been detected in Jurassic and Permian evaporite varves which also record a strong 2.7 k.y. periodicity. Furthermore, the ^{14}C record

(proxy for solar activity) in Holocene tree rings contains a ≈200 yr and 2.4 k.y. periodicity (Suess, 1980; Damon and Linwick, 1986; Stuiver and Braziunus, 1989) further supporting the link between fluctuating solar activity and climate.

CONCLUSIONS

1) Deep-water deposits of the Lower Mississippian Paine Member are composed of decimeter-scale, rhythmic interbeds of limestone and argillite which are bundled into four 4th order shallowing-upward sequences.

2) Limestone layers represent distal storm deposits, whereas argillite layers record intervals of little or no storm activity. Rhythmic interbedding of these contrasting rock types suggests paleoclimatic fluctuations controlled ramp-slope sedimentation patterns.

3) Spectral analysis of the fluctuating siliciclastic component (insoluble residues) indicate a dominant 0.7-2.9 k.y. periodicity in the deposits. A similar ≈2.5 k.y. periodicity is recorded in several terrestrial and marine systems and may represent one of several harmonics of the periods related to the Earth's changing orbital

parameters (Milankovitch-type periods) or the ≈2.5 k.y. periods may be due to fluctuations in solar activity.

4) No Milankovitch-type periods (≈20-100 k.y.) are recorded in the insoluble residue times-series data from the deep-water deposits; however, the range of thicknesses of the 4th order shallowing-upward sequences suggests 0.04-1.0 m.y. relative sea level fluctuations affected long-term depositional patterns along the ramp-slope. Similar periods of sea level fluctuation controlled the deposition of cyclic sequences in time-equivalent shallow and deeper ramp deposits in Wyoming and southwestern Montana.

5) The strong periodicity detected in the Lower Mississippian deposits suggests other rhythmically bedded, deep-water sequences may preserve a similar record of short-term paleoclimatic fluctuations.

REFERENCES

Aigner, T., 1985, Storm Depositional Systems: *in* Friedman, G. M., Neugebauer, H. J., and Seilacher, A., eds., New York, Springer-Verlag, 173 p.

Anderson, R. Y., 1982, A long geoclimatic record from the Permian: Jour. Geophys. Research, v. 87, p. 7285-7294.

Anderson, R. Y., Gardner, J. V. and Hemphill-Haley, E., 1989, Variability of the Late Pleistocene-Early Holocene oxygen-minimum zone off northern California: Geophysical Monograph v. 55, p. 75-84.

Arthur, M. A., Dean, W. E., Bottjer, D. J. and Scholle, P. A., 1984, Rhythmic bedding in Mesozoic-Cenozoic pelagic carbonate sequences: The primary and diagenetic origin of Milankovitch-like cycles: *in* Berger, A. L., and others, eds., Milankovitch and Climate: Dordrecht, Netherlands, D. Reidel, p. 191-222.

Arthur, M. A., and seven others., 1986, Rhythmic bedding in Upper Cretaceous pelagic carbonate sequences: varying sedimentary response to climatic forcing: Geology, v. 14, p. 153-156.

Bathurst, R. G. C., 1975, Carbonate Sediments and Their Diagenesis: Elsevier, Amsterdam, 658 p.

Benoist, J. P., Glangeaud, F., Martin, N., Lacoume, J. L., Lorius, C. and Oulahman, A., 1982, Study of climatic series by time-frequency analysis: *in* Preceedings of the ICASSP82, New York: IEEE Press, p. 1902-1905.

Bray, J. R., 1971, Solar-climate relationships in the post-Pleistocene: Science, v. 171, p. 1242-1243.

Calvet, F and Tucker, M. E., 1988, Outer ramp cycles in the Upper Muschelkalk of the Catalan Basin, NE Spain: Sed. Geol., v. 57, p. 185-198.

Cole, T. W., 1973, Periodicities in solar activity: Solar Physics, v. 30, p. 103-110.

Damon, P. E. and Linwick, T. W., 1986, Geomagnetic-heliomagnetic modulations of atmospheric radiocarbon production: Radiocarbon, v. 28, p. 266-278.

Dansgaard, W., Johnsen, S. J., Clausen, H. B., Dahl-Jensen, D., Gundestrup, N., Hammer, C. H. and Oescheger, H., 1984, North Atlantic oscillations revealed by deep Greenland ice cores: Geophysical Monograph, v. 29, p. 288-298.

Dean, W. E., Gardner, J. V. and Cepek, P., 1981, Tertiary carbonate-dissolution cycles on the Sierra Leone Rise, eastern equatorial Atlantic Ocean: Marine Geology, v. 39, p. 81-101.

deBoer, P. L. and Wonders, A. A., 1984, Astronomically induced rhythmic bedding in Cretaceous pelagic sediments near Moria (Italy): *in* Berger, A. L., and others, eds., Milankovitch and Climate: Dordrecht, Netherlands, D. Riedel, p. 177-190.

Denton, G. H. and Karlen, W., 1973, Holocene climatic variations-their pattern and possible cause: Quat. Research, v. 3, p. 155-205.

Eder, W., 1982, Diagenetic redistribution of carbonate, a process in forming limestone-marl alternations (Devonian and Carboniferous, Rheinisches Schiefergebirge, W. Germany): *in* Einsele, G., and Seilacher, A., eds., Cyclic and Event Stratification, New York, Springer-Verlag, p. 99-112.

Einsele, G., 1982, Limestone-marl cycles (periodites): diagnosis, significance, causes-a review: *in* Einsele, G., and Seilacher, A., eds., Cyclic and Event Stratification, New York, Springer-Verlag, p. 8-53.

Fischer, A. G. and Schwarzacher, W., 1984, Cretaceous bedding rhythms under orbital control?: *in* Berger, A. L., and others, eds., Milankovitch and Climate, Dordrecht, Netherlands, D. Reidel, p. 163-175.

Friedman, G. M. and Sanders, J. E., 1978, Principles of Sedimentology: Wiley, New York, 792 p.

Hallam, A.,1964, The origin of minor limestone/shale cycles: Geology, v. 14, p. 609-612.

Handford, C. R., 1986, Facies and bedding sequences in shelf-storm-deposited carbonates, Fayetteville Shale and Pitkin Limestone (Mississippian), Arkansas: Jour. Sed. Petrology., v. 56, p. 123-137.

Hays, J. D., Imbrie, J. and Shackleton, N. J., 1976, Variations in the earth's orbit: pacemaker of the ice ages: Science, v. 194, p. 1121-1131.

Herbert, T. D. and Fischer, A. G., 1986, Milankovitch climatic origin of mid-Cretaceous black shale rhythms in central Italy: Nature, v. 321, p. 739-743.

Kanasewich, E. R., 1981, Time Sequence Analysis in Geophysics: Third edition, University of Alberta Press, Edmington, Canada, 480 p.

Kate, W. G., ten and Sprenger, A., 1989, On the periodicity in a calcilutite-marl succession (SE Spain): Cretaceous Research, v. 10, p. 1-31.

King, D. A., 1990, Upper Cretaceous marl-limestone sequences of Alabama: Possible products of sea-level change, not climate forcing: Geology, v. 18, p. 19-22.

Koerschner, W. F. III and Read, J. F., 1989, Field and modelling studies of Cambrian carbonate cycles, Virginia Appalachians: Jour. Sed. Petrology, v. 59, p. 654-687.

Kreisa, R. D., 1981, Storm-generated sedimentary structures in subtidal marine facies with examples from the Middle and Upper Ordovician of southwestern Virginia: Jour. Sed. Petrology, v. 51, p. 823-848.

LeTreut, H. and Ghil, M., 1983, Orbital forcing climatic interactions and glaciation cycles: Jour. Geophys. Research, v. 88, p. 5167-5190.

LeTreut, H., Portes, J., Jouzel, J. and Ghil, M., 1988, Isotopic modeling of climatic oscillations: Implications for a comparative study of marine and ice core records: Jour. Geophys. Research, v. 93, p. 9365-9383.

Palmer, A. R., 1983, The Decade of North American Geology 1983 geologic time scale: Geology, v. 11, p. 503-504.

Pedersen, G. K., 1985, Thin, fine-grained storm layers in a muddy shelf sequence: an example from the Lower Jurassic in the Sentille 1 well, Denmark: Jour. Geol. Soc. London, v. 142, p. 357-374.

Pestiaux, P., Duplessy, J. C. and Berger, A., 1987, Paleoclimatic variability at frequences ranging from 1 cycle/10,000 years to 1 cycle/1000 years: evidence for nonlinear behaviour of the climate system: *in* Rampino, M. R., and others, eds., Climate-History, Periodicity, and Predictability, Van Nostrand Reinhold., Co., p. 285-299.

Pisias, N. G., Dauphin, J. P. and Sancetta, C., 1973, Spectral analysis of Late Pleistocene-Holocene sediments: Quat. Research, v. 3, p. 3-9.

Purser, B. H. and Evans, G., 1973, Regional sedimentation along the Trucial Coast, SE Persian Gulf: *in* Purser, B. H., ed., The Persian Gulf: New York, Springer-Verlag, p. 211-231.

Ricken, W., 1986, Diagenetic bedding, Lectures Notes in Earth Sciences, New York, Springer-Verlag, v. 6 210 pp.

Ricken, W., 1989, Independent measurement of time and sediment influx in bedding cycles and larger sequences: International Geological Congress Meeting with abstr. 28th Ann., v. 2, p. 696.

Rodriguez, J. and Gutschick, R.C., 1970, Late Devonian-Early Mississippian ichnofossils from western Montana and northern Utah: *in* Crimes, T.P., and Harper, J.C. eds., Trace Fossils: Seel House Press, Liverpool, p. 407-438.

Ross, C. A. and Ross, J. R. P., 1987, Late Paleozoic sea levels and depositional sequences: *in* Ross, C. A., and Haman, D., eds., Timing and Depositional History of Eustatic Sequences: Constraints on Seismic Stratigraphy: Cushman Foundation for Foraminiferal Research, Spec. Pub. 4, p. 137-149.

Ross, C. A. and Ross, J. R. P., 1988, Late Paleozoic transgressive-regressive deposition: *in* Wilgus, C.K. and others, eds., Sea-Level Changes: An Integrated Approach: S.E.P.M. Spec. Pub. 42, 156-181.

Sandberg, C. A., Gutschick, R. C., Johnson, J. G., Poole, F. G. and Sando, W. J., 1983, Middle Devonian to Late Mississippian geologic history of the Overthrust belt region, western United States: *in* Powers, R. B., ed., Geologic Studies of the Cordilleran Thrust Belt, v. 2: Denver, Rocky Mountain Assoc. Geol., p. 691-719.

Sando, W. J., 1976, Mississippian history of the northern Rocky Mountains region: Jour. Research U. S. Geological Survey, v. 4, p. 317-338.

Sando, W. J., 1985, Revised Mississippian time scale, western interior region, conterminous United States: U. S. Geological Survey Bull. 1605-A, p. A15-A26.

Smith, D. L., 1977, Transition from deep- to shallow-water carbonates, Paine Member, Lodgepole Formation, central Montana: *in* Enos, P. and Cook, H. E., eds., S.E.P.M. Spec. Pub. 25, p. 87-201.

Sneeden, J. W., Nummendal, D. and Amos, A. F., 1988, Storm- and fair-weather combined flow on the central Texas continental shelf: Jour. Sed. Petrolgy, v. 58, p. 580-595.

Stone, R. A., 1972, Waulsortian-type bioherms (reefs) of Mississippian age, central Bridger Range, Montana: *in* Montana Geol. Soc. Guidebook, p. 37-55.

Stuiver, M. and Braziunus, T. F., 1989, Atmospheric ^{14}C and century-scale solar oscillations: Nature, v. 338, p. 405-408.

Suess, H. E., 1980, The radiocarbon record in tree rings of the last 8000 years: Radiocarbon, v. 22, p. 200-209.

Swift, K. J. P. and Nummedal, D., 1987, HCS, tropical hurricanes, and intense winter storms: Sedimentology, v. 34, p. 338-344.

Yiou, P., Genthon, C., Jouzel, J., Ghil, M., LeTrout, H., Barnola, J. M., Lorious, C. and Korotkevitch, Y. N., 1989, High frequency paleovariablility in climate and $C0_2$ levels from Vostok ice-core records: *in* Kein, R., ed., Interaction of the Global Carbon and Climate System, Electric Power Res. Inst. Report, (in press).

Weedon, G. P., 1986, Hemipelagic shelf sedimentation and climatic cycles: the basal Jurassic (Blue Lias) of south Britian: Earth Planetary Sci. Letters., v. 76, p. 321-335.

APPENDIX

Stratigraphic Section Locations:

Hartville Canyon, Wyoming, (HC)

Section is located on the east side of the Platte River, in S1/2 NE1/4 sec. 27, T.27N., R.66W., northeast of the town of Guernsey, Platte County, Wyoming.

Red Canyon, Wyoming, (RC)

Section is located on Hermit Rock 71/2° quadrangle map. Location is on the north side of Red Canyon Creek in the northern Laramie Range, N1/2 NW1/4 sec. 15, T.31N., R.74W., southwest of the town of Douglas, Converse County, Wyoming.

Blue Creek, Wyoming, (BC)

Section is located on Turk Springs 71/2° quadrangle map. Location is on the north side of Blue Creek in N1/2 NW1/4 sec 1, T.42N., R.85W., east side of the Bighorn Mountains, east of the town of Barnum and Kaycee, Johnson County, Wyoming.

South Rock, Wyoming, (SR)

Section is located on Stone Mountain 71/2° quadrangle map. Location is on the north side of South Rock Creek, in SW1/4 sec. 25, T.52N., R.84W., east side of the Bighorn Mountains, west of the T-bar-T Dude Ranch, Johnson County, Wyoming.

Big Goose, Wyoming, (BG)

Section is located on Beckton 71/2° quadrangle map. Location on north and south side of Big Goose Creek, NE1/4 sec. 3 and NW1/4 sec. 2, T.54N., R.86W., and SW1/4 sec. 35, T.55N., R.86W., east side of the Bighorn Mountains, west-southwest of the city of Sheridan, Sheridan County, Wyoming.

Little Tongue, Wyoming, (LT)

Section is located on Dayton South 71/2° quadrangle map. Location on north side of U.S. Highway 14; NE1/4 sec. 27, and SE1/4 sec. 15, T.56N., R.87W., east side of the Bighorn Mountains, west of the town of Dayton, Sheridan County, Wyoming.

Little Bighorn Canyon, Wyoming, (LBC)

Section is located on Bull Elk Park 71/2° quadrangle map. Location on north side of the Little Bighorn River, NW1/4 sec. 20, T.58N., R.89W., north east side of the Bighorn Mountains, Sheridan County, Wyoming.

Clarks Fork Canyon, Wyoming, (CF)

Section is located on Deep Lake 15 minute map. Location on north side of the Clarks Fork of the Yellowstone River at Clarks Fork Canyon, NE1/4 sec. 7, SE1/4 sec. 6, SW1/4 sec. 5, T.56N., R.103W, southeast side of the Beartooth Mountains, Park County, Wyoming.

Shoshone Canyon, Wyoming, (SH)

Section is on Cody 71/2° quadrangle map. Location on the north side of Shoshone River NE1/4 sec. 5, NW1/4 sec. 4, T.52N., R.102W. West of the town of Cody, Park County, Wyoming.

Benbow, Montana, (B)

Section is on Mt. Wood 15 minute map. Location on hairpin turn of Benbow Mine Road, sec. 20 and 29, T.5S., R.16E., east side of the Beartooth Mountains, Stillwater County, Montana.

Baker Mountain, Montana, (BM),

Section is on McLeod Basin 71/2° quadrangle map. Location on west side of the East Boulder River, NW1/4 sec. 35, and NE1/4 sec. 34, T.3S., R.12E., northeast side of the Beartooth Mountains, Sweetgrass and Park County, Montana.

Livingston, Montana, (L)

Section is on Brisbin 71/2° quadrangle map. Location on east side of the Yellowstone River, south of the town of Livingston, NW1/4 sec. 1, NE1/4 sec. 2, T.3S., R.9E., and SE1/4 sec. 35, R.2S., R.9E., north side of the Beartooth Mountains, Park County, Montana.

Sacajawea Peak, Montana,(S)

Section is on Sedan 15 minute map. Location on north side of Sacajawea Peak, N1/2, sec. 27, T.2N., R.6E., tallest peak in the Bridger Range, Gallatin County, Montana.

Logan, Montana, (LO)

Type section of Madison Group. Section is on north side of the Gallatin River, SE1/4 SW1/4 sec. 25, T/2N., R.2E., north of the town of Logan, Gallatin County, Montana.

Dry Fork, Montana, (DF)

Type section of the Paine and Woodhurst Members of the Lodgepole Formation. Section is on the north side of the Dry Fork of Belt Creek, at the intersection of Currie Coulee with Dry Fork, Little Belt Mountains, SE1/4 sec. 35, T.16N., R.7E., Cascade County, Montana.

Ashbough Canyon, Montana, (AC)

Section is on the Ashbough Canyon 71/2° quadrangle map. Location on the north side of Ashbough Canyon, S1/2 sec. 28, T.9S., R.8W., Blacktail Mountains, Beaverhead County, Montana.

Little Flat Canyon, Idaho, (LF)

Section is on Hatch 71/2° quadrangle map. Location on south side of Little Flat Canyon, S1/2, sec. 20 and NW1/4 sec. 29, T.7S., R.40 E., Chesterfield Range, Bannock County, Idaho.

Wiggins Fork, Wyoming, (W)

Section is on Mason Draw 71/2 ° quadrangle map. Location on east side of the Wiggins Fork, south of Black Mountain and south of the town of Dubious, SW1/4 sec 7, T.42N., R.105W., Fremont County, Wyoming.

Washakie Reservoir, Wyoming, (WR)

Section on Moccasin Lake 71/2° quadrangle map. Location on Indian reservation land, north side of the Little Wind River and west of Washakie Reservoir, difficult to get permission to enter; S1/2 sec. 18, T.1S., R.2W., east side of the Wind River Range, Fremont County, Wyoming.

VITA

I was born in Denver, Colorado on June 16, 1959. I graduated from Bonita Vista High School in San Diego, California in 1977. I graduated from U. C. Santa Cruz in 1981, then went to work for the U.S. Geological Survey in Denver for two years. I then attended Oregon State University where I received my M.S. in geology in 1986. I moved across the country to attend V.P.I. where I finished my Ph.D. in August 1990. As of August, I will be employed as an Assistant Professor of Geology at the Department of Geological Sciences at the University of New Mexico.
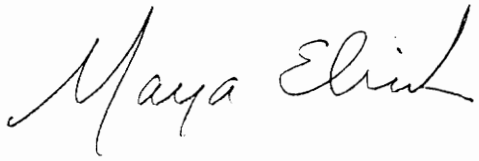
For those of you wondering if there is a light at the end of the tunnel.....yes, there is.